REPLACEMENT OF ELECTRONICS WITH FLUID INTERACTION DEVICES

Prepared for

NATIONAL AERONAUTICS AND SPACE ADMINISTRATION

CONTRACT NAS 3-6201

By

THE BENDIX CORPORATION
RESEARCH LABORATORIES DIVISION
Southfield, Michigan

Summary Report

NASA CR-54758
BRLD NO. 2946

TASK-1

REPLACEMENT OF ELECTRONICS WITH FLUID INTERACTION DEVICES

Prepared Under
the Direction of:

M. H. Cardon, Project Engineer
Machine and Propulsion Controls Department
Energy Conversion and Dynamic Controls Laboratory

Approved by:

L. B. Taplin, Manager
Energy Conversion and Dynamic Controls Laboratory
Technical Director, Fluid State Programs

Prepared for

NATIONAL AERONAUTICS AND SPACE ADMINISTRATION

August 31, 1965

CONTRACT NAS 3-6201

Technical Management
NASA Lewis Research Center
Cleveland, Ohio
Advanced Development and Evaluation Division
Dr. William Griffin

By

The Bendix Corporation
Research Laboratories Division
Southfield, Michigan

REPLACEMENT OF ELECTRONICS WITH FLUID INTERACTION DEVICES (U)

by
M. H. Cardon

ABSTRACT

The report covers the design and analysis of an actuation system that uses fluid circuits instead of electronics. The objective is to develop an all-pneumatic servo actuator with performance equal to the electropneumatic unit but with much more reliability for adverse environments. The system will use a piston-cylinder with rack and pinion that produces 180 degrees rotary output. The system will have a 6 cps bandwidth, 0.2 degrees resolution, and 300 in-lb stall torque. The working fluid is dry hydrogen with 215 psia supply and 50 psia exhaust. Experimental data on vortex amplifiers for this system are also presented.

TABLE OF CONTENTS

LIST OF ILLUSTRATIONS

LIST OF TABLES

SECTION 1

INTRODUCTION

This report presents results of Task 1 of a two task effort to develop a pneumatic actuation system in which the electronics that formerly provided the error detection, frequency compensation, and amplification have been replaced with fluid interaction devices.

The objective of Task I was to design and analytically study an all-pneumatic servo actuator with performance characteristics comparable to an existing electropneumatic system. Both static and dynamic performance characteristics were to be established. Characteristics specifically called out for study were linearity and gain of output shaft angular position versus applied signal to the input transducer; pressures; flows; and required performance characteristics of all fluid interaction elements to be used in the servo loop. These characteristics were to be studied over a specified range of supply and exhaust gas pressures and temperatures. The study was also to provide a description of components selected for use in the system along with experimental evidence to justify and support performance calculations.

The existing electropneumatic system specified as a starting point for this study is a control drum actuation system for a nuclear rocket engine. That system uses a General Electric AG-20 actuator motor with electronics located in a shielded region some distance from the actuator motor.

The actuator motor has two pistons mounted on opposite ends of a short rack that drives a pinion gear. The pinion gear is coupled directly to the load. The load of the actuation system consists of a control drum with friction and inertia, and a scram spring. The drum has a limited rotational travel requirement of 180° and a normal operating range of 15° to 165°.

The supply gas to the system is hydrogen at a pressure of 215 psia and at a temperature ranging from 100°R to 600°R. The exhaust pressure is 50 psia. Another requirement of this actuation system is that the actuator motor must operate in a specified radiation environment without shielding.

A block diagram of the pneumatic control drum actuation system illustrating the components that are to be replaced is shown in Figure 1-1.

The reason for desiring to substitute fluid interaction or flueric circuits for electronics is to allow the drum position control loop to be closed at the actuator motor location, thus minimizing the number of electrical connections exposed to the actuator motor environment and increasing reliability.

This change in location of part of the control loop is practical with mechanical-pneumatic circuits -- but not with electronics -- due to the superior tolerance to nuclear radiation of these circuits compared to unshielded electronic circuits.

Reliability is further improved by using a minimum number of moving parts and by using the same fluid as a power supply for both the actuator motor and the other pneumatic components. In this case, the other pneumatic components are passive elements such as orifices, and active elements using fluid interaction methods to obtain desired functions.

Fluid interaction devices perform summing and amplification functions without the use of mechanical moving parts. By the proper direction of fluid streams through orifices, connecting channels, and within chambers, the fluid streams interact providing the desired operational characteristics.

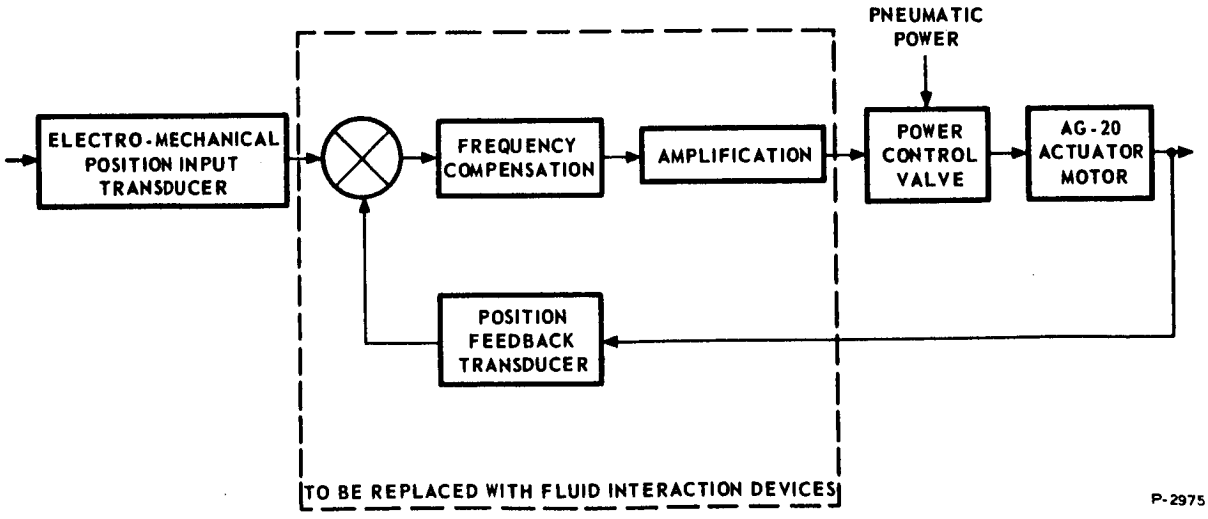

Figure 1-1 - Block Diagram of Pneumatic Control Drum Actuation System

The orifices, channels, and chambers can be made of stable materials that are relatively unaffected by nuclear radiation and temperature extremes.

The Task I objective was met by the means of the studies documented in this report. These studies used both linearized and nonlinear models of the actuator motor and the other portions of the actuator system. The linear model was used for hand and digital computer computations while the nonlinear model was used as a basis for analog computer simulation of the actuator system.

These studies resulted in generation of tentative specifications for the flueric circuits and other components required to build a prototype system using the AG-20 actuator motor.

The report also presents experimental data supporting the feasibility of constructing flueric circuits meeting the requirements of the prototype system.

The prototype actuator system will have a 6 cps bandwidth, 0.2 degrees resolution, and 300 lb-in stall torque. The working fluid for the complete system including flueric circuits is dry hydrogen at the same temperatures and pressures as the original supply for the AG-20 actuator motor. All of the required new components can be mounted on the AG-20 actuator motor within the allowed envelope.

SECTION 2

SUMMARY AND CONCLUSIONS

A control drum actuation system using the AG-20 actuator motor has been designed and studied analytically. The electronic system formerly used to perform the error detection, amplification, and compensation functions has been replaced by fluid interaction devices. In the study it was established that the actuation system required (1) error rate compensation to meet system bandpass and dynamic resolution specifications, (2) a low frequency lag-lead network to meet steady-state resolution requirements, (3) load pressure feedback to provide the necessary damping, and (4) velocity limiting to limit actuator velocity to the maximum allowable.

In the final design, compensation is provided by rate feedback and a lag-lead network, the damping is controlled by dynamic pressure feedback in the flapper-nozzle power control valve, and velocity limiting is accomplished by the rate feedback loop which overrides the position loop when the actuator approaches the maximum specified velocity. The performance characteristics of the actuation system are summarized in Table 2-1.

Vortex amplifiers of 0.25 inch chamber diameter are used to implement the compensation and amplification network. The gains required of these devices are within their experimentally proven capability, and their output noise level is well below the maximum allowed in the system. By use of these small vortex amplifiers and by proper circuit design, the gas consumption of the actuation system was kept well below that specified (0.0117 lb/sec compared to the 0.04 lb/sec allowed). All the orifices of these small size vortex amplifiers are equivalent to standard drill sizes.

The position input transducer, compensation and amplification networks, rate sensor, and position feedback transducer are packaged in a housing 7.75 inches in diameter and 7.25 inches high. The housing is bolted directly to the actuator utilizing an existing mounting pad.

Table 2-1 - Summary of Performance Characteristics

Characteristic	Specified	Performance of Actuation System Employing Fluid Interaction Devices		
		100°R	190°R	600°R
1. Gas Consumption of Actuation System	0.04 lbm/sec of H_2 at 100°R	0.01175 lbm/sec	0.00743 lbm/sec	0.00418 lbm/sec
2. Static Position Resolution	±0.2 degree	same as 190°R	±0.1 degree	same as 190°R
3. Transient Response to an 18 Degrees Step Input	a) Rise time to 62.5% of step command - 0.055 second	-0.070 second* +0.084 second	-0.068 second* +0.080 second	-0.051 second* +0.060 second
	b) Settling time to 0.9% of command - 0.15 second	-0.204 second +0.230 second	-0.188 second +0.212 second	-0.136 second +0.160 second
	c) Allowable overshoot 6 degrees	-4.00 degrees +1.15 degrees	-2.3 degrees +1.72 degrees	-1.15 degrees +1.15 degrees
4. Frequency Response to a ±2 Degree Input	a) 90 degrees phase shift at 6 cps	83 degrees at 6 cps	65 degrees at 6 cps	54 degrees at 6 cps
	b) 180 degrees phase shift at 12 cps	157 degrees at 12 cps	157 degrees at 12 cps	85 degrees at 12 cps
	c) Less than ±3 db output shaft variation from 0 to 8 cps	+3 db -2.5 db	+2.2 db -2.0 db	+1.6 db -0 db
5. Maximum Dynamic Resolution at 3 deg/sec Slewing Velocity	±0.5 degree	approx. same as 190°R	+0.175 degrees -0.175 degrees	approx. same as 190°R
6. Maximum Slewing Velocity	±300 deg/sec	-315 deg/sec +258 deg/sec	-286 deg/sec +275 deg/sec	-328 deg/sec +328 deg/sec

P-275

*±polarity symbols indicate direction of rotation

From the analytic study it is concluded that a control drum actuation system in which the electronics that formed the error detection, amplification, and compensation networks are replaced by fluid interaction devices, can be built and that:

(1) The system will have performance capabilities equivalent to a similar electropneumatic system.

(2) The use of fluid interaction devices in place of electronic circuits will require only a 17 percent increase in gas consumption over that required by the power control valve and actuator motor.

(3) The fluid interaction devices can be packaged in a compact housing that can be readily mounted on the actuator-motor.

(4) The performance characteristics required of the fluid interaction devices have been proven experimentally to be within the capabilities of the vortex amplifiers specified.

SECTION 3

SYSTEM DESIGN

A nuclear rocket engine control drum actuation system in which the error detecting, frequency compensation, and amplification are performed by fluid interaction devices was to be designed and analyzed. It was specified that the General Electric AG-20 actuator-motor be used in the system. A preliminary analysis of system requirements indicated the need for error rate compensation to meet the system bandpass and dynamic resolution specification, a low frequency lag-lead network to meet steady state resolution requirements, and load pressure feedback to meet the damping requirement.

The initial system design employed position feedback only, and the error rate compensation was to be accomplished by generating a lead signal in the compensation network. The resulting in a network had a lag-lead-lead-lag characteristic. A flapper-nozzle type servovalve that inherently provides load pressure feedback was selected for the power control valve. Vortex devices were used to implement the amplification and compensation networks. A detailed analysis of this actuation system, however, established that lag-lead-lead-lag compensation in the position loop was not adequate, that the maximum actuator velocity would have to be limited, and that a reduction in gas consumption was mandatory.

The actuation system was then redesigned. The final design included rate feedback, a lead-lag compensation network, and dynamic load pressure feedback. The velocity limiting was provided by having the rate feedback signal override the position error signal when the actuator approached a maximum specified velocity. The gas consumption was reduced by using the exhaust flow from the first stage vortex amplifiers as the supply flow for the following stages of vortex amplifiers and reversing the direction of flow through the position input nozzles and position feedback transducers. Also the chambers of the vortex devices were reduced from a chamber diameter of 0.5 inch to a chamber diameter of 0.25 inch.

This section of the report describes the AG-20 actuator-motor and the load; the originally proposed actuation system design with fluid interaction elements; and the final design. The operation and the mechanical details of the final system design are also covered.

3.1 AG-20 ACTUATOR AND LOAD

The AG-20 actuator-motor is a piston-cylinder device in which the linear motion of the piston is converted to a rotary motion by the means of rack and pinion. The load consists of the control drum, its associated friction, and a scram spring.

The power control valve, the AG-20 actuator-motor, and the load are illustrated in Figure 3-1. The power control valve is of the flapper-nozzle type which has dynamic load pressure feedback. This valve is discussed in detail in subsequent paragraphs and is shown here only to help illustrate how the actuator-motor functions. The actuator-motor is shown in Figure 3-2.

The actuator-motor has two separate pistons which are mounted on opposite ends of a short rack. The rack drives a pinion gear that is coupled directly to the load. The intermediate volume between the pistons is kept at a constant pressure, which prevents any cross port leakage between the cylinder chambers V_1 and V_2. In mid-position each chamber has a volume of 4.36 cubic inches. The actuator-motor has a displacement in terms of output shaft rotation of 2.2 cubic inches per radian.

The load has a maximum rotation of zero to 180° and a working rotation of 15° to 165°. The scram spring has a mid-position torque of 106.8 lb-in and a spring rate of 24.3 lb-in per radian. The spring force acts to reduce the angle of rotation of the load. The control drum has a polar moment of inertia of 0.24 in-lb-sec^2. The static friction load is 54 lb-in and the dynamic friction load is 47 lb-in.

3.2 INITIAL DESIGN

A block diagram of the initial system design, which employed position feedback only and used a lag-lead-lead-lag compensation network, is shown in Figure 3-3, and a schematic of the system is shown in Figure 3-4. In this design, the pneumatic position input and position feedback signals are generated using a conventional flapper-nozzle technique. An electrical torque motor strokes the position input flapper and a cam, coupled directly to the output shaft of the actuator-motor, actuates the position feedback flapper. The error detecting, amplification, and frequency compensation networks were implemented using vortex amplifiers. The lag-lead-lead-lag compensation was mechanized using both positive and negative feedback around an amplification circuit. The use of a positive feedback circuit permitted using smaller lag compensation

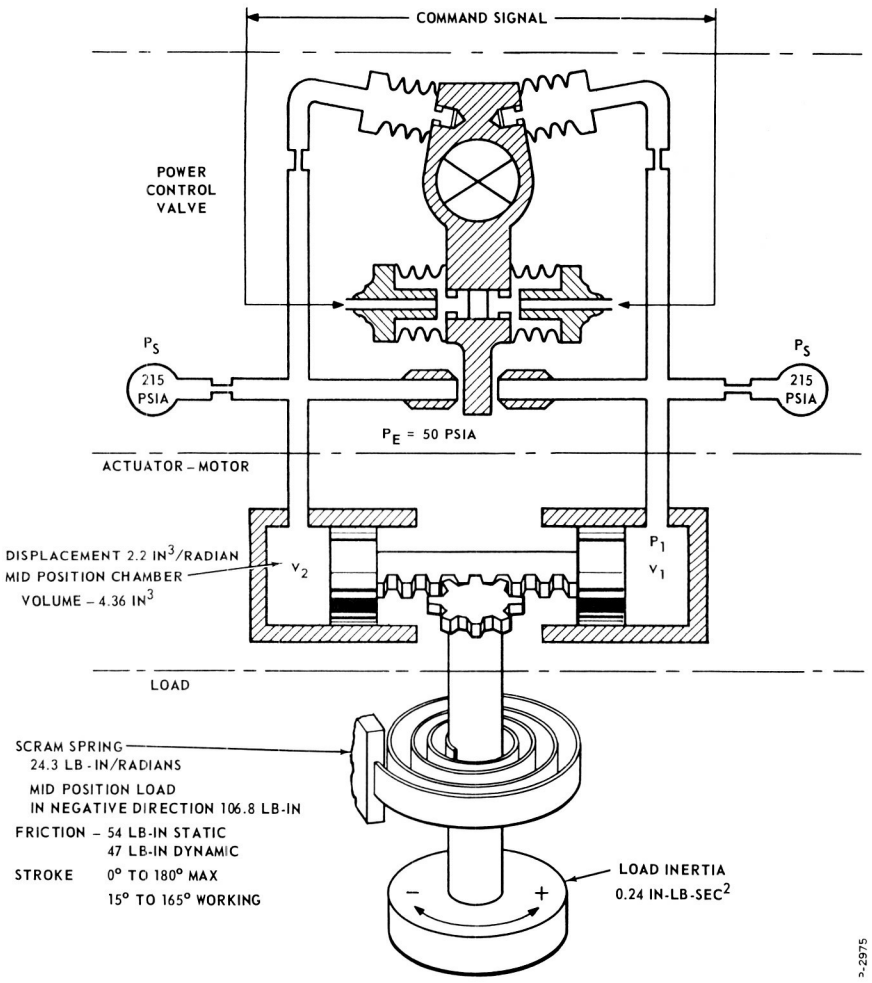

Figure 3-1 - Schematic of Valve, Actuator Motor, and Load

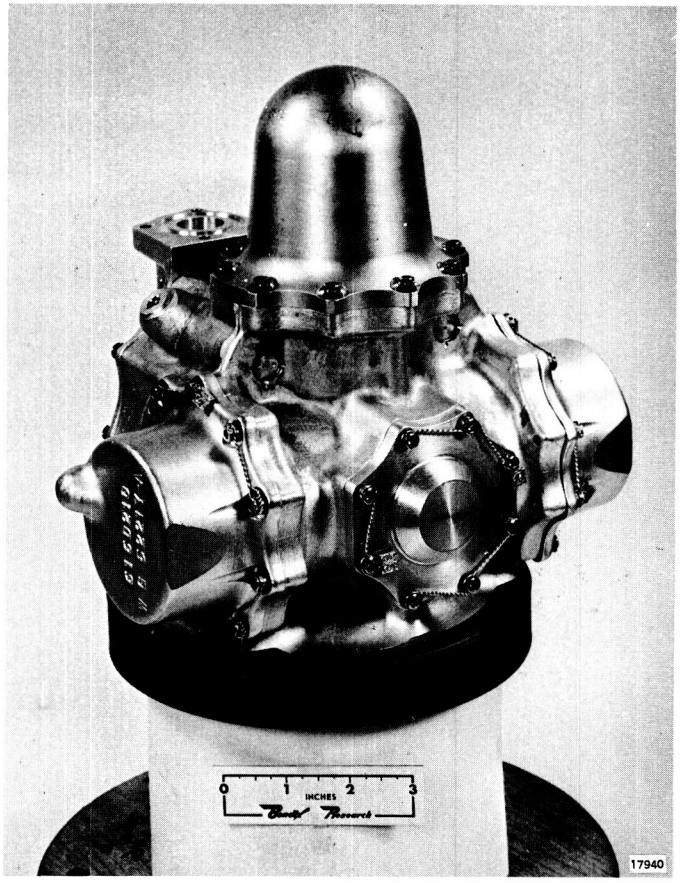

Figure 3-2 - General Electric AG-20 Actuator Motor

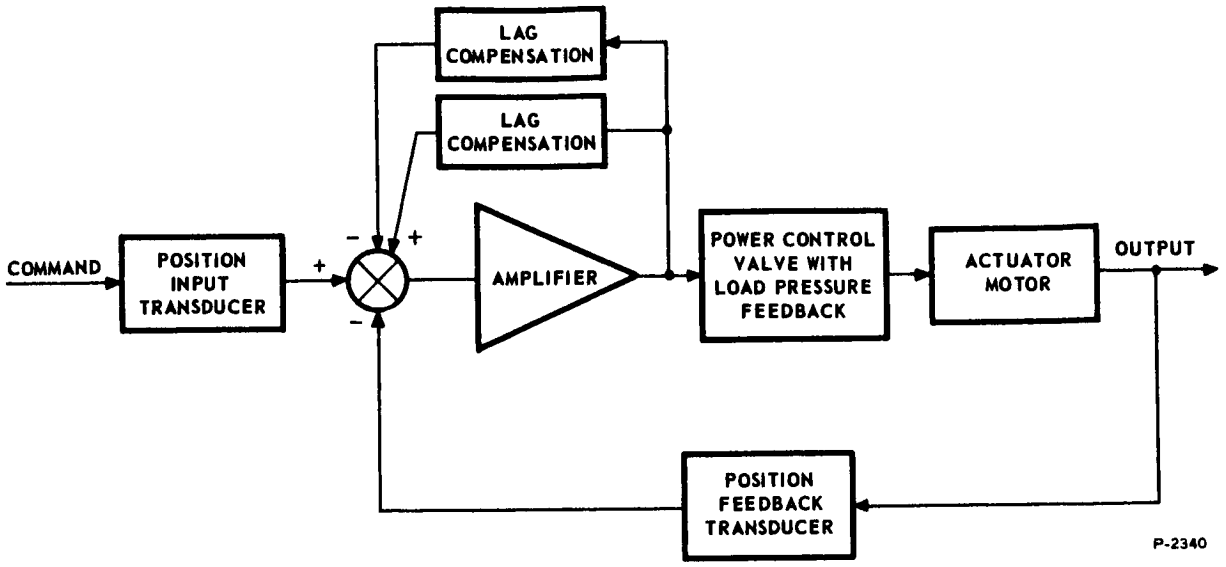

Figure 3-3 - Block Diagram of Originally Proposed Fluid Interaction Actuation System

volumes. The feedback around the amplification circuit was accomplished by using a Vorjet amplifier, since this device can operate with a control pressure considerably below its supply pressure (See Appendix II). As mentioned previously, the power control valve was of the flapper-nozzle type, which inherently provided the required damping by means of negative pressure feedback.

3.3 FINAL DESIGN

In arriving at the final actuation system design, several system configurations were analyzed before a final configuration was selected. A block diagram of the final actuation system is shown in Figure 3-5. The final design included a position input transducer, error detecting and amplification network, rate feedback, summing network, power control valve with dynamic load pressure feedback, position feedback transducer, and actuator-motor.

In conformance with the objective of the contract, the position error detecting and amplification network, compensation network (with the exception of the frequency variant load pressure feedback in the power control valve), summing network, and differentiating and amplification portions of the rate feedback circuit are made up of fluid interaction devices and passive components.

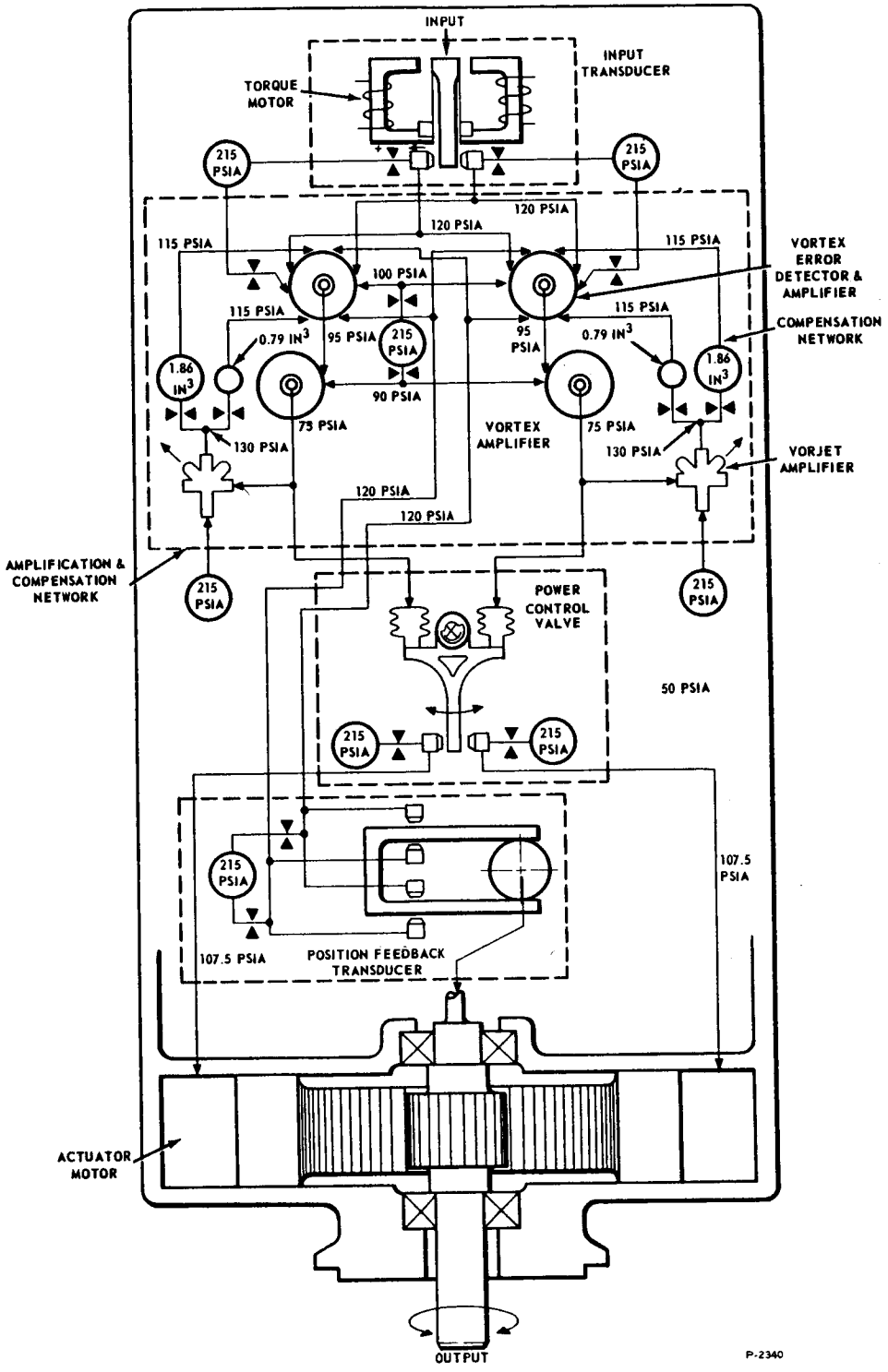

Figure 3-4 - Schematic of Originally Proposed Fluid Interaction Actuation System

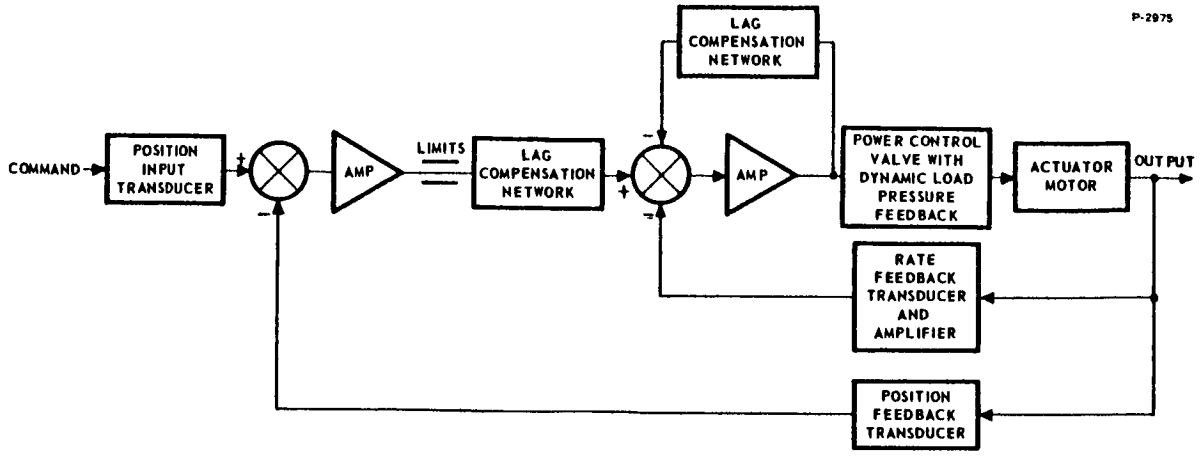

Figure 3-5 - Block Diagram of Final Design of Fluid Interaction Actuation System

The power control valve was increased in size by a factor of 1.8 over that used in the initial system, to improve the transient response. This increase in size, however, increased the inherent load pressure feedback such that the static performance of the actuator deteriorated. The static performance was then improved by incorporating frequency variant (or dynamic load pressure) feedback in the valve. (Dynamic pressure feedback in the flapper-nozzle valve takes exception to the requirement that the frequency compensation shall contain no moving mechanical parts). This approach is recommended because a fluid-interaction servovalve in which the incorporation of dynamic load pressure feedback is quite feasible is now under development. Alternate methods of improving static performance either increase gas consumption or introduce appreciable complexity.

The rate feedback now provides the necessary error rate compensation. The rate signal is generated by pseudo differentiating the position signal. The differentiation is performed using a volume-orifice network. To compensate for the effects of supply gas temperature change, the volume used in the circuit increases with increasing gas temperature.

A lead-lag signal is generated inside the rate loop to compensate for a lag in the rate signal generator. This lead signal is generated by feeding a portion of the output signal to the power control valve back through a lag network. Lag compensation is used in the position channel prior to the summation of the position error and rate signals to compensate for the lead generated in the rate loop.

The gas consumption was reduced by operating the signal processing network of the system at a lower pressure, using the exhaust of forward stages of the signal processing network to supply following stages, changing the direction of the gas flow so that it enters the nozzles of the input and position transducers rather than exhausting from them, replacing the Vorjet amplifiers with a pressure follower circuit, and reducing the size of the vortex elements to be used.

A schematic of the final actuation system is shown in Figure 3-6. The various networks illustrated are all implemented using vortex devices and passive components.

3.3.1 System Operation

Following an input command signal through the system (Figure 3-6), an input electrical signal which causes the flapper to move in the plus (+) direction reduces the total effective area of nozzles 1 and 1' of the position input and position feedback transducers and increases the total area of nozzles 2 and 2'. The result is a decrease in the pressure signal to vortex amplifier V_2 and an increase in the signal to vortex amplifier V_1. The increase in the input signal to vortex amplifier V_1 results in a decrease in its output to V_3, and, consequently, an increase in the output of V_3. The reverse is true for vortex amplifier V_2 and V_4. The input signals are amplified by vortex amplifiers V_1 and V_2, and V_3 and V_4. The maximum outputs of amplifiers V_3 and V_4 are limited by the proper arrangement of the saturation points of the position input and position feedback transducers and of the amplifiers. This limiting feature is essential in controlling the maximum velocity of the actuator and will be discussed later.

The outputs of V_3 and V_4 pass through the T_5 volumes after which they are summed with the outputs of the rate channel. This sum is then amplified by V_9 and V_{10}. The T_5 volumes are used in generating a lag in the position error signal. The increased signal from V_3, as long as the signal from V_7 is not decreasing, causes the output of V_9 to decrease, and the decreased signal from V_4 causes the output of V_{10} to increase.

The outputs of V_9 and V_{10} are directed to amplifiers V_{11} and V_{12}, respectively, where they are summed with the feedback signals generated in the T_3 lag circuit. To generate the lead-lag characteristics, the output signals of V_{11} and V_{12} are fed back to their inputs through pressure follower circuits employing

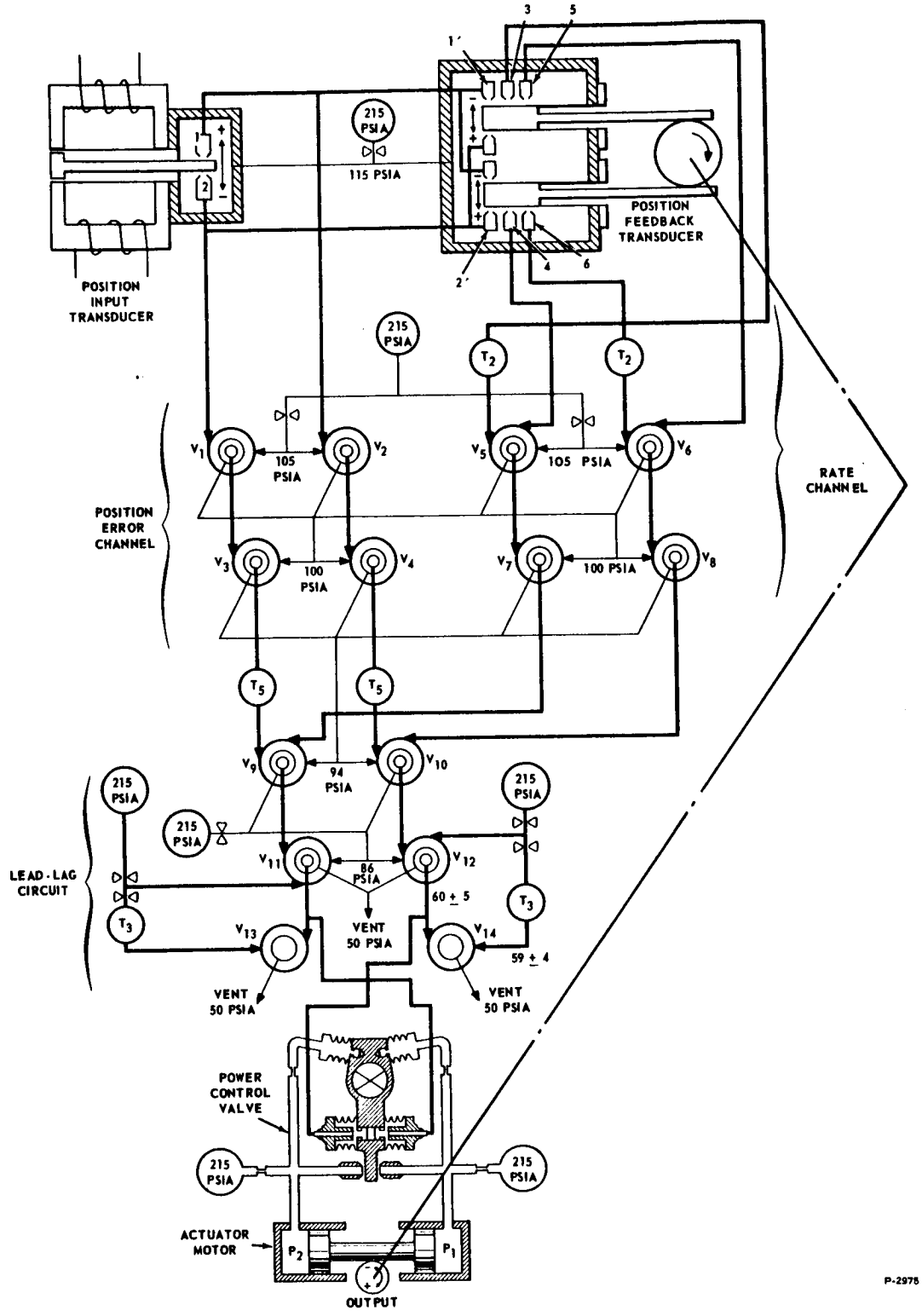

Figure 3-6 - Schematic of Final Design of Actuation System

vortex valves V_{13} and V_{14}. An increasing signal from V_{13} causes an increase in the feedback signal to V_{11}. Chamber T3 in conjunction with accompanying restricting orifices provides the necessary lag in the feedback path.

Changes in the output of V_{11} and V_{12} are fed back negatively. Very fast changes in their outputs will result in little or no change in feedback signal while slow changes are fed back, reducing the outputs of V_{11} and V_{12} as the case may be.

The outputs of V_{11} and V_{12} are also fed to input bellows that move the flapper of the power control valve. In this case the output of V_{11} is increasing and the output V_{12} decreasing, causing the flapper to move in the direction which increases P_1 and decreases P_2. The pressure difference in P_1 and P_2 forces the piston to move in the plus direction. As the piston rotates the cam of the position transducer, the position feedback transducer flapper moves in a direction to increase the area of nozzle 1' and decrease the area of nozzle 2'. When the areas of nozzle 1 and 1' are equal to areas of nozzles 2 and 2' the difference in the output signals becomes zero and actuator comes to a stop.

Following a signal through the rate circuit, as the position transducer moves in a positive direction, the area of nozzle 3 will increase and the area of nozzle 4 will decrease. The output of nozzle 3 passes through volume T_2 to vortex amplifier V_5 and the output of nozzle 4 is summed with the output of nozzle 3 at V_5. Because of volume T_2 there is a lag in the change of the signal coming from nozzle 3. This lag causes the total input signal to V_5 to decrease. This decrease in the total input signal is approximately proportional to the rate of change of the input signal. If the rate of change is very slow, the increase in the signal from nozzle 3 is about equal to the decrease in the signal from nozzle 4 and the total input signal changes very little. The reverse process takes place with the nozzle 5 and 6, resulting in an increasing total signal to amplifier V_7 as the velocity of the actuator increases in the positive direction.

The outputs of vortex amplifiers V_5 and V_6 are amplified by vortex amplifiers V_7 and V_8, respectively. The output of V_7 is fed to V9 and decreases as the actuator acquires a positive velocity. The output of V_8 is fed to V_{10} and is above the mean value for a positive velocity. The rate feedback is negative, since a positive velocity signal to V_{10} is opposite in sign to the input generated by a positive position error.

The gain of the rate feedback is adjusted according to the limits that are set in the position error channel such that as the velocity of the actuator approaches the maximum specified velocity, the rate feedback signal exceeds the position error signal and the system essentially becomes a rate servo operating on a constant input (the position error limit value) and therefore maintains a fixed maximum velocity.

3.3.2 Mechanical Configuration

The mechanical configuration of the position control system is shown in Figure 3-7. The position input transducer, error detecting network amplification and compensation network, rate sensing network, summing network, and position feedback transducer comprise the signal processing elements of the system. All these elements are mounted in a single housing that is bolted directly to the actuator-motor in place of the housing that formerly covered the electrical potentiometers.

The power control valve is mounted on a sub-plate that is fitted over the original valve supply and load ports and provides a means of communicating the supply gas and exhaust of the actuator with the signal processing elements. This sub-plate is used so that the actuator-motor will not have to be altered. The former cover is still used to cover the valve.

The cam of the position feedback transducer is coupled to the output shaft of the actuator-motor through a ball bearing mounted shaft which has a seal on its input end. This seal prevents the high pressure gas in this area of the actuator-motor from passing into the instrument housing, which is maintained at the specified 50 psia exhaust pressure. The shaft is coupled to the output shaft of the actuator using the existing coupling.

The instrumentation potentiometer which will be used in the position control system evaluation tests is mounted directly over the input shaft and is coupled to it using a zero back lash flexible coupling.

All the signal processing elements are mounted on a common porting plate which can be easily removed from the housing. All communicating passages for gas flow to and from the porting plate have metallic face seals and all connections are automatically made when the porting plate is bolted in place. The complete signal processing portion of the system can be bench checked and then mounted on the actuator without disturbing any of the components.

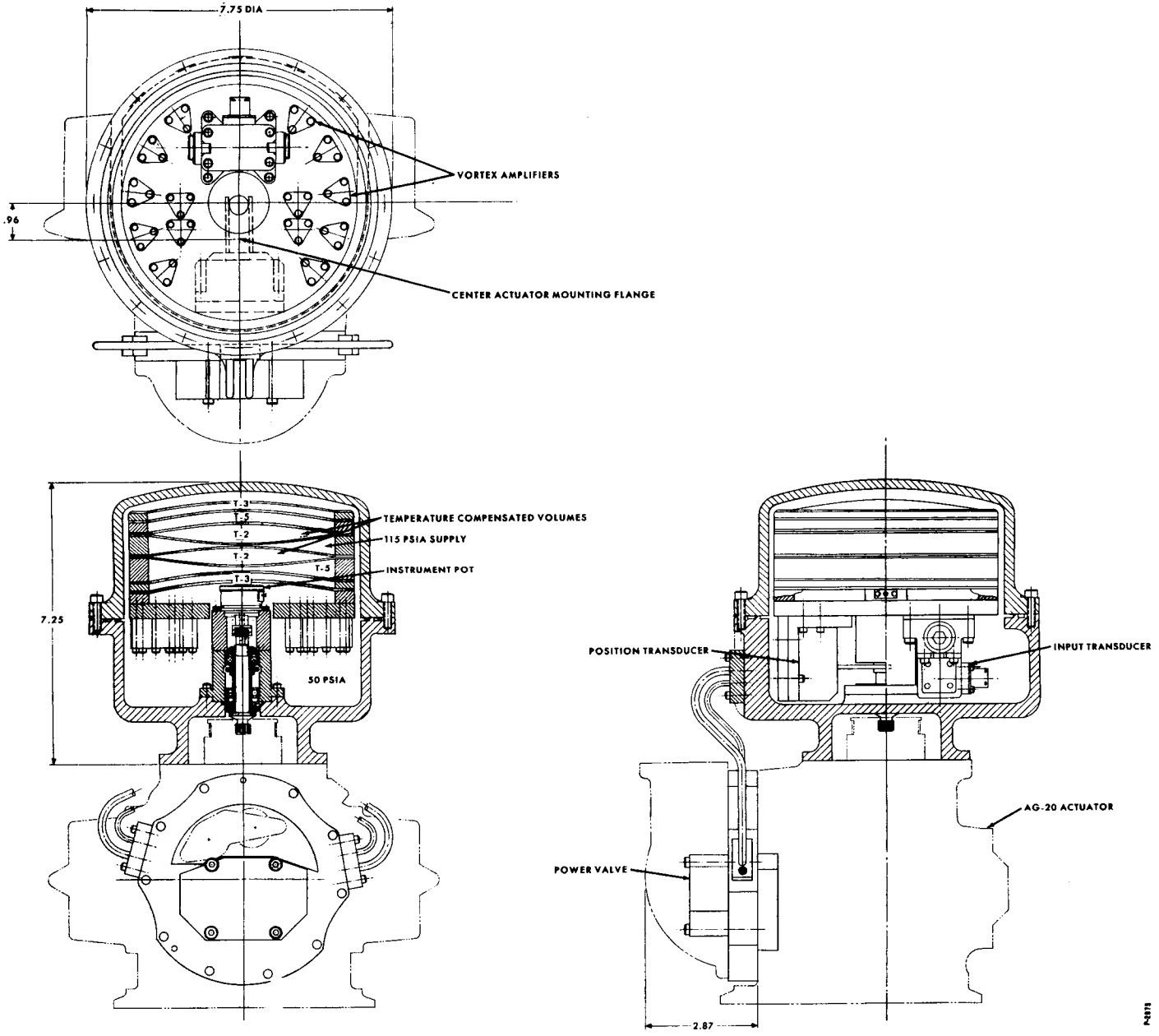

Figure 3-7 - Installation Drawing of Position Control System

The lag volumes used in the various networks are all mounted on the top of the porting plate and are arranged with volumes containing the highest pressure at the center and those with the lowest pressure on the outside. This arrangement reduces the pressure differentials across the volume chamber walls and allows substantially lighter construction techniques to be used.

The instrument housing is 7.25 inches high and 7.75 inches in diameter. While this is not extremely large, if one had the opportunity to completely integrate the fluid interaction signal processing elements with the power control valve and actuator-motor, a much cleaner and more compact design could be achieved.

SECTION 4

SYSTEM ANALYSIS

The system analyzed included the AG-20 actuator-motor, its load, power control valve, and a fluid interaction circuit to replace the electronics of the original actuation system. In the analysis, the actuator and its load were first analyzed and the compensation requirements defined. A system was then analyzed which attempted to compensate the actuator with only position and load pressure feedback. This was followed by the analysis of a system incorporating position feedback, rate feedback, and frequency varient load pressure feedback.

The analysis included (1) hand computations using a simple linear model, (2) digital computations based on a more complete linear model, and (3) an analog simulation of the AG-20 actuator-motor and actuator system control signal paths.

The following conclusions are drawn from the system analysis:

(1) The actuation system cannot be adequately compensated using position feedback and load pressure feedback only.

(2) Both rate feedback and frequency varient load pressure feedback are required.

(3) A limited position error signal is needed to effectively limit the maximum actuator velocity.

(4) When items 2 and 3 are available, dynamic and static performance requirements can be met with the exception of step response time.

(5) The signal-to-noise ratio of the vortex amplifiers chosen is high enough to allow proper system operation.

(6) Gas consumption can be kept well below the specification value of 40×10^{-3} lb/sec. A value of 11.75×10^{-3} lb/sec at 100°R, including the actuator-motor consumption, appears to be practical.

4.1 ACTUATOR-MOTOR AND POWER CONTROL VALVE

In the analysis of the actuator-motor the torque-speed requirements were established and a power control valve was then sized to meet these requirements. After the valve was sized, the dynamic characteristics of the actuator-motor, power control valve, and load were determined using linearized techniques. Once the dynamic characteristics of the actuator and load were known, the compensation requirement was defined.

In this section the actuator torque-speed requirements, reduced to differential pressure-volume flow requirements, and the required minimum valve size will be presented. Also, the neutral stability frequency will be derived, and the dynamic characteristics of the actuator and load in the form of Bode plots will be presented, followed by a discussion of the compensation requirements.

It was concluded from the analysis that (1) error rate or lead compensation is required to achieve the specified dynamic response, (2) a low frequency lag-lead compensation is required for static stiffness, and (3) negative load pressure feedback should be used to achieve optimum damping.

4.1.1 Differential Pressure Versus Load Volume Flow

Using the parameter values of Table 4-1 and the specified characteristics (Appendix I) the torque-speed requirements were determined and converted to the required differential pressure versus load volume flow characteristics. The most severe loading conditions occur when the actuator is at the 165 degree position of its travel and moving against the scram spring. Also, actuator velocities are slowest with a supply gas temperature of 100°R. Therefore, the differential pressure versus load volume flow requirements, illustrated in Figure 4-1, are for 100°R condition. A valve sized to meet these requirements will be large enough for all other actuator positions and specified supply gas temperatures. The reverse "S" shaped curve shown in the figure, defines the differential pressure-load volume flow required by the actuator to respond to a 12 cps, 2 degrees amplitude input signal. It will be noted that the differential pressure never reverses sign. This is a result of the scram spring load. To meet the transient response specification the actuator must travel at approximately its maximum velocity of 300 deg/sec against the scram spring. The differential pressure and load volume flow required for

Table 4-1 - Parameter Values Used for Performance Analysis

Actuator and Load Parameter	Specified	Used In Performance Analysis	Remarks
Mid-Position Volume (V_o)	3.71 in^3 (minimum) 3.85 (maximum)		
P_1 Line	0.317 in^3		The value used in the performance analysis includes the estimated volume in the power control valve.
P_2 Line	0.381 in^3		
Total	4.23 in^3 (maximum)	4.36 in^3	
Displacement Volume	2.2 in^3/rad	2.2 in^3/rad	
Actuator Friction	Equivalent to ± 10 psi pressure differential		
Load Friction	32 lb-in static	54 lb-in static	In the performance analysis the actuator friction was added to the load friction.
	25 lb-in dynamic	47 lb-in dynamic	
Actuator Inertia	0.00183 in-lb-sec^2		The actuator inertia is considered negligible and was not included in the performance analysis.
Load Inertia	92.5 lbm-in^2 (0.24 in-lb-sec^2)	0.24 in-lb-sec^2	
Actuator Spring Load	75 in-lb @ 15° and 124 to 145 in-lb @ 180°	75 in-lb @ 15° 24.3 in-lb/rad gradient	
Leakage	60 x 10^{-6} lb/sec of He @ room temperature for 2 pistons		This leakage was not considered in the performance analysis because it is two orders of magnitude below the power control valve flow

P-2975

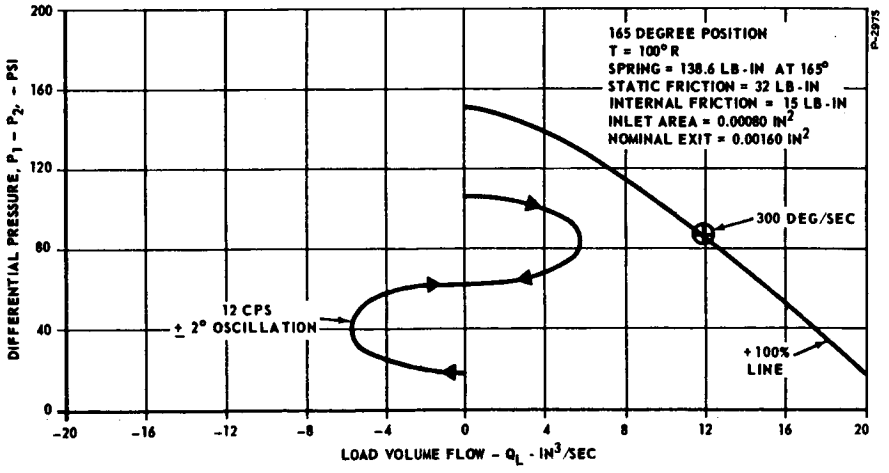

Figure 4-1 - Differential Pressure Versus Load Volume Flow Required of Power Control Valve

the specified transient response under the above condition is indicated in Figure 4-1 as the 300 deg/sec point.

With a valve sized to meet transient response requirements at 100°R and at the 165 degree position the system will exceed the maximum specified velocity at other positions when moving with the scram spring force, and at higher supply gas temperatures, indicating a need for velocity limiting if the specification requirement of a maximum velocity of 300 deg/sec is to be met.

4.1.2 Power Control Valve Capacity

A flapper-nozzle type servovalve was selected for this application because of its simplicity, absence of close fitting parts with relative motion, and inherent negative load pressure feedback. The desirability of the first two points is self evident, and the desirability of the last is covered in Section 5.5.

The valve was sized to meet the pressure and flow requirements for transient response using the technique described in Appendix VI. In Figure 4-1 the resulting pressure-flow characteristic for the valve with the flapper in a hard-over position is shown passing through the 300 deg/sec point. The pressure and flow requirements to meet the frequency response fall below this curve, indicating that the valve has sufficient capacity to meet frequency response requirements.

A schematic of a flapper nozzle valve defining the inlet orifice and exit orifice is shown in Figure 4-2. (The exit orifice varies as the flapper moves. The nominal exit orifice is defined as the exit orifice area when the flapper is centered between the two nozzles.) For the curve shown in Figure 4-1 the inlet orifice area was 0.00080 in^2 and the nominal exit orifice area was 0.00160 in^2.

4.1.3 Dynamic Characteristics

A schematic of the power control valve, actuator-motor, and load is shown in Figure 4-3. A block diagram of this actuator and

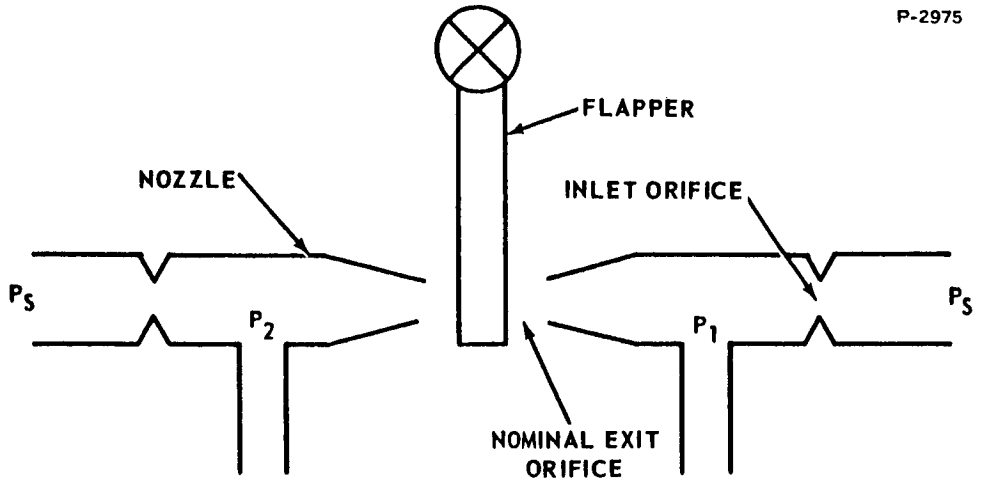

Figure 4-2 - Schematic of Flapper Nozzle Valve

load without friction is illustrated in Figure 4-4. Symbols used in the figures and their units are:

SYMBOL	DEFINITION	
ΔE_4	input signal ΔP	psi
A	effective area of actuating bellows of power control valve	in^2
ℓ	length from center of bellows to flapper pivot	in
$A\ell$	effective area of bellows times ℓ	in^3
D	maximum power control valve flapper deflection at nozzle	in
%D	percent of maximum power control valve flapper deflection	
Q	load volume flow	in^3/sec

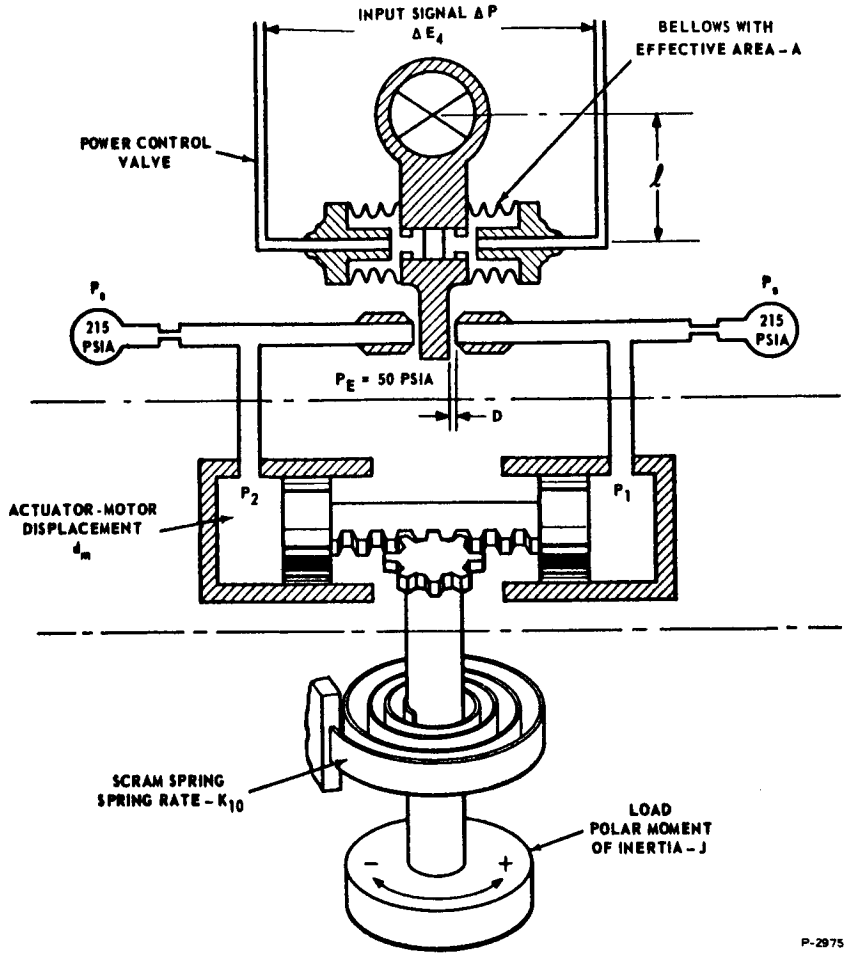

Figure 4-3 - Schematic of Power Control Valve, Actuator Motor, and Load

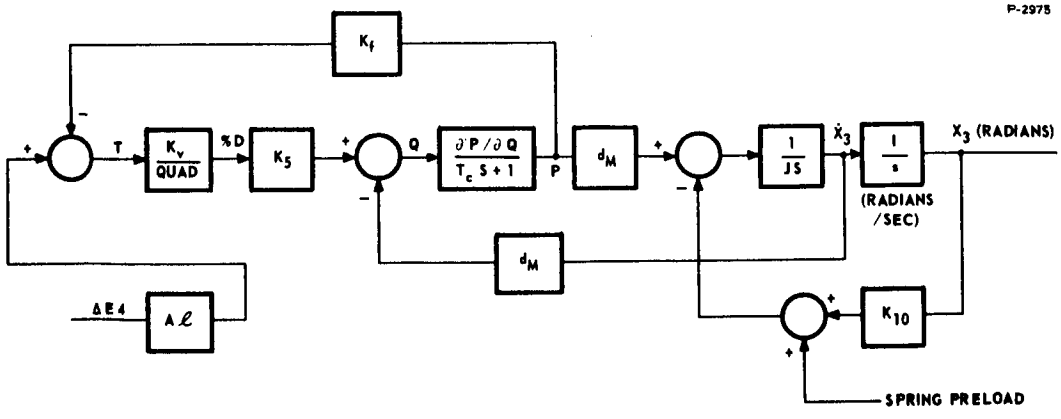

Figure 4-4 - Block Diagram of Actuator and Power Control Valve, Without Friction

SYMBOL	DEFINITION	
K_5	power control valve flow constant	0.52 $in^3/sec/\%D$
P	mean load pressure	107.5 psia
V	actuator volume under compression	4.36 in^3
$\frac{\partial P}{\partial Q}$	slope of the actuator differential pressure versus load volume flow characteristic curve	3.48 $\frac{lb\text{-}sec}{in^5}$
γ	ratio of specific heats	
T_c	compressibility time constant = $\frac{(\partial P/\partial Q)\, V}{2\, \gamma\, P}$	sec
d_M	displacement of actuator motor	2.2 in^3/radian
J	polar moment of inertia	0.24 lb-in-sec^2
K_{10}	spring rate of scram spring	24.3 lb-in/radian
K_V	% deflection of flapper per lb-in	400 %D/lb-in
K_f	pressure feedback gain	lb-in/psi
X_3	load position	radians
$\dot{X}_3$	load velocity	radians/sec

Using the block diagram of Figure 4-4, the linearized equation of motion is

$$\frac{\Delta X_3}{\Delta E_4} = \frac{\dfrac{A\ell K_v K_5 \dfrac{\partial P}{\partial Q} \dfrac{d_M}{K_{10}}}{1 + \dfrac{\partial P}{\partial Q} K_f K_v K_5}}{\dfrac{T_c J}{K_{10}\left(1 + \dfrac{\partial P}{\partial Q} K_f K_v K_5\right)} S^3 + \dfrac{J}{K_{10}} S^2 + \dfrac{T_c + \dfrac{d_M^2 \dfrac{\partial P}{\partial Q}}{K_{10}}}{1 + \dfrac{\partial P}{\partial Q} K_c K_v K_5} S + 1} \qquad (4\text{-}1)$$

If $j\omega$ is substituted for the Laplace operator S in equation (4-1), the resulting transfer function will represent the response to steady state sinusoidal inputs. Using the digital computation method described in Appendix V, the frequency response characteristics of the actuator and load at 100°R were calculated. These characteristics are shown in the form of Bode plots in Figures 4-5 and 4-6 respectively, without pressure feedback.

The method of servo analysis used was to examine these Bode plots and then from a general knowledge of the relations between open loop Bode plot response and closed loop response, to decide what compensation should be used.

From examination of Figures 4-5 and 4-6, it was apparent that the effect of temperature was to increase damping of the response. This same conclusion can be reached by detailed examination of the parameter changes versus temperature in equation (4-1). It was also apparent that a substantial increase in damping would make the actuator and load response less variable with temperature and therefore easier to compensate.

In order to see this more clearly, consider a very general cubic response. The generalized cubic response can be written as

$$\frac{\Delta X_3}{\Delta E_4} = \frac{K}{\frac{1}{B}\left(\frac{j\omega}{\omega_{NS}}\right)^3 + \frac{A}{B}\left(\frac{j\omega}{\omega_{NS}}\right)^2 + \left(\frac{j\omega}{\omega_{NS}}\right) + 1} \qquad (4\text{-}2)$$

where $j\omega$ has been substituted for S. Now by comparison with equation (4-1), the various coefficients can be derived. The quantity ω_{NS} is called the neutral stability resonant frequency and is by definition the frequency at which the cubic response exhibits 180 degrees phase lag. This means the output must be real and negative relative to the input. It follows that the imaginary components of the complex number representing the response at $\omega = \omega_{NS}$ must sum to a zero value. Therefore from equation (4-1)

$$(j\omega_{NS})^3 \left(\frac{T_c J}{K_{10}}\right) + j\omega_{NS} \left(T_c + \frac{dm^2 \frac{\partial P}{\partial Q}}{K_{10}}\right) = 0 \qquad (4\text{-}3)$$

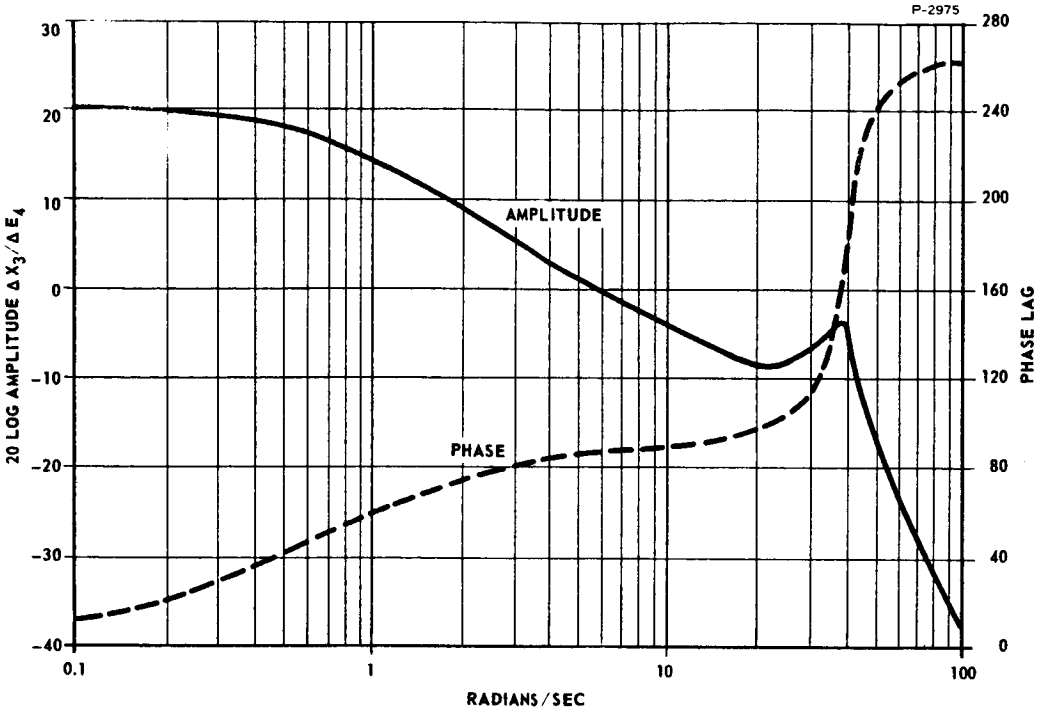

Figure 4-5 - Calculated Actuator Response at 100 °R Without Pressure Feedback

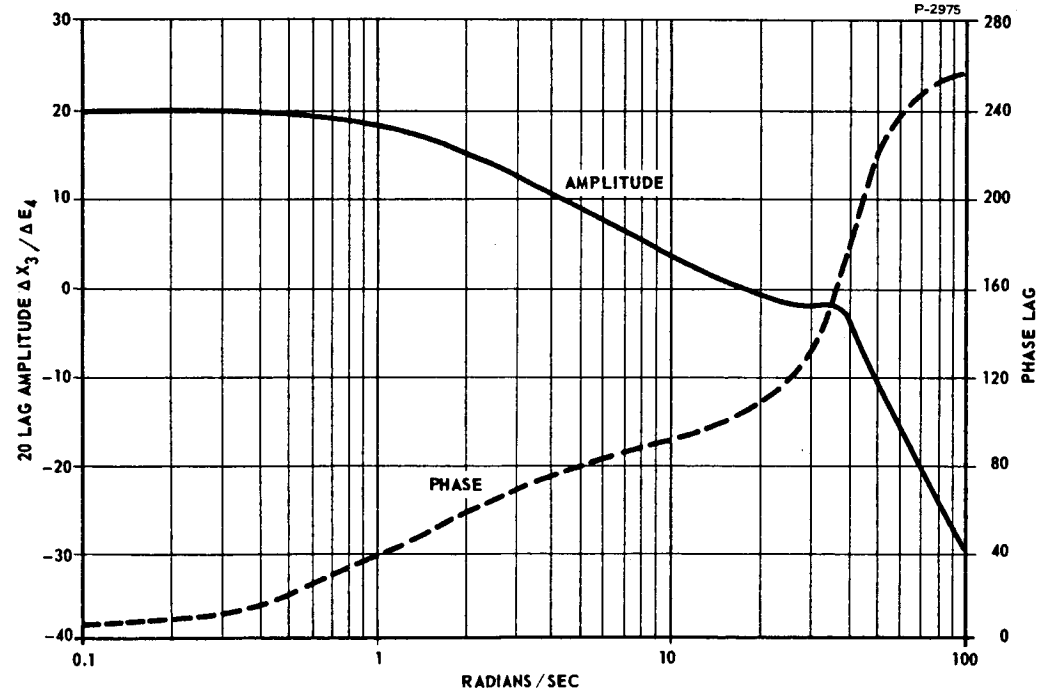

Figure 4-6 – Calculated Actuator Response at 600 °R Without Pressure Feedback

$$(j\omega_{NS})^2 = -\left(\frac{T_c K_{10} + dm^2 \frac{\partial P}{\partial Q}}{T_c J}\right) \tag{4-4}$$

$$\left(\omega_{NS}\right)^2 = \frac{K_{10}}{J} + \frac{dm^2 \frac{\partial P}{\partial Q}}{T_c J} \tag{4-5}$$

since

$$T_c = \frac{\left(\frac{\partial P}{\partial Q}\right) V}{2 \gamma P} \tag{4-6}$$

$$\omega_{NS}^2 = \frac{K_{10}}{J} + \frac{dm^2 \quad 2 \gamma P}{JV} \tag{4-7}$$

Note that ω_{NS} does not change with temperature except to the extent that the parameters involved in equation (4-7) change. These parameters are all relatively unaffected by temperature, except for γ. The γ of hydrogen does change appreciably when the gas temperature is below 200°R.

Now by substitution of numerical values, ω_{NS} is found to be 38.6 radians/sec at γ = 1.4.

The amplitude response at ω equal to ω_{NS} is also important. It may be calculated by substitution in the even order terms. After simplification, this equation is

$$\frac{A\ell K_v K_5 \frac{\partial P}{\partial Q} V}{(1 + \frac{\partial P}{\partial Q} K_f K_v K_5)(2 d_M \gamma P)} = \text{Amplitude at } \omega = \omega_{NS} \tag{4-8}$$

The A and B parameters in equation (4-2), if calculated, would allow prediction of the shape of the amplitude response of the cubic versus frequency by reference to charts. In this case, the function under consideration has only a few parameters that can be varied since most of the parameters are fixed by actuator motor design. It is therefore easier to try various values of K_f and calculate the complete frequency response on a digital computer.

Figures 4-7 and 4-8 show the results for a nominal servovalve and a realizable value of K_f.

4.1.4 Compensation Requirements

When the loop input is considered to be the pneumatic position command signal and the feedback signal is the pneumatic position signal, the actuation system has unity feedback. The pneumatic position feedback signal has very little dynamic error relative to the actual output position and the closed loop frequency response of the actual output position versus the position command is equal to the unity feedback closed loop response, GH/1 + GH, times 1/H. H is defined as the transfer function of the feedback portion of the closed loop and G is defined as the transfer function of the forward portion of the loop.

The unity feedback closed loop response can be approximated from the open loop Bode plot of GH by taking the zero db line at frequency where GH is greater than zero db and the GH plot at frequencies where GH is less than zero db. The approximation is least accurate where GH is approximately zero db.

If the closed loop is to have not over 90-degree phase lag at 6 cps, then GH and the zero db line must intersect somewhere near that frequency, that is near or above 37.6 radians/sec. This is the region where the approximation is least accurate, but it is at least a preliminary guide.

Then from system design charts such as those first published in Chestnut and Mayer, Volume One, Chapter 14,* it can be seen that the GH curve should cross the zero db line at 20 db/decade slope and should maintain this slope for some distance on each side of the intersection.

To obtain this characteristic with the actuator-plus-load response seen in Figures 4-5 and 4-6, it would be necessary to construct an antiresonance circuit. This is difficult under the best of conditions, where the actuator resonance is precisely known and where both the actuator resonance and the compensation circuit are independent of temperature. To avoid the difficulties of that approach, negative pressure feedback is used to produce a response like that in Figures 4-7 and 4-8. Then the required compensation for proper linearized closed loop response is lead in the circuit ahead of the actuator. This is equivalent to position error plus the rate-of-change-of-position error or "error rate" compensation.

*See "Servomechanisms and Regulating System Design" by Harold Chestnut and R. W. Mayer, John Wiley & Sons, Inc., New York, 1957, pp. 398-439.

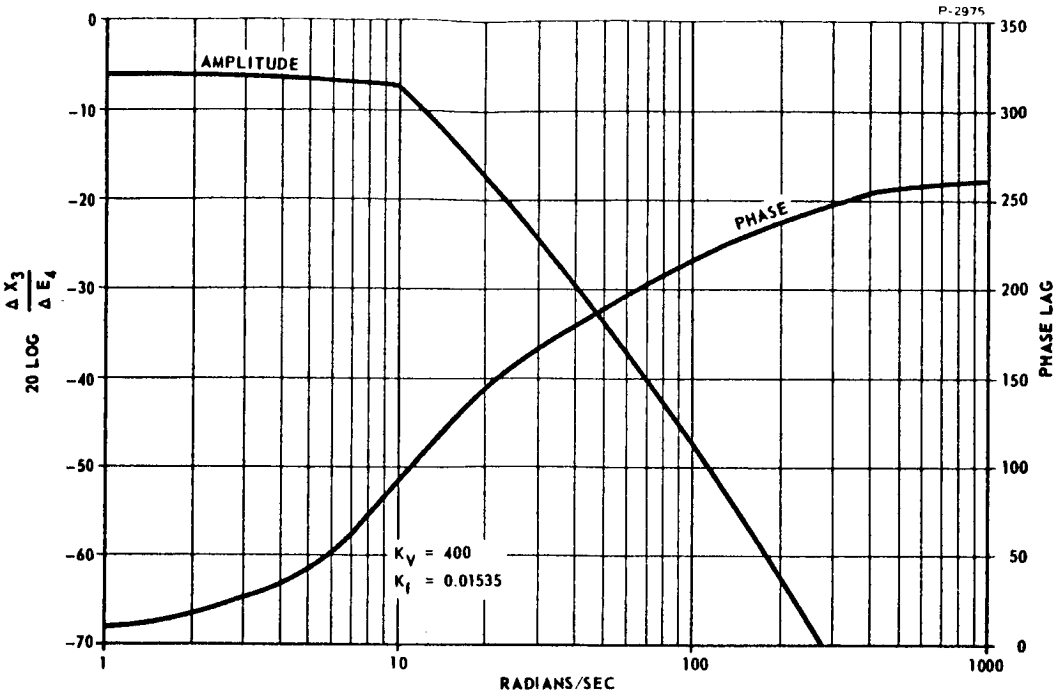

Figure 4-7 - Actuator and Power Control Valve With Pressure Feedback, at 100°R

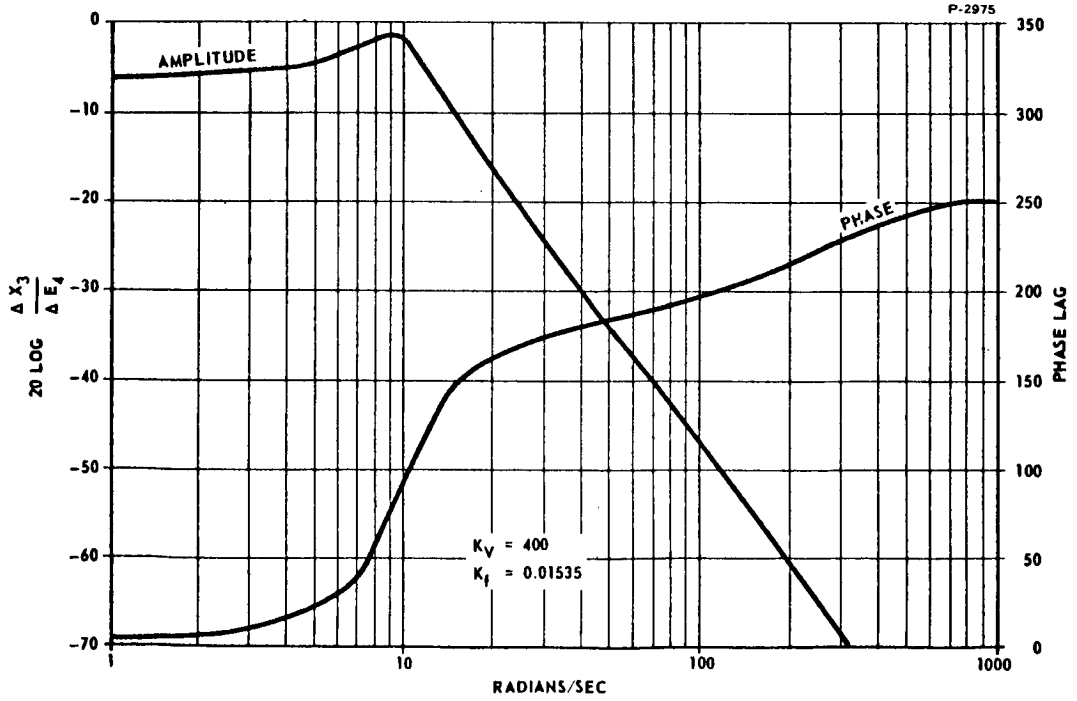

Figure 4-8 - Actuator and Power Control Valve with Pressure Feedback, at 600°R

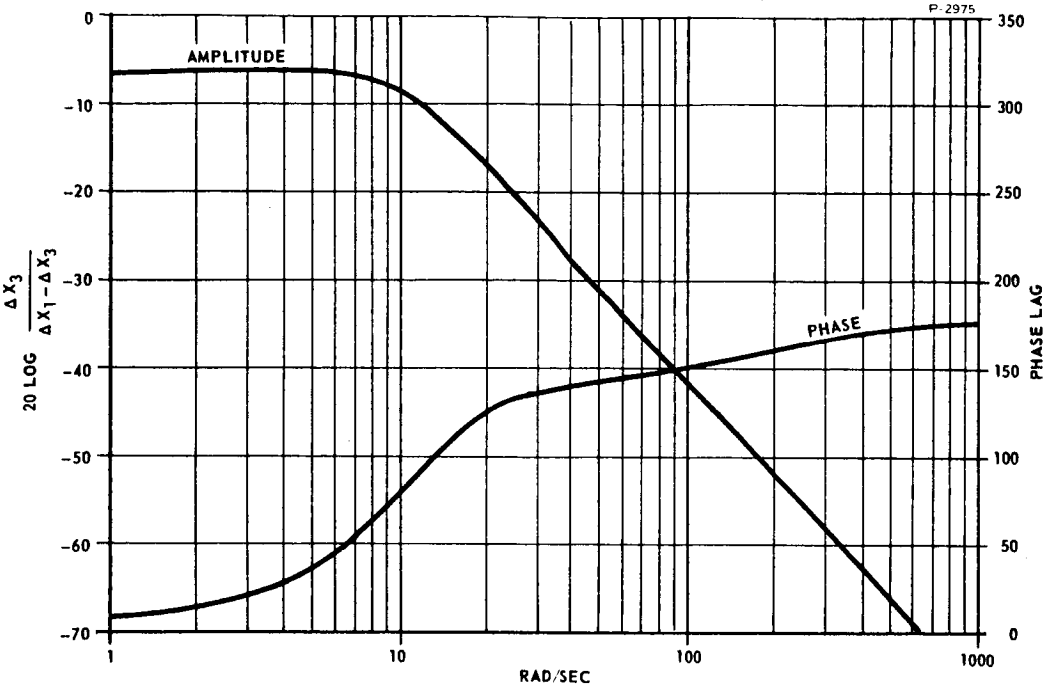

Figure 4-9 - Open Position Loop at 100 °R With Ideal Lead

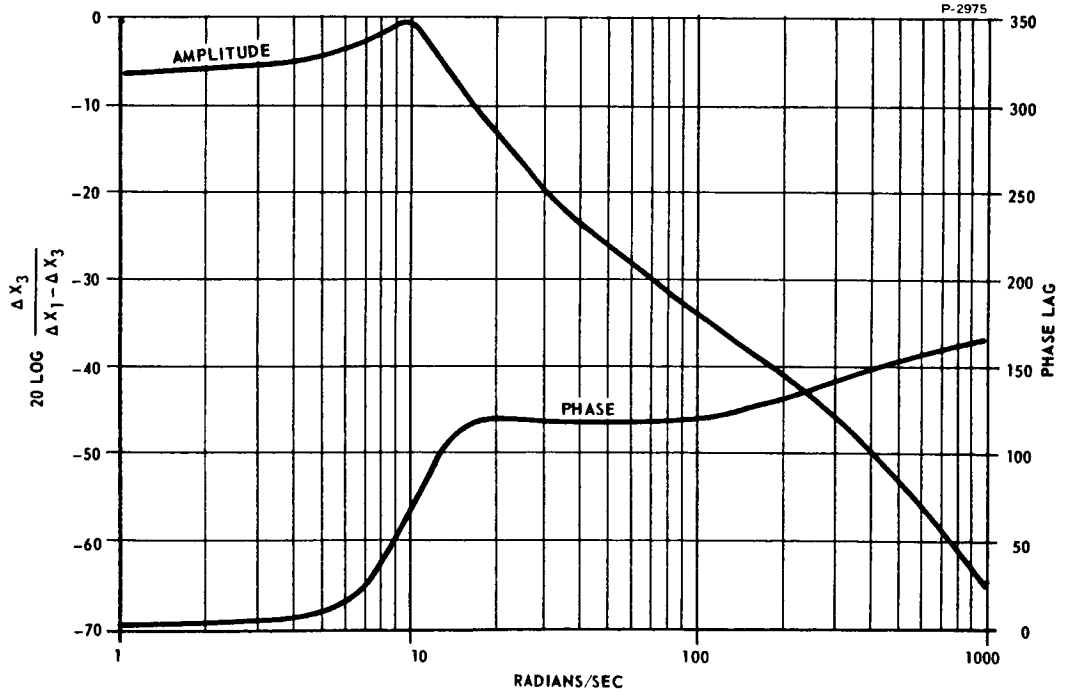

Figure 4-10 - Open Position Loop at 600 °R With Ideal Lead

If pure lead is available, the lead-plus-actuator response may be made equivalent to Figures 4-9 and 4-10, where ΔX_1 is the system command signal. The lead time constant is 0.044 sec at 100°R and 0.02 sec at 600°R, to simulate the effects of temperature on a lead generated by flueric elements.

Now the system can have a gain of 27 db ahead of the actuator with a crossover frequency of 40 radians/sec at 100°R. On a purely linearized basis, the closed loop response at 100°R would be as shown in Figure 4-11.

From equations (4-1) and (4-8), it can be seen that the gain at very low frequencies and the gain at ω_{NS} are equally affected by the negative pressure feedback coefficient. Thus raising pressure feedback to lower the gain at ωNS causes the low frequency gain of the actuator to be decreased also. This means that increases in negative pressure feedback allow increases in gain in the position loop ahead of the actuator, but these increases do not improve resolution since a

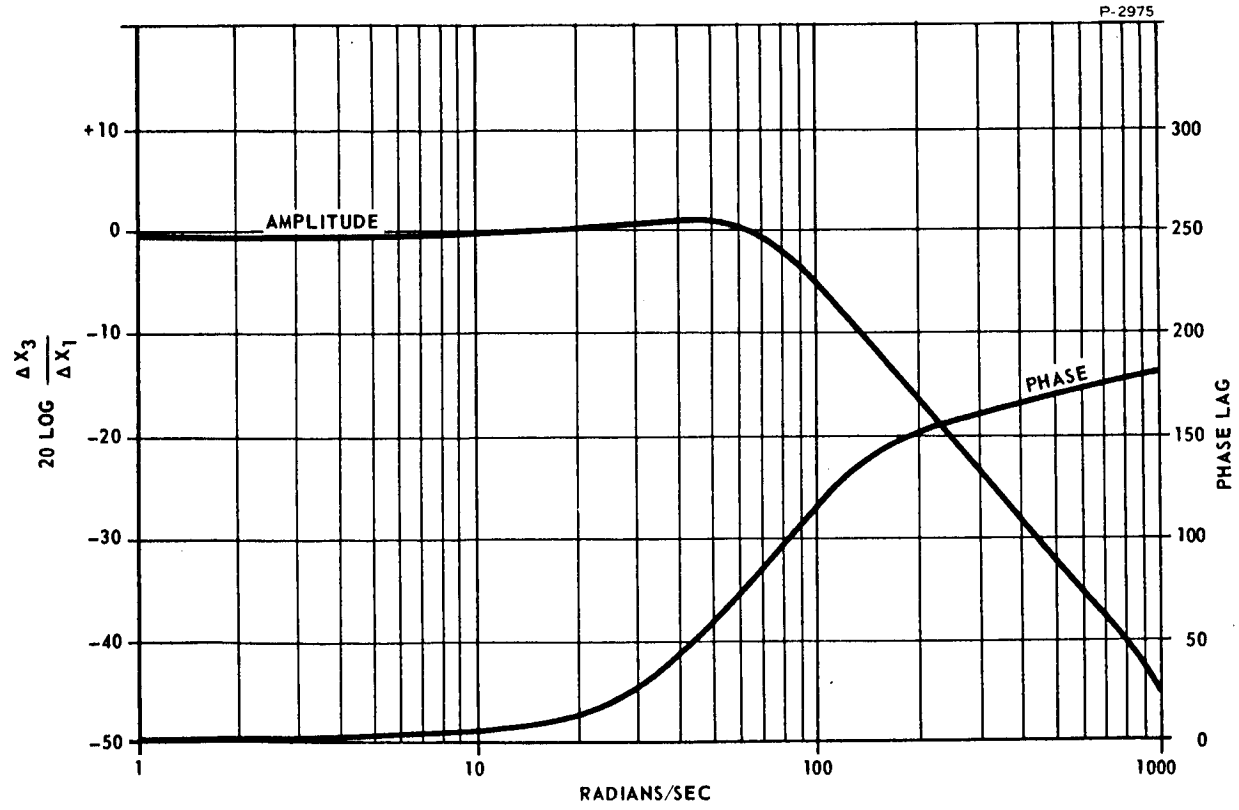

Figure 4-11 - Closed Loop With Ideal Lead at 100°R

larger pressure input to the power control valve is required to achieve a given pressure differential across the actuator piston. Calculation of resolution was not performed at this point in the analysis since the linearized model excluded friction. See Section 4.2 for further development of this problem.

Since the static resolution requirements are higher than the dynamic requirements, static gain must be increased by inserting a lag-lead in the position error compensation. This gives a lag-lead-lead circuit. It is not possible to mechanize a device with more leads than lags as this would require infinite gain at a sufficiently high frequency. The required compensation must then be lag-lead-lead-lag, to use position feedback only.

4.2 ACTUATION SYSTEM WITH POSITION AND LOAD PRESSURE FEEDBACK

The preliminary analysis reported in Section 4.1 established the need for lag-lead-lead-lag or "notch" compensation if actuator position and load pressure are the only feedbacks used. In this section, the feasibility of generating the required networks is explored and the performance limitations are presented. The results show that adequate performance is apparently not possible with only these feedbacks with circuits using state of the art fluid interaction devices.

4.2.1 Constraints of Circuits Using Fluid Interaction Devices

Scaling from test data currently available indicates a probable phase lag equivalent to a 0.001 second time constant for each vortex amplifier stage used, at 100°R supply gas temperature. The cumulative effects of these lags make it necessary to minimize the number of series stages.

Since it is desirable to minimize the volumes used to generate the compensation lag at the lowest frequency, the original scheme called for using positive feedback through a lag circuit to generate this lowest frequency lag and using negative feedback through a second lag circuit with a smaller time constant to generate lead. This concept requires creation of closed loops within the fluid interaction circuit package. To maintain stability during large transient, it is necessary in this system that each of these individual closed loops in itself be stable. The individual amplifier lags limit the open loop gain of each loop. This, in turn, sets a minimum value on the second lag time constant in the compensation notch circuit and therefore imposes a practical limit on the frequency span of the lead-lag portion of the compensation.

A detailed algebraic study also shows that as one increases the frequency span of the lead-lag portion of the compensation, the frequency span of the lag-lead is decreased. The limiting factor though is the amount of lead phase shift which can be generated. If this could be made sufficient, gain could be increased, increasing the amplitude crossover frequency of the open position loop, until the gain at 6 cps was sufficient to minimize the effects of friction.

4.2.2 Gain Required for Adequate Dynamic Response

The presence of friction in the system and the fact that the input signal amplitude for frequency response tests is specified make it

necessary to study the distribution of gains in the system. If the amplitude crossover frequency of the position loop is held to 40 radians/sec at 100°R, the gain in the fluid interaction circuits cannot exceed 22.39 psi/radian at that frequency. (Refer to Section 4.1.3). For a 2 degree input signal, the total differential pressure at ΔE_4 in Figure 4-4 will be only 0.78 psi. This input will produce a differential pressure in the actuator of

$$\Delta E_4 \left(\frac{A\ell}{K_f} \right) = \Delta P \qquad (4\text{-}9)$$

or

$$(0.78)(5.87) = 4.59 \text{ psid}$$

if the actuator does not move. This pressure is below the value required to overcome friction. With friction present, the ΔP required to produce a 2 degree output signal at 40 radians/sec is 55.8 psid for acceleration plus about 22 psid to overcome friction. Since this peak requirement occurs around zero velocity, the required ΔE_4 is about 13.2 psid.

If the output signal at 40 radians/sec has about 90 degree phase lag, the position error signal available is about 1.4 degrees or 0.0244 radians. The gain needed is then $\frac{13.2 \text{ psid}}{0.0244 \text{ radians}}$ or 540 $\frac{\text{psid}}{\text{radian}}$. This is 24.1 times the available gain, or an increase of 27.65 db. It would then be necessary to make the open loop gain crossover about 240 radians/sec at 100°R. This is possible with ideal lead (Figure 4-9). In practice, a final lag in the compensation at 800 radians/sec is sufficient to make the loop unstable. This is in the vicinity of or better than the best that can be currently mechanized for a lead-lag circuit using only flueric amplifiers and passive components.

When one then puts in a reasonable lag for the position error detector, realistic dynamics for the power control valve, and an allowance for the circuitry needed to generate the low frequency lag-lead compensation, it clearly becomes unrealistic to pursue this design concept further.

4.3 ACTUATION SYSTEM WITH RATE AND DYNAMIC LOAD PRESSURE FEEDBACK

To properly compensate the actuation system, a more effective means than a lead in the position error channel must be used. The use

of rate feedback was investigated and found to be effective. A system using rate feedback was designed and analyzed. The system was designed to limit its maximum velocity by having the rate signal override the position error signal when the maximum desired velocity was exceeded. In the analysis it was found that with the power control valve sized to meet all torque-speed requirements, except transient response, the transient response was less than desired. Valve size was increased to increase the torque available for acceleration and thereby reduce the time required for the actuator to accelerate to its maximum velocity. While increasing the valve size improved the transient response, it was not possible to meet the specified response at lower supply gas temperatures.

Increasing the valve size made it necessary to use dynamic load pressure feedback. This became necessary because the optimum negative load pressure feedback became sufficient to require either an unreasonable input bellows area or a large input pressure difference. Either of these choices would have increased control complexity and probably would have increased gas consumption.

An analysis using linear techniques which illustrates the effects of rate feedback is presented. Also presented is a discussion of the approach taken to incorporate rate feedback and velocity limiting in the system, and to incorporate frequency varient load pressure feedback in the power control valve. The analysis concludes with presentation of parameter values for the final design.

4.3.1 Effect of Rate Feedback

Figure 4-12 shows a simplified block diagram of the actuator and power control valve with rate feedback added.

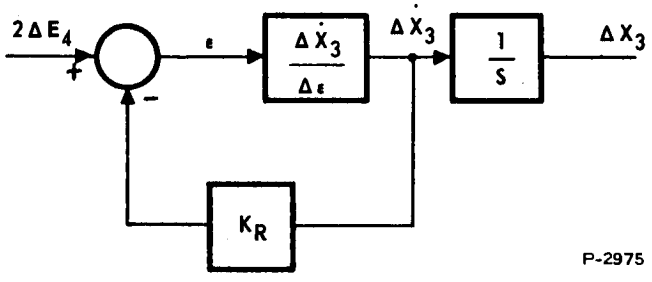

Figure 4-12 - Actuator with Rate Feedback

Since,

$$\frac{\Delta \dot{X}_3}{\Delta \epsilon} = \frac{(S)\ \Delta X_3}{\Delta E_4}\Bigg|_{\substack{\text{pressure} \\ \text{feedback}}} = \frac{G\,(S)}{C_1 S^3 + C_2 S^2 + C_3 S + 1} \tag{4-10}$$

where

$$G = \frac{A \ell K_V K_5 \frac{\partial P}{\partial Q} \frac{dm}{K_{10}}}{1 + \frac{\partial P}{\partial Q} K_f K_V K_5} \tag{4-11}$$

$$C_1 = \frac{T_c J}{K_{10}\left(1 + \frac{\partial P}{\partial Q} K_f K_V K_5\right)} \tag{4-12}$$

$$C_2 = \frac{J}{K_{10}} \tag{4-13}$$

$$C_3 = \frac{T_c + \frac{dm^2 \frac{\partial P}{\partial Q}}{K_{10}}}{\left(1 + \frac{\partial P}{\partial Q} K_f K_V K_5\right)} \tag{4-14}$$

Then the equation for motion becomes

$$\frac{\Delta \dot{X}_3}{\Delta E_4} = \frac{G(S)}{C_1 S^3 + C_2 S^2 + C_3 S + 1 + G K_R S} \tag{4-15}$$

Therefore,

$$\frac{\Delta X_3}{\Delta E_4}_{\text{rate feedback}} = \frac{G}{C_1 S^3 + C_2 S^2 + C_4 S + 1} \tag{4-16}$$

where

$$C_4 = C_3 + G K_R$$

or

$$C_4 = \frac{T_c + \dfrac{dm^2 \dfrac{\partial P}{\partial Q}}{K_{10}} + A\ell K_V K_5 \dfrac{\partial P}{\partial Q} \dfrac{dm}{K_{10}} K_R}{1 + \dfrac{\partial P}{\partial Q} K_f K_V K_5} \qquad (4\text{-}17)$$

In effect, the "S" coefficient in the denominator has been made much larger by the addition of $G K_R$ to the previous coefficient, C_3. The 180 degree phase shift point is still the point where the S^3 and S terms are equal in magnitude and opposite in sign; i.e.,

$$C_4 = C_1 \omega^2$$

$$\omega^2 = \frac{C_4}{C_1}$$

$$\omega^2 = \frac{T_c + \dfrac{dm^2 \dfrac{\partial P}{\partial Q}}{K_{10}} + A\ell K_V K_5 \dfrac{\partial P}{\partial Q} \dfrac{dm}{K_{10}} K_R}{\dfrac{T_c J}{K_{10}}}$$

$$\omega^2 = \frac{T_c K_{10} + dm^2 \dfrac{\partial P}{\partial Q} + A\ell K_V K_5 \dfrac{\partial P}{\partial Q} dm K_R}{T_c J}$$

Thus, substituting

$$T_c = \frac{V}{2 \gamma P} (\partial P / \partial Q)$$

into the equation gives

$$\omega^2 = \frac{K_{10}}{J} + \frac{2 \gamma P dm^2}{J V} + \frac{2 \gamma P A\ell K_V K_5 dm K_R}{J V} . \qquad (4\text{-}18)$$

Therefore the frequency at which the 180 degree point occurs has been moved to a higher value. Each time this happens, the amplitude of $\Delta X_3/\Delta E_4$ at the 180 degree point changes in proportion to $C_2(j\omega)^2 + 1$, the real part of the denominator with S replaced by $j\omega$. Since K_{10} is 24.29 lb-in/radian and J is 0.24 lb-in-sec^2, the S^2 term is dominant for ω^2 greater than 100. Thus, moving ω from 40 to 80 radians causes the amplitude of $\Delta X_3/\Delta E_4$ for frequencies near 40 radians/sec to be lowered 4 to 1 or -12 db, allowing the position error gain (ahead of ΔE_4) to be increased proportionately. Observing previous dynamic results, the position error gain at the position loop crossover frequency needs to be raised about 20 to 1.

This conclusion can be verified very simply by the dynamic position error required to overcome friction, which was about 10 degrees in the position-feedback-only case. The dynamic specifications call for the frequency response at ±2 degrees amplitude. Dynamic error must therefore be less than 2 degrees in the frequency range where the amplitude response is specified. While the nonlinearity actually present is caused by coulomb friction plus stiction (the difference between static friction and friction at a finite speed), the waveforms produced are very similar to those caused by the much simpler nonlinearity "deadband." To get an idea of the tolerable dynamic error level, we note that the output of a circuit containing deadband is down 32 percent or about 3.3 db when the magnitude of the deadband is about 0.25 of the amplitude of the input signal. This gives an allowable dynamic error of 0.50 degree to get amplitude response within system specifications. Dividing the measured dynamic error of 10 degrees previously required to overcome friction by the allowable 0.50 degree value gives the approximate desired 20 to 1 increase in gain at the mid-frequency range.

A 20 to 1 gain increase in the frequency range around 40 radians/sec, means that the frequency at which the actuator has a 180 degree phase lag, ω_{NS} must be increased enough to allow about a 26 db gain increase relative to the position-feedback-only system. A value of 24 db will result if ω_{NS} is made 160 radians per second. (This value is adequate for linearized results when an analog study is also being performed.) Then,

$$160^2 = \frac{K_{10}}{J} + \frac{dm^2\, 2\gamma P}{J V} + \frac{2\gamma P A K_V K_5\, dm\, K_R}{J V}$$

and upon substituting numerical values into this equation and solving for K_R,

$$K_R = 4.07 \frac{\text{lb-sec}}{\text{in}^2} . \qquad (4\text{-}19)$$

This demonstrates the potential dynamic performance benefits of rate feedback and provides a starting place for an analog study.

The static resolution requirement, however, is still not met, since there is still a 0.5 degree position error required to start the actuator versus the desired 0.2 degree value; but, potentially there are several ways of getting the increased static gain. For example, a 4 to 1 frequency span lag-lead circuit in the position error channel would be more than adequate. (Since the span would be 2 octaves, the static gain would be raised 12 db or 4 to 1 over the high frequency gain.)

4.3.2 Incorporation of Rate Feedback into System

The rate feedback scheme must consider all of the practical constraints on the system:

(1) Rate must have a maximum limit, nominally 300 deg/sec.

(2) The rate signal must be developed without using any mechanical sensor more complex than a flapper valve; a flyball governor, for example, was ruled out.

(3) The rate limit must remain substantially the same at all temperatures to allow the best possible transient response to steps.

(4) Gas flow (weight) for control purposes must be minimized.

From these constraints, it follows that a limited position error signal must be obtained, since the position error signal is the rate command signal. This requirement led to the evolution of a position summing circuit, in place of the separate input position and feedback position transducers once considered. At first glance the original separate flapper-nozzle circuits seem to perform the same function, since the signals were previously subtracted by being fed into a summing amplifier in a manner which causes each to cancel some or all of the effect of the other. Unfortunately, if the vortex amplifier gain is made

high enough to cause saturation for a position error of a few degrees, it is possible to set up a situation where the same minimum pressure output signal is obtained for either a large positive or a large negative position error signal. Because of bias problems, this situation can be shifted from one stage to another; but, it can be eliminated only by revising the position error forming circuit. The circuit shown in Figure 3-6 cannot go into a false output sign condition regardless of the magnitude of the instantaneous error signal. The combined gain of vortex amplifiers V_1 and V_2 times the gain of vortex amplifiers V_3 and V_4 is capable of being set high enough to cause the output pressures of V_3 and V_4 to saturate for small plus or minus position error signals. The magnitude of the position error desired at saturation was determined during the analog study and is reflected in the component specifications, Section 4.3.1 The rate signal must be generated at the same pressure levels as the position error signal to allow signal comparison. The signal is, therefore, developed by adding a position signal and a lagged position signal of opposite sign. In effect each side of the push-pull circuit can be approximately represented by:

$$\Delta X_3 \left(K - \frac{K}{T S + 1} \right) = \Delta X_3 \frac{(K T) S}{T S + 1} \qquad (4\text{-}20)$$

where ΔX_3 is the output shaft rotation in radians. The rate signal is therefore not pure but accompanied by a lag. There is a practical minimum lag to allow enough signal to be generated. This minimum lag is about 0.01 second and is provided by tank T_2 (pneumatic capacitance) in conjunction with the pneumatic resistance of the inlet and outlet orifices to this volume.

To avoid changes in the rate limit as a function of temperature, either the position error limits must be adjusted or the rate signal must be made invarient with temperature. The method which appears most feasible is that of adjusting the volume of T_2 as the temperature changes, thereby keeping the effective lag constant with temperature.

It is necessary to shift the point in the system where rate is summed with position error to some point ahead of E_4 to allow compensation to be added to the rate loop. As a minimum, lead-lag must be added to compensate for the lag in the rate signal generator.

4.3.3 Dynamic Load Pressure Feedback

Next, a method for obtaining the required static resolution must be established. One method would be to use a lag-lead network in the position error channel. Since only a 4 to 1 gain increase at static conditions is needed, it could be generated by using different gains for each side of the push-pull position error circuit and lagging one side. Unfortunately, any lag in getting position error to the saturation value adversely affects the large step performance. In addition, the analog study revealed that the power control valve flow and pressure feedback values had to be increased to obtain the system performance specified for large signal inputs. This created a problem with the magnitude of the pressure differential needed at point ΔE_4 in the system. To reduce the required differential, which in turn has a substantial effect on control operating pressures and therefore on the weight of the gas used for control, it was decided to incorporate a lagged positive pressure feedback to cancel part of the negative pressure feedback. This amounts to incorporating a lag-lead circuit inside the rate loop. It could be incorporated in other ways, but the way illustrated is the most direct and efficient. If a fluid state power control valve is later used in place of the flapper-nozzle valve, it appears that it would be practical to incorporate pressure feedback in a manner analogous to the feedback in the present mechanical flapper. The driving gas flow for the power valve would then be obtained from the output amplifiers, V_{11} and V_{12}, and would be at least partially compensated by reduced vent flow from these stages so that the weight of the gas used for both computation and control would remain nearly the same.

Lag in the position error channel is still needed for stability. This lag cancels the effects of the lead present in the closed rate loop response because of the rate sensor lag. It also affects the ability of the position loop to properly damp, following an input signal which is large enough to cause saturation. A lag can be found which is large enough to obtain small signal stability but not large enough to obtain properly damped system response for large signal inputs. The value, therefore, was defined during the analog simulation.

4.3.4 Value of Parameters of Final Design

As a result of these complicated and interacting constraints, the final system simulated was as shown in Figure 4-13. The portions of

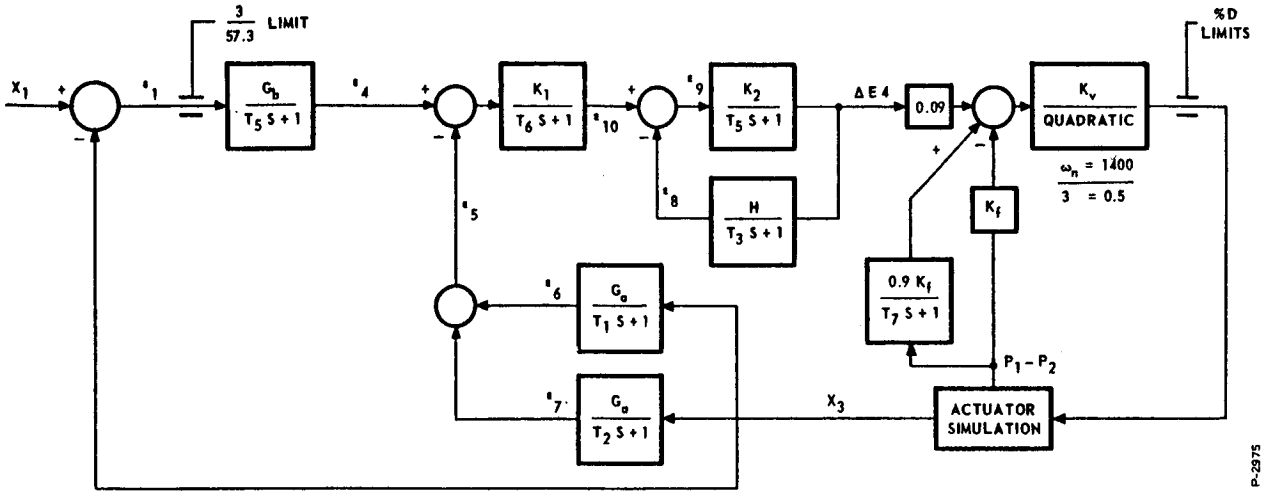

Figure 4-13 - Block Diagram of Actuation System With Position and Rate Feedback

the actuator simulation not detailed remained as shown in Appendix VI. The vortex amplifiers were not simulated in detail but rather by lumped time constants and gains very much like those indicated on the block diagram. After considerable experimentation, a set of values was chosen which seemed to best meet the sometimes conflicting demands of static and dynamic resolution, frequency response, and relative invariance of response over the temperature range. These values are listed in Table 4-2.

Table 4-2 - Parameter Values Used in the Performance Evaluation of Control System with Rate Feedback

Definitions	Symbol	Value at Temperature Indicated				Remarks
		Unit	100°R	190°R	600°R	
Rate channel gain	G_A	$\frac{psi}{rad}$	194	194	194	Gains were assumed to remain constant with temperature.
Position error channel gain	G_b	$\frac{psi}{rad}$	194	194	194	
Summer circuit gain	K_1	$\frac{psi}{psi}$	3	3	3	
Compensation forward gain	K_2	$\frac{psi}{psi}$	16	16	16	
Compensation feedback gain	H	$\frac{psi}{psi}$	0.5	0.5	0.5	
Lag of "fast" side of rate sensor	T_1	sec	0.001	0.001	0.001	This lag will actually vary with temperature but was held constant to keep $(T_2 - T_1)$ constant.
Lag of "slow" side of rate sensor	T_2	sec	0.011	0.011	0.011	This rate sensor lag is to be compensated to keep $(T_2 - T_1)$ invariable with temperature.
Compensation feedback lag	T_3	sec	0.0176	0.0142	0.008	For T_3 through T_7 no temperature compensation assumed.
Compensation forward lag	T_4	sec	0.001	0.00056	0.00045	
Position error channel lag	T_5	sec	0.044	0.0355	0.020	
Summer stage lag	T_6	sec	0.001	0.00056	0.00045	
Positive pressure feedback lag	T_7	sec	0.066	0.0533	0.03	
Negative pressure feedback gain	K_f	$\frac{lb\text{-}in}{psid}$	0.0384	0.0384	0.0384	
Power control valve flapper gain	K_v	% deflection/lb-in	200	200	200	This is essentially set by flapper valve spring rate.
Valve scale-up factor			1.8	1.8	1.8	Represents flow increase factor compared to valve which meets frequency response torque-speed requirements.
Position error limits			± 3°	± 3°	± 3°	
% Deflection of power control valve flapper	%D limits	%	± 95	± 95	± 95	
Load-plus-actuator friction	Friction	lb-in	max.	max.	max.	Maximum equals 47 lb-in static and 40 lb-in dynamic.
Supply pressure	P_s	psia	215	215	215	Unless otherwise noted on results.
Exhaust pressure	P_v	psia	50	50	50	

P-2975

4.4 DYNAMIC CHARACTERISTICS OF FINAL DESIGN

After a set of parameter values was determined which appeared to meet specifications at all temperatures, it was necessary to verify these values at 190°F and to check the 90 degree phase lag point and response of the system to 18 degree steps in input at 100°R and 600°R. The parameter values of Table 4-2 were used. These values reflect expected parameter value changes with temperature. There may be some additional small effects on gain, particularly at 100°R where the gas properties are considerably altered, but it is believed that all major effects have been accurately simulated. The dynamic characteristics of the simulated system are summarized and compared with the specified characteristics in Table 4-3.

The simulated system met all specifications with the exception of the response time required to make an 18 degree step.

4.4.1 Frequency Response

Bode plots of the actuation system response at 100°R, 190°R, and 600°R are shown in Figures 4-14, 4-15, and 4-16 respectively. Samples of the strip chart data taken in the frequency response evaluation are shown in Figure 4-17.

4.4.2 Dynamic Resolution

The static resolution was established for the 190°R supply gas case only, and a plot of position output versus input signal is shown in Figure 4-18. The dynamic resolution over the specified range of supply gas temperatures should be approximately the same.

4.4.3 Transient Response

Samples of the strip chart data taken when evaluating the transient response of the actuation system to 18°, 2.86°, and 0.56° step input signals are shown in Figures 4-19, 4-20, and 4-21, respectively.

The transient response deserves special comment because it is by far the most difficult part of the dynamic response to meet and imposes a considerable burden on the system gas flow weight, even to meet the values of Table 4-5.

At a rate of 300 degrees per second, the actuator is moving only 0.3 degree per millisecond. The required 62.5 percent of 18 degrees is 11.25 degrees and would take 37.5 milliseconds at this slewing rate.

Table 4-3 - Summary of Dynamic Characteristics of Final Performance Evaluation

SPECIFICATION ITEM	SPECIFICATION	RESULTS AT TEMPERATURES LISTED			UNITS	REMARKS
		100°R	150°R	600°R		
Frequency response at ±2° input	(1)Phase shift at 6 cps no more than 90°.	83	65	54	degrees	Response at any one temperature can be improved at the expense of that at the others.
	(2)Phase shift at 12 cps no more than 180°.	157	157	85	degrees	
	(3)Output Shaft amplitude variation from 0 to 8 cps less than ± 3 db	+3 -2.5	+2.2 -2.0	+1.6 -0	db	
Maximum dynamic Resolution at 3 deg/sec	± 0.5°	approx. ± 0.175	+0.175 ± 0.175	approx. ± 0.175	degrees	Maximum -0.5 deviation of minus to plus turnaround. Maximum + 0.42 on plus to minus turnaround.
Maximum slewing velocity	± 300 °/sec	-315 +258	-286 +275	-328 +328	degrees/ sec	Controlled by position error limits Recorded values from 18° step data These are peak values
Transient response to 18° step input	(1)Rise time to 62.5% of command 0.055 sec.	-0.070 +0.084	-0.068 +0.080	-0.051 +0.060	sec	Signs refer to step direction.
	(2)Settling time to within 0.9% of command 0.15 sec.	-0.204 +0.230	-0.188 +0.212	-0.136 +0.160	sec	
	(3)Allowable overshoot 6°	-4.00 +1.15	-2.3 +1.72	-1.15 +1.15	degrees	

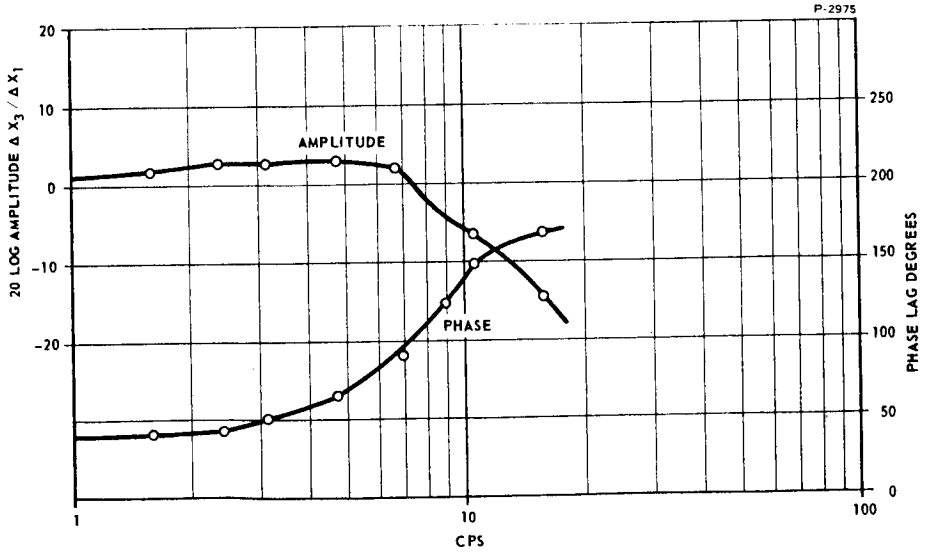

Figure 4-14 - Bode Plot of Actuation System Response at 100°R

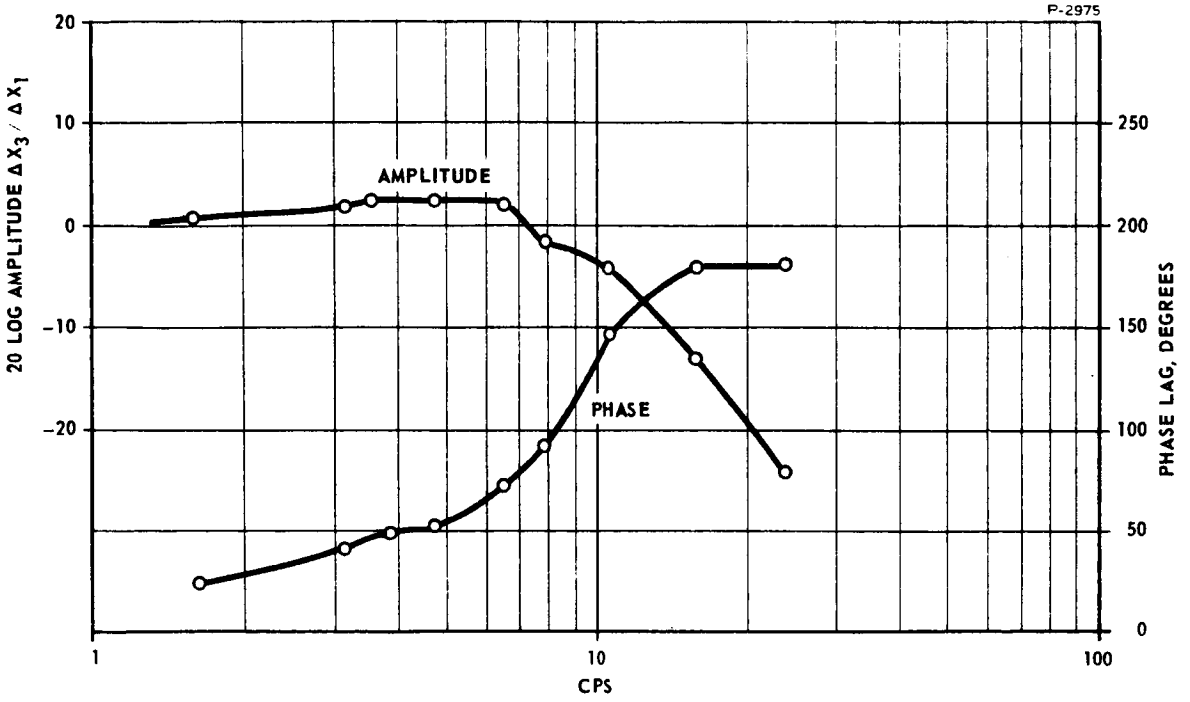

Figure 4-15 - Bode Plot of Actuation System Response at 190°R

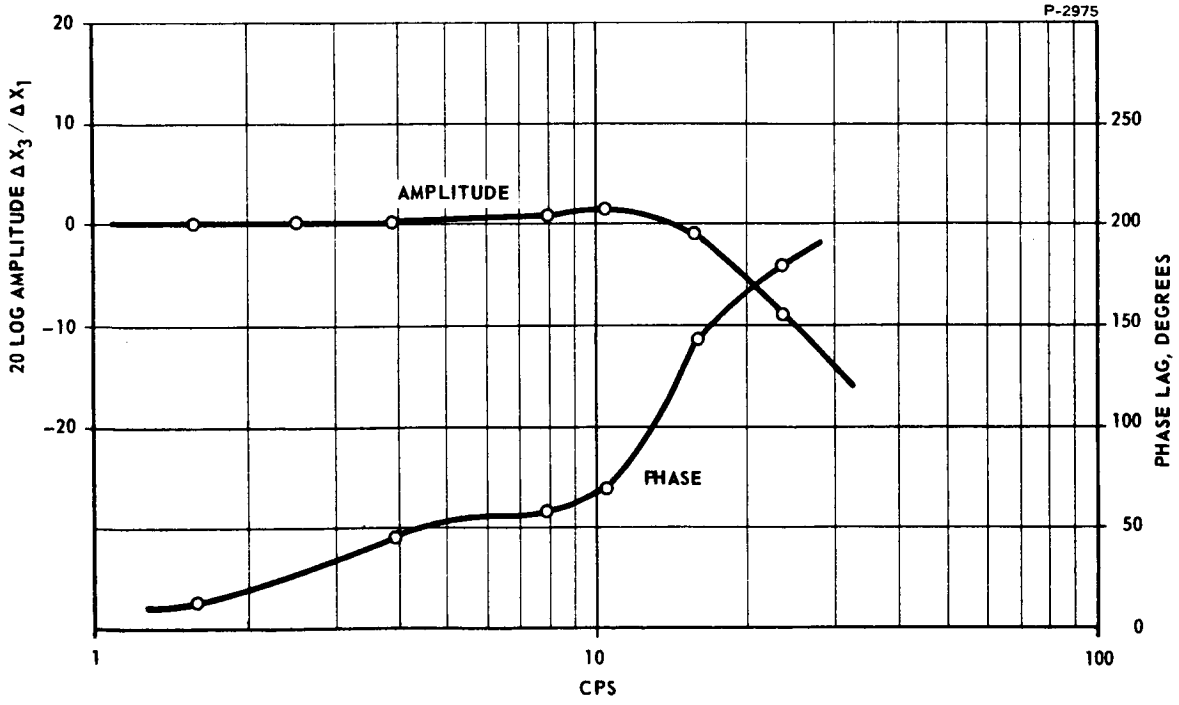

Figure 4-16 - Bode Plot of Actuation System Response at 600°R

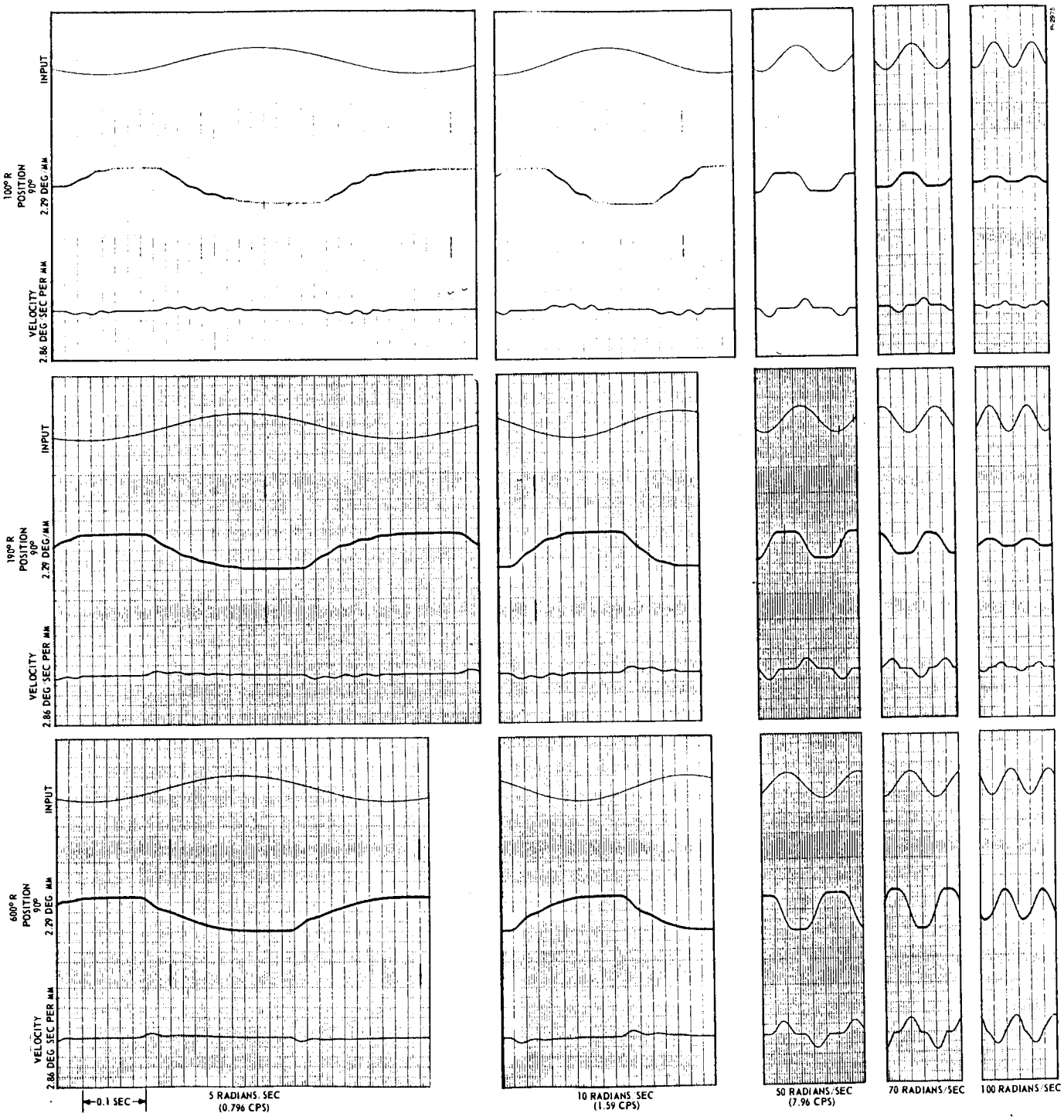

Figure 4-17 - Samples of Frequency Response of Actuator

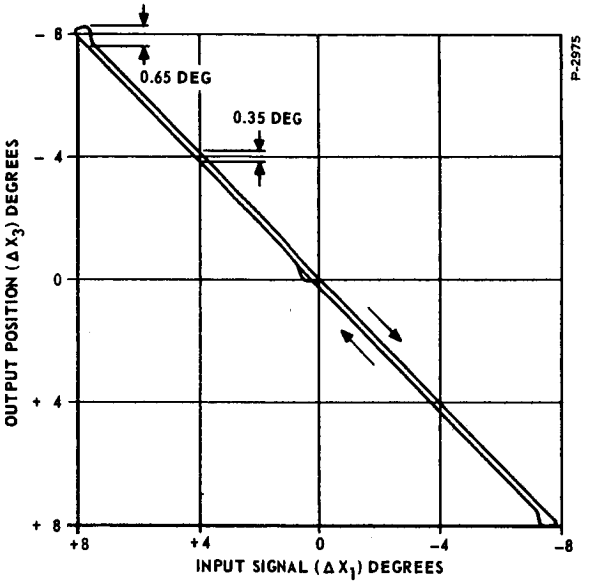

Figure 4-18 - Response of Actuation System at 190°R to 3 deg/sec Position Ramp

In the simulation the flapper of the power control valve reached 95 percent of its stroke in the first 5 milliseconds following the application of a step input to the input transducer, and is providing very superior performance. (The analog simulation contains no lags in X_1.) The actuator P_1 and P_2 chambers must now be charged with gas. If the volume lags at a particular temperature are only 0.010 second and the volumes are assumed to start charging at time zero, which is generous since the valve is not fully open yet, the value of $(P_1 - P_2)$ available at time 0.010 second is 63.2 percent of the available head. The maximum differential pressure available is 155 psi, of which 34 psi is already in use at mid-stroke just to hold the scram spring. Therefore of the remaining 121 psi of pressure differential, not over 76.5 psi will be available in 0.010 second. Of this, 22 psid is required to overcome breakout friction (after which friction decreases slightly). Then an approximate average torque during the first 0.010 second is

$$\frac{(2.2 \text{ in}^3/\text{rad})\,(76.5 - 22)}{2} = 60 \text{ lb-in}$$

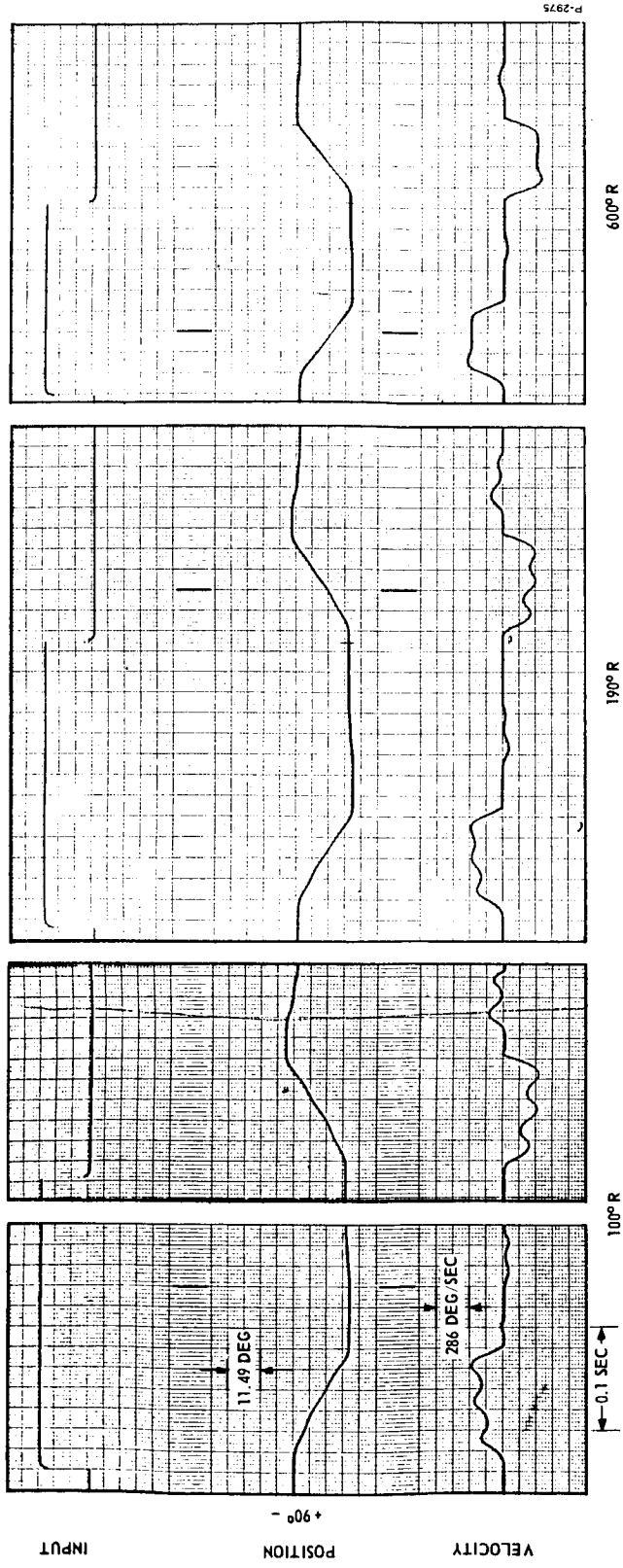

Figure 4-19 - 19 degree Step Response

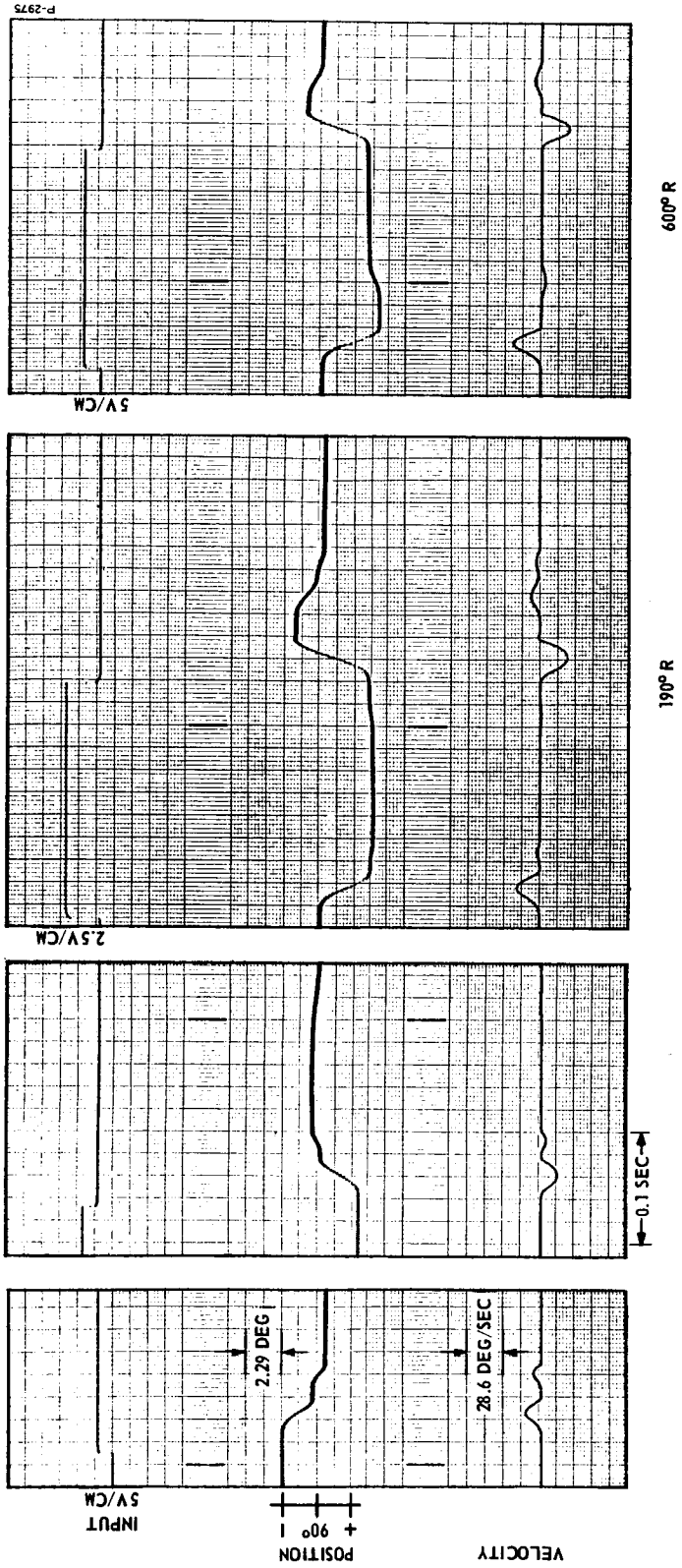

Figure 4-20 - 2.86 degree Step Response

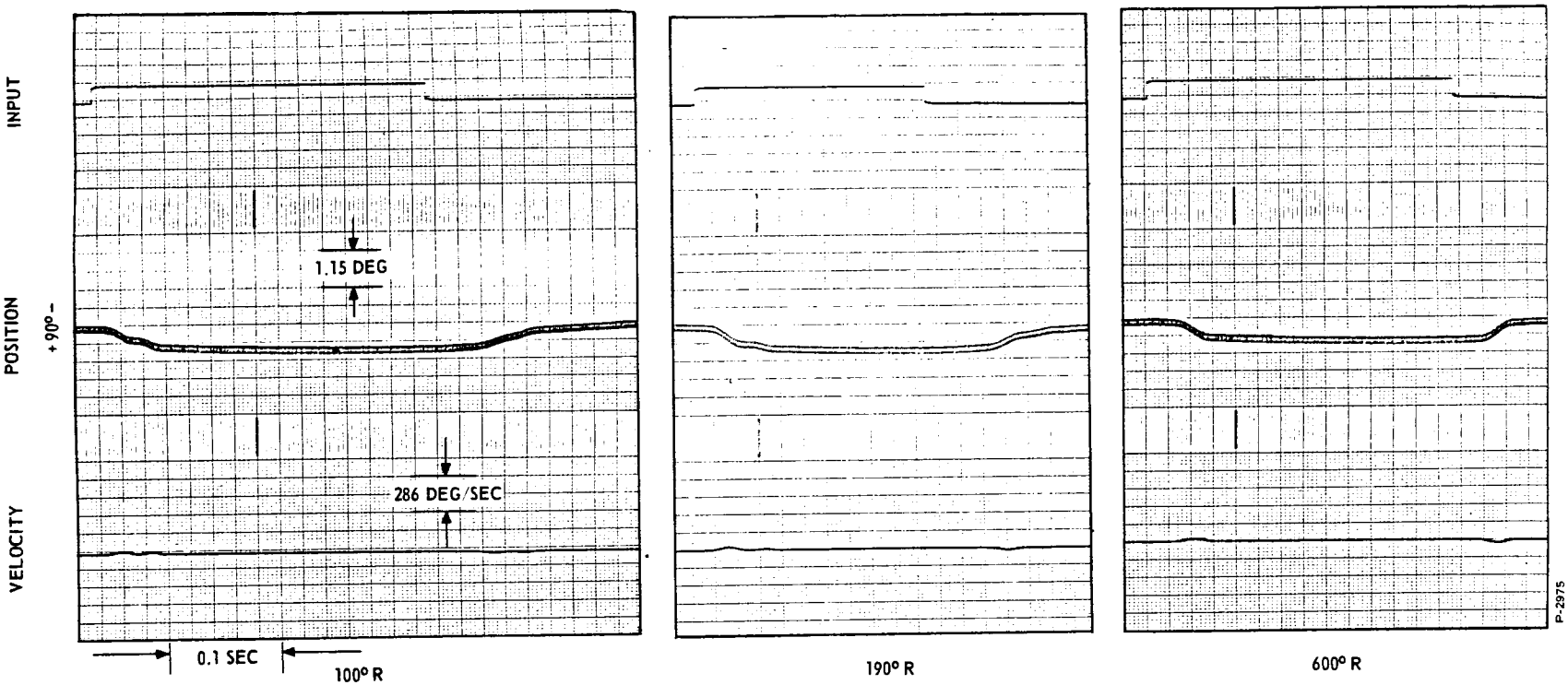

Figure 4-21 - 0.56 degree Step Response

This torque acting for 0.010 second on a polar moment of inertia of 0.24 lb-in-sec^2 produces a velocity of 2.50 radians/second. The rotation is then 0.0125 radian or only 0.715 degrees in the first 0.010 second, going in the positive direction from mid-stroke, and under very favorable assumptions. In the next 0.010 second period, the available differential could possibly rise to 82 psid, so the torque could average 170 lb-in. This would increase velocity by 7 radians per second if it were not for the velocity limit. Thus the actuator could under ideal conditions, reach the limit velocity in slightly over 0.010 milliseconds and therefore under the conditions stated should be able to make 11.25 degrees in about 47 to 50 milliseconds.

One of the stated conditions was volume lags in the piston actuator of 0.010 second each. With a valve which satisfies the torque-speed requirements for all other dynamic conditions, the lags at 100°R are about 0.1 second. At 600°R they are about 0.045 second. Increased valve quiescent flow (1.8 times nominal) brings these lags down to about 0.025 second at mid-stroke at 600°R. Beyond that amount of valve scaleup, the other assumptions such as the instant opening of the flapper valve begin to be important and large flows are sacrificed to trim milliseconds off the step response. If the specified response is to be met, friction reduction, higher available pressure differential, spring preload reduction and possibly unbalanced piston sizes to help hold the spring preload would all help. Otherwise flow must be sacrified to get a very high acceleration capability in the actuator.

Unfortunately, there is no simple answer to this problem. A spool valve is not necessarily the answer, since in this case the resistance of one land takes the place of two orifice resistances effectively in parallel on one side of a flapper valve system. Accordingly, a spool valve has to have a high maximum flow area to get low volume time constants. If the spool valve could be manufactured perfectly enough, it could result in less actuator gas consumption. In practice, the necessary clearances to assure operation over the temperature range would reduce its flow advantage and the intermittent changes in total actuator flow would increase transient temperature changes in the actuator with possible adverse effects on the pistons.

4.4.4 Dynamic Stiffness

Dynamic loading errors can best be assessed on the analog computer with friction simulated. It has been estimated that vibration loads along the axis of the piston cause 1.13 lb-in of peak load torque

per g. Thus checks with simulated 4g and 20g loads tell us both the vibration sensitivity and the sensitivity to dynamic torque loads from any other cause. The analog results show the degrees/g disturbance to be -38.8 db at the worst. The frequency range of 1.5 cps to 15.9 cps was checked with a simulated ± 20g signal at a simulated temperature of 190 degrees. The worst case was at 1.59 cps and amounts only to 0.23 degree peak-to-peak motion.

When a vibration signal is first applied, the actuator simulation would sometimes show a transient shift of as much as 0.3 degree, not actually following the input, but apparently seeking a new condition of balance. After 0.2 to 0.5 second, this shift has almost completely disappeared and if the actuator is following at all, it is doing so around the original mean position. This phenomenon is due to the fact that the volume lags of P_1 and P_2 in the piston actuator are not matched and are variable. Therefore sine wave loads do not result in pure sine wave P_1 and P_2 variations so the average pressures shift in value until the loop can make corrections.

The theoretical inverse stiffness without friction is shown in Figure 4-22 for the 100°R case, which is the worst case. The worst point, at 10.5 cps, is equivalent to 1740 lb-in per radian. Then without friction a 10 cps, 20 g signal could cause a 0.745 degree deflection of the actuator. As shown by the analog study, actual results with friction are more favorable.

4.5 STATIC CHARACTERISTICS OF FINAL DESIGN

The simulated actuation system met all the static specifications. The results of the static evaluation are shown in Table 4-4 and compared to the specified values.

4.5.1 Static Resolution

The static resolution was evaluted using 0.6 deg/sec ramp input signal. The resulting plot of output position versus input signal is shown in Figure 4-23.

4.5.2 Static Stiffness and Static Position Offsets

The static stiffness of the servo actuator loop is calculated as follows:

(a) External torque (Δ L) times $\dfrac{\Delta (P_1 - P_2)}{\Delta L}$

Table 4-4 - Summary of Static Characteristics of Final Performance Evaluation

SPECIFICATION ITEM	SPECIFICATION	RESULTS AT TEMPERATURES LISTED			UNITS	REMARKS
		100°R	150°R	600°R		
Travel	0° to 180°: ±1° max. 150° to 165°: ±1°: working	-- --	-- --	-- --		These are mechanical limits not simulated for performance study
Static resolution	±0.2°	same	±0.1	same	degrees	Tested with 0.6 deg/sec ramp
Static linearity of output shaft position to electrical command	-4% of full travel (spec) ±1% of full travel goal					See Figure 4-24 and text for discussion of contributing factors

P-2975

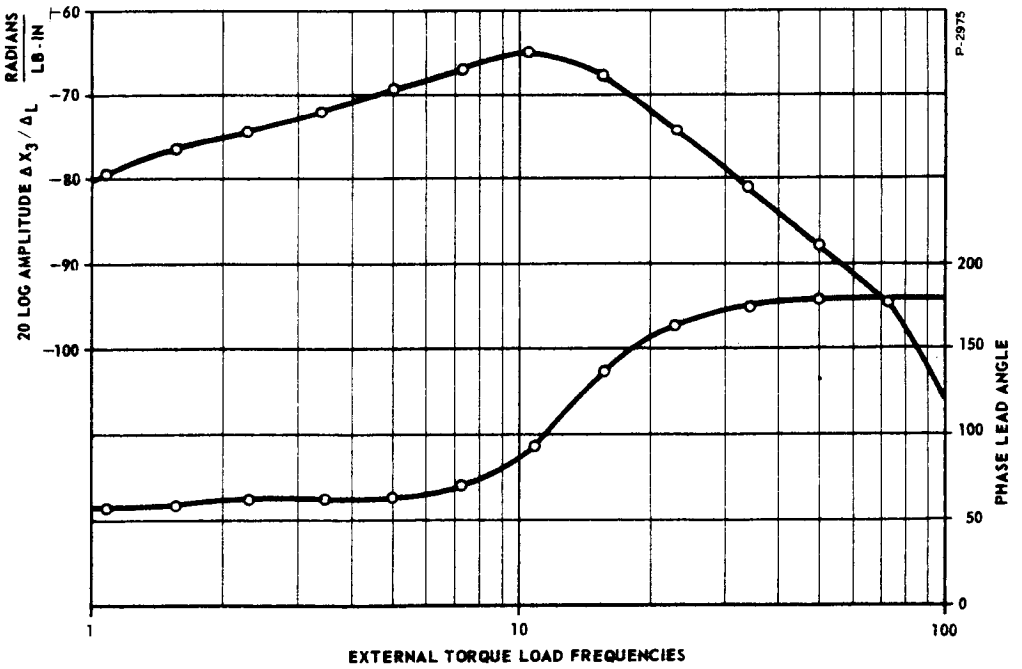

Figure 4-22 - Dynamic Output Stiffness Versus Frequency

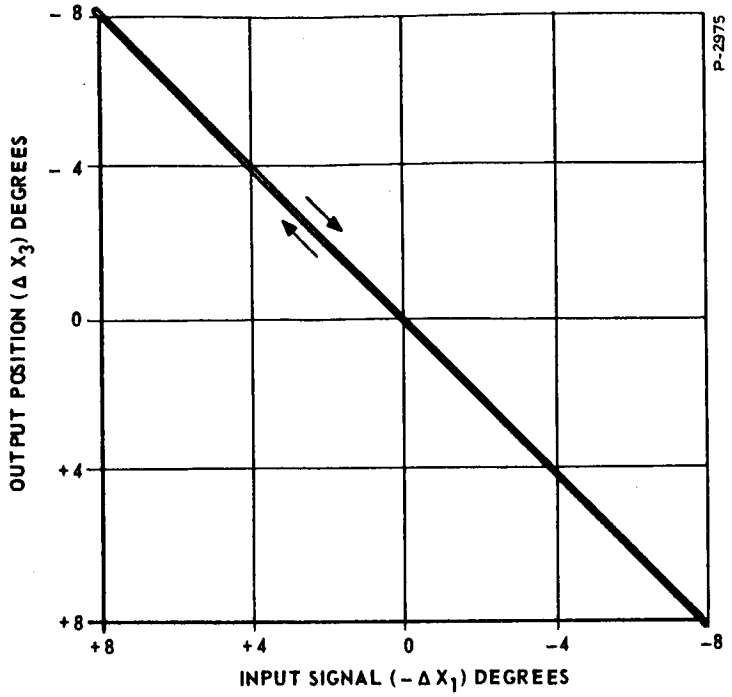

Figure 4-23 - Response of Actuation System at 190°R to 0.6 deg/sec Position Ramp

equals $\Delta (P_1 - P_2)$

$$\text{and } \frac{\Delta (P_1 - P_2)}{\Delta L} = \frac{1}{\text{Actuator volume displacement per radian}} = \frac{1}{2.2} = 0.455 \text{ radian/in}^3 \quad (4\text{-}20)$$

$$\text{(b) } \Delta (P_1 - P_2)(K_f - 0.9\, K_f) = \text{Net torque on the power control valve flapper due to pressure feedback} \quad (4\text{-}21)$$

$$K_f - 0.9\, K_f = 0.00383 \frac{\text{lb-in}}{\text{psid}}$$

using the final value of K_f from Table 4-3.

(c) $\dfrac{\Delta (P_1 - P_2)}{(\partial P/\partial Q)\,(K_s)\,(K_v)}$ = Torque on the power control valve flapper due to deflection against a spring necessary to obtain the desired pressure differential (4-22)

where

$K_5 = \Delta Q/\Delta\%$ deflection

$$\frac{1}{\partial P/\partial Q\,(K_5)\,(K_v)} = \frac{1}{(3.48)\,(0.52)\,(200)} = 0.00276 \text{ in}^3$$

(d) Total input torque to the power control valve flapper is then:

$\Delta (P_1 - P_2)\,(0.00383 + 0.00276)$ = Valve input torque (4-23)

or substituting for $(P_1 - P_2)$

$\Delta L\,(0.455)\,(0.00659) = \Delta L\,(0.003)$ = Valve input torque, lb-in (4-24)

(e) This torque can be converted to position error by:

$$\frac{\text{Valve input torque}}{(G_b)\,(K_1)\,\dfrac{K_2}{1 + K_2 H}\,(A\ell)} = \frac{\text{Valve input torque}}{93}, \text{ radian} \quad (4\text{-}24)$$

and then substituting for valve input torque:

$\Delta L \dfrac{(0.003)}{93} = \Delta L\,(32.2 \times 10^{-6})$ = Radians position error per lb-in of external torque

Then $(32.2)\ 10^{-6}\ \dfrac{\text{radians}}{\text{lb-in}}$ is the inverse static stiffness and the static stiffness is:

31,000 lb-in/radian or 540 lb-in/deg

From this figure, it is then possible to calculate static position offsets due to spring load, and if friction is considered to contribute a position uncertainty depending on the final direction of motion before

stopping, a zone of uncertainty can also be calculated. For 32 lb-in static friction in the load plus 15 lb-in actuator friction, the "uncertainty" zone is:

$(32 + 15)(0.00185) = \pm 0.087$ degrees, centered on the spring

line. This is actually far in excess of what a real system would do, as noise and vibration both tend to make the actuator approach the offset line dependent on spring load only.

The offset is -0.21 degree at $90°$

-0.256 degree at $165°$

-0.1295 degree at $15°$

due to spring preload. Thus if the system is adjusted to give -0.1295 degree offset at 15 degrees, the maximum static deviation from the hypothetical gain curve would be -0.343 degree, which means the input has to go more positive to get 180 degrees position. The maximum amount is only 0.02 milliamperes, too small to plot clearly.

The static accuracy therefore depends primarily on torque motor linearity and position transducer cam accuracy. The torque motor linearity from published data is $\pm 2\%$. Figure 4-24 then shows the envelope of possible positions versus current, making no allowance for soft stop action. Repeatability and matching between actuators will definitely be better than absolute position linearity versus input current.

4.6 SIGNAL TO NOISE RATIO

Since a certain amount of noise inevitably appears in the servo loop, it is necessary to examine the extent of performance degradation with noise level.

The noise spectrum used for analog tests was chosen arbitrarily but with the intent that the servo bandpass would be included so that degradation would definitely occur at a sufficiently high level of input. The noise used had an approximately constant power density spectrum from 1 to 200 cps, taking into consideration the time scale of the analog simulation. Since the servo bandwidth is from zero frequency to about 10 cps, at least, the noise signal does contain frequencies which will propagate through the servo loop. Frequencies below 1 cps are low enough to allow the loop to follow them and therefore are more in the nature of drift or offset rather than noise.

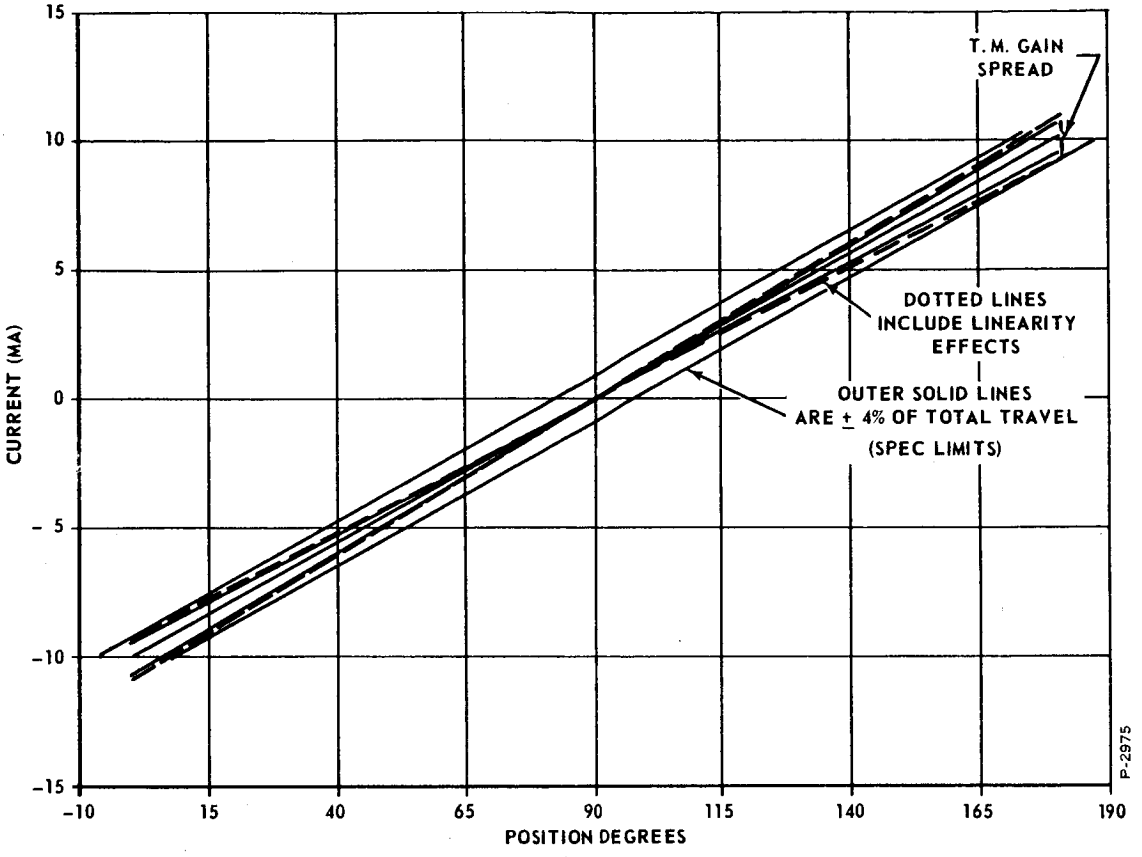

Figure 4-24 - Output Position Versus Input Current

The test signal was injected at the position error point. It therefore receives some immediate filtering but also receives a maximum amount of gain. Figure 4-25 shows characteristic performance.

The conclusion of this examination was that the vortex valve type chosen for the V_1 and V_2 stage does have sufficiently low inherent noise to allow successful loop operation at the gain levels determined by system analysis.

There are three inherent sources of noise:

(a) the input signal

(b) the pressure supply to the actuator and control

(c) internal noise generated in the amplifier circuits.

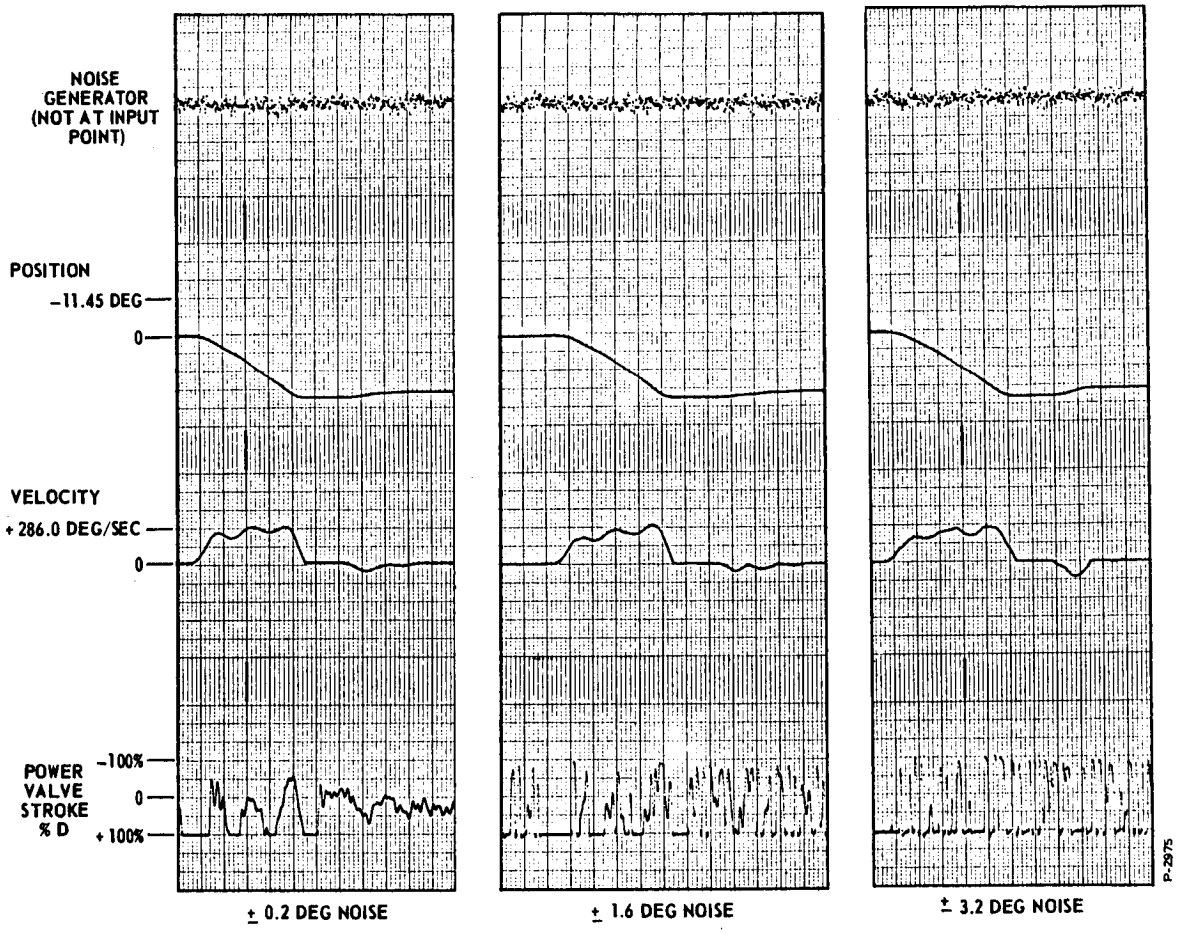

Figure 4-25 - Effect of Noise on Actuation Performance

The input signal noise to the system is very likely not to be random but rather composed of discrete frequencies. Sixty and 400 cps components are both likely. These will be attenuated by the lag circuits used on the input and, therefore, are not likely to cause difficulty unless they are rather large. A typical input specification might call for ± 10 mv or less noise on a ± 10 V input signal which would be equivalent to ± 90 degrees demand. The specified noise would then be ± 0.09 degree. This is a level of noise demonstrated to have little or no effect on performance. This input signal noise figure was actually part of the specification of a recent control rod contract and can, therefore, be assumed to be realistic.

Pressure supply fluctuations affect both the pneumatic amplifiers and the actuator itself. Figure 4-26 shows the extent of the effect on the actuator itself. Effects on the actuator via the amplifier will be minimized by the push-pull circuitry used and by careful attention to mechanical symmetry in the layout of manifolds. It is felt that at worst the total effect might be twice the effect produced by oscillating actuator supply pressure only. This effect is in the order of tenths of a degree of position offset or fluctuation.

Internal noise is generated by flow irregularities in the amplifiers, attachment effects, and organ pipe effects. The small size of the proposed vortex valve tends to push natural frequencies of cavities and lines outside the servo loop bandpass, thus minimizing noise effects. Figure 4-27 shows typical noise at pressures and flows in the range of planned operation. Under planned input stage conditions, the 0.25-inch diameter valve will have an inherent noise level of less than 0.1 psi. The inherent noise of the first amplifier will determine the major portion of the noise which gets through to the power valve. The analog runs show that actuator performance starts to deteriorate at ±3.2 degrees injected noise, largely due to power valve saturation. This situation will be helped in the actual circuit, as compared to the analog, by limiting the amplitude of the input signal to the power valve. The noise value at which response definitely starts to deteriorate is equivalent to ±0.175 psi at the output of each side of the first position amplifier stage (V_1 and V_2 outputs)

The actual unfiltered noise output of V_1 and V_2 measures about 0.2 psi peak to peak at the points in question, under realistic loading. When filtering of the amount the next stage would normally introduce (0.0005 second) is added, the level is down to about 0.09 psi peak to peak.*

Further filtering does not result in substantial improvements as the noise does have some low frequency components.

It is therefore established that a realistically loaded 0.25 in diameter vortex amplifier can be made to have inherent noise in the servo bandpass below the level at which performance deteriorates, and therefore the input stages as drawn can be mechanized with a high

*The signal to noise ratio for the 0.25 in diameter vortex amplifier shown in Figure 4-27 is approximately 700:1 with the 0.005 second filtering effect of the next stage.

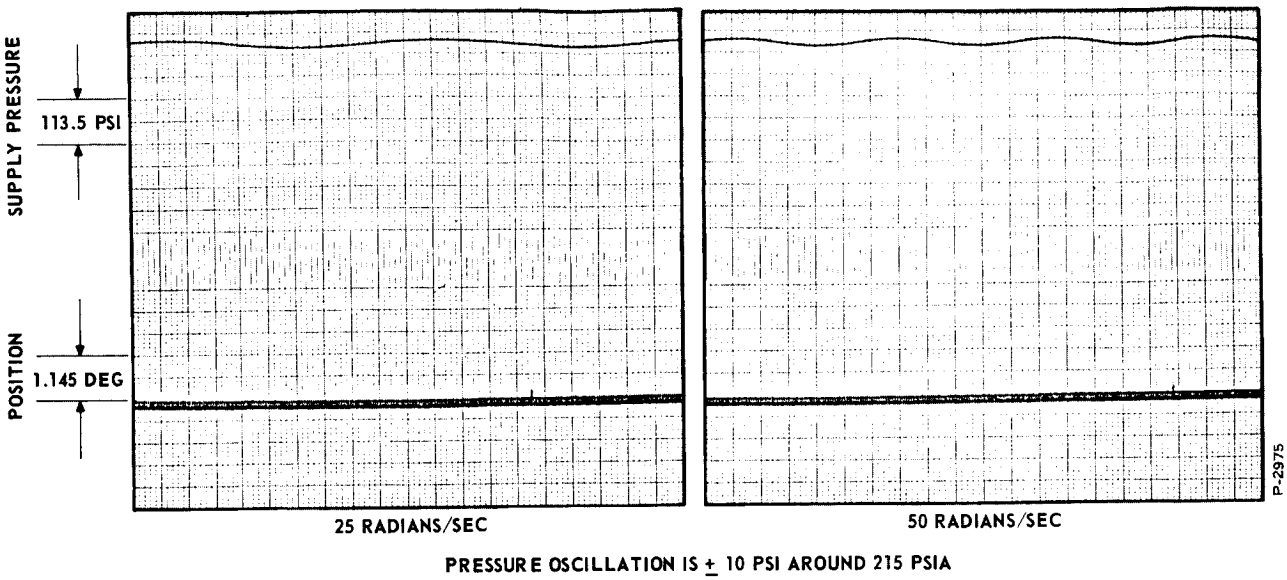

Figure 4-26 - Effect of Actuator Pressure Oscillation

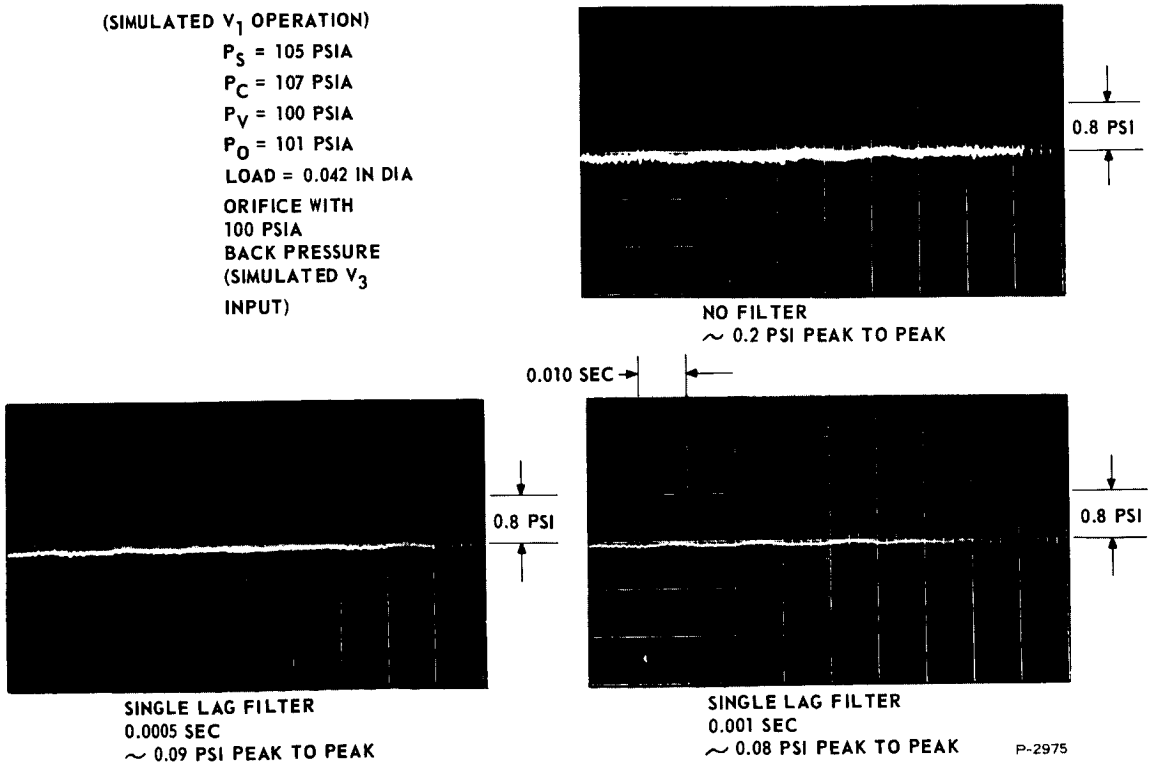

Figure 4-27 - 0.25 in. Chamber Diameter Vortex Valve Noise Characteristics

probability of proper performance. This is actually the only valid criterion for allowable noise since the input stage noise is amplified enough to completely dominate the noise reaching the power valve. (This is assuming subsequent stages do not have entirely unreasonable noise levels.)

4.7 GAS CONSUMPTION

Table 4-5 shows the estimated consumption for the currently proposed circuit with the consumption broken down by components. The estimated values are well below specification.

A significant saving could be made in the actuator itself if lower transient performance could be accepted. The control circuit flow would still be a minor portion of total flow. See Subsection 4.4.3 for a discussion of the practical limitations.

Table 4-5 - Hydrogen Weight Flow Versus Temperature

Component	Conditions	Weight Flow at Various Temperatures, lb/sec x 10^{-3}						
		100°R	190°R	250°R	300°R	400°R	500°R	600°R
Flapper Valve	Minimum to meet torque-speed requirements	5.58	3.50	3.05	2.79	2.41	2.16	1.97
Flapper Valve	Minimum to meet Section 4.4 performance	10.05	6.31	5.50	5.03	4.35	3.89	3.55
V_{13} and V_{14} vents (0.250 in diameter chambers)	Quiescent condition, which is also approx. max. flow condition for the pair	0.776	0.511	0.446	0.407	0.353	0.315	0.288
V_{11} and V_{12} vents (0.250 in diameter chambers)	Same assumptions as V_{13} and V_{14}. Probe flow is 20% of max. possible vent flow	0.924	0.067	0.530	0.484	0.427	0.324	0.342
Totals	Minimum performance system	6.28	4.62	4.126	3.68	3.19	2.80	2.6
	Performance as per Section 4.4	11.75	7.43	6.48	5.92	5.13	4.53	4.18

P-2975

4.7.1 Calculation Method

The weight flow calculations were done as follows:

(a) For the flapper valve, digital computer calculations of the nominal valve size were made for 100°R and 600°R. Larger valve sizes and intermediate temperature points were scaled.

(b) For the control system, there are only four points where flow is consumed (V_{11}, V_{12}, V_{13}, V_{14}). A definite size valve (0.250 in diameter chamber) with a definite exit orifice (0.036) was used. The quiescent condition is representative since the circuit is push-pull. V_{13} and V_{14} were assumed to have a quiescent turndown equivalent to an orifice coefficient of 0.55, which is definitely in line with the operating conditions shown. V_{11} and V_{12} were also assumed to have equivalent exit coefficients of 0.55 as a result of turndown. In addition, probe flow recovery was estimated from test data as being 0.2 of the maximum exit flow with an orifice coefficient of 1. Flows were then calculated at 100°R and 600°R, using graphs of R and γ to choose values consistent with the temperatures and pressures involved. This has the effect of raising the 100°R weight flow value substantially over what one would get by scaling 600°R data on the basis of temperature only. The weight flow at intermediate temperatures was scaled from the 600°R data. As a result, the 600°R and 100°R weight flow data are as accurate as available data on hydrogen can make them. Intermediate values down to 250°R are essentially as accurate as the 600°R data. The 190°R values may be on the low side as this is the region where R and γ start to change. The error is at most on the order of 10 percent.

Complete flow calculations for the other amplifiers have not been made, but enough has been done to verify that upstream flows are definitely low enough to justify the flow salvaging scheme shown and to obviate venting any other points to exhaust pressure.

The equation used for weight flow calculations in the vortex valve is

$$W = \frac{C_d A C_3 P_s f_1 \left(\frac{P_v}{P_s}\right)}{\sqrt{RT}} \qquad (4\text{-}25)$$

where

C_d = dimensionless orifice coefficient

A = area of exit orifice (in^2)

P_s = vortex valve or amplifier chamber

P_v = vent pressure (psi)

$$f_1\left(\frac{P_v}{P_s}\right) = \frac{\left(\frac{P_v}{P_s}\right)^{\frac{1}{\gamma}} \sqrt{1 - \left(\frac{P_v}{P_s}\right)^{\frac{\gamma - 1}{\gamma}}}}{\left[\left(\frac{P_v}{P_s}\right)^{\frac{1}{\gamma}} \sqrt{1 - \left(\frac{P_v}{P_s}\right)^{\frac{\gamma - 1}{\gamma}}}\right]_{max.}}$$

γ = ratio of specific heats, $\frac{C_p}{C_v}$

T = temperature, degrees Rankine

R = gas constant in/°R

$$C_3 = \frac{\sqrt{\gamma_g}}{\left(\frac{\gamma + 1}{2}\right)^{\left(\frac{\gamma + 1}{2(\gamma - 1)}\right)}} \frac{in^{\frac{1}{2}}}{sec}$$

This function was "invented" to replace the usual C_2 coefficient to get R to appear only one place in the computation. The graphs used were:

C_3 versus γ

γ versus P for lines of T for hydrogen

R versus P for lines of T for hydrogen

f_1 versus pressure ratio for various values of γ.

(Tabulated values rather than plots are shown in Appendix VI, as the plots are all very similar.)

The flapper valve computations involved essentially the same equation with the graphic data put in by means of linear approximations. See Appendix VI for details and the graphic data used in the computations.

SECTION 5

COMPONENT DESCRIPTION AND CHARACTERISTICS

The performance analysis of Section 4 was based on the general characteristics of the type of components expected to be used. The generalized transfer functions resulting from the analysis were then used to determine final component specifications. A number of component rearrangements and rescalings have been necessary to design a practical system and to minimize gas consumption.

In this section the transfer functions used in the performance analysis are related to the gain and time constant requirement of components. A detailed description of the components follows, including specifications and performance characteristics. Mechanical analyses are presented where necessary to verify the feasibility of the mechanical design selected. In the case of vortex elements that are used to implement the amplification and frequency compensation, circuit, test data showing their operating characteristics are presented.

5.1 GAIN REQUIREMENTS

The discussion presented is concerned primarily with translating the generalized transfer functions of the performance analysis into gain and time constant requirements of the various subsystems. Figure 5-1 shows the performance analysis results in a very generalized form.

$G_b K_1$ equals the gain of the position error detection circuit times the position error amplifier gain times the gain of the position error and rate feedback summing amplifier. $G_a K_1$ is the rate sensor amplifier gains times the gain of the position error and rate feedback summing amplifier. The gains shown are the total gain for a channel.

These gains may be related to sections of the proposed hardware by reference to Figure 3-6. $G_b K_1$ is the gain of the error detection circuit (2 - 2' side only) times the gains of V_1, V_3, and V_9 times 2. This doubling takes into account the other side of the push-pull circuit. $G_a K_1$ is the gain of the differentiator circuit of the rate sensor made up of nozzles 3 and 4 and T_2 (Figure 3-6) times gains of V_5, V_7, and V_9 times 2. Here, the doubling accounts for the push-pull action.

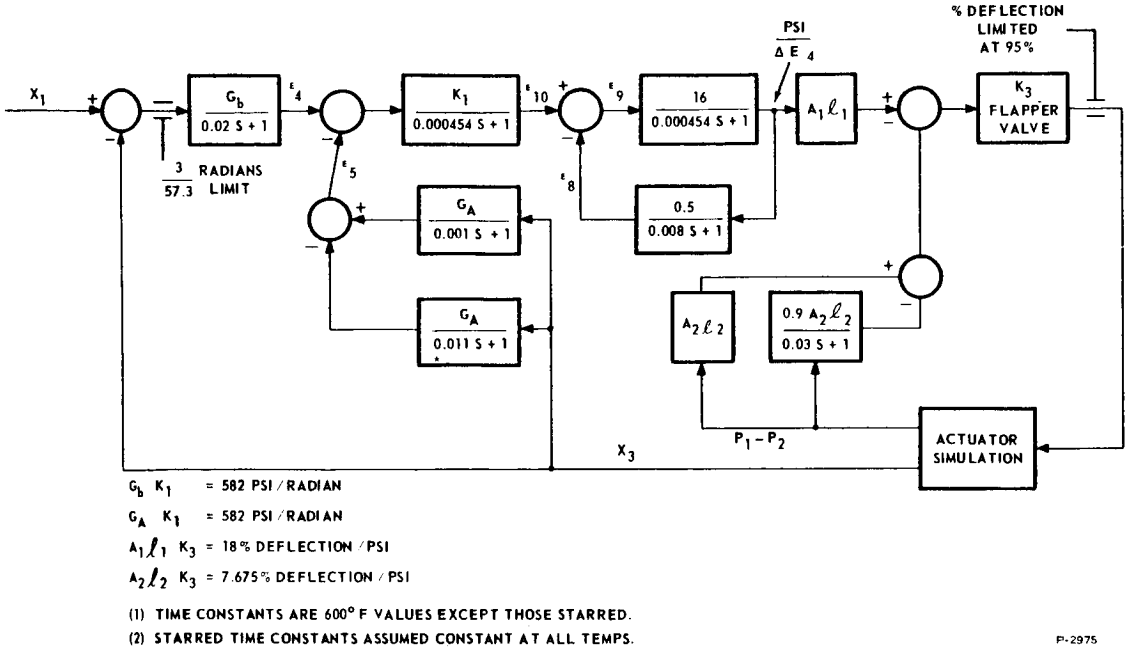

Figure 5-1 - Generalized Performance Analysis Results

Amplifiers V_9 and V_{10} are used to form the summing circuit for ϵ_4 and ϵ_5, and are the lag shown under K_1, and the gain K_1. The tanks marked T_2 on Figure 3-6 are the temperature compensated 0.011 second lag shown in the rate circuit. The 0.001 second lag is due to the volume between nozzle 4 and V_5 (and the corresponding section of the other side of the circuit).

This volume was assumed to be temperature compensated in the analog. In the actual mechanization, however, the temperature compensation (change in volume with temperature) takes place in the T_2 volume only. In the actual system operation, it is only important that the required difference in the lags remains constant throughout the range of operating temperatures.

The practical arrangements for G_b K_1 must now be made, including the limit. There is some difference in performance depending on whether the limit is ahead of G_b K_1 or after G_b, but this difference, being on the leading edge of large steps, is of minor importance. Thus, there is some flexibility in the mechanization. The mechanization consists of a limited linear range pneumatic summer (error detection circuit) feeding a string of amplifiers. The lag shown with G_b is a pneumatic resistance-capacitance circuit.

The amplifier stages are coupled similar to a direct coupled direct current amplifier. Therefore, a series of regulated pressures must be used or, if push-pull circuitry is utilized, simple dropping resistances (orifices) may be used. Push-pull circuits with their higher available gain reduces the number of cascaded stages and, therefore, minimizes amplifier phase lags. Push-pull circuits also have the benefit of minimizing performance shifts due to pressure level changes during transients. This is because one lag tank charges as the other discharges and the average pressure and, therefore, average time constant remains very nearly at one value.

Because push-pull circuits allow simple dropping orifices to be used in place of regulators and have the other advantages mentioned above, they are used throughout.

The noise level in the error detector and first amplifier section is critical because of the large gains in the rest of the circuit. Prime consideration is given to noise reduction, therefore, even at the expense of gain.

The most effective placement of the lag tanks was evaluated. The first thought was to connect these tanks in the error detector because some volume and, therefore, some lag is unavoidable.

Initial estimates of error detector time constants indicated a natural lag large enough to constitute a serious problem. (A value of 0.006 second at 100°R was estimated early in the program.) At that time, separate dividers were used to generate command and feedback networks. The present estimate based on the Figure 3-6 mechanization, the pressure levels, and volumes for the connecting lines estimated from the component layout of Figure 3-7 shows that the error detector time constants can be reduced to less than 0.001 second at 100°R.

Thus, it is possible to place the lag tank where it will filter the noise and provide the necessary compensation function. This location is on the input lines to V_5 and V_6. The preceding stage pressure pickup orifice and the following stage inlet orifice act as resistors, and the tanks act as a capacitance. Figure 5-2 shows the equivalent pneumatic and electrical circuits. The electrical circuit time constant is $\frac{R_1 R_2}{R_1 + R_2} C$. The equation for the pneumatic time constant will have an analogous form with the resistances calculated around the mean value of pressure.

The rate channel is similar to the position error channel, except that half of each signal is lagged ahead of the amplifier, and the paired

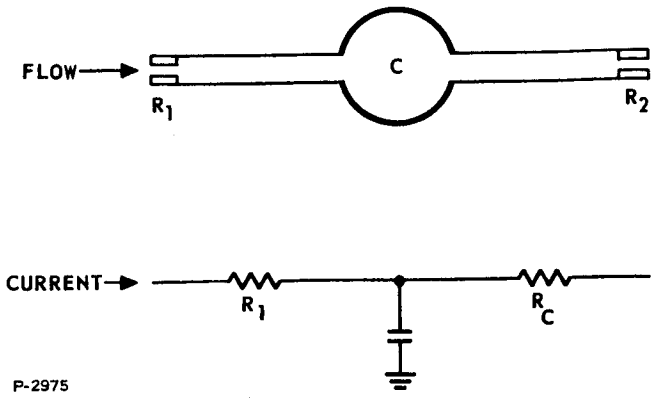

Figure 5-2 - Equivalent Pneumatic and Electrical Lag Circuits

signals to amplifiers V_5 and V_6 are matched so that for zero motion, no output results. It might have been possible to simplify this arrangement somewhat by taking advantage of the inverting properties of the coupled amplifiers with a supply line resistance, but the present circuit has advantages of complete symmetry, and lag variations are minimized by having the pressures in the two T_2 tanks maintain a constant average.

Since amplifier V_3 and V_4 of the error detector circuit and amplifiers V_7 and V_8 of the rate sensor have essentially the same saturation pressures, it is necessary to be sure the rate signal can override the position error signal. This will be done by making the rate signal ports on V_9 and V_{10} larger than the position error ports. The gain will, therefore, be different (higher) for the rate channel. This higher gain will be compensated for by reducing the differentiator gain a proportionate amount.

The limits on V_3 and V_4 outputs must be wide enough, in equivalent degrees, to allow for required offsets to hold the spring and, at the same time, must be as narrow as practical to insure best transient performance and to limit the change in signal required from the rate circuit. A value of 3 degrees was chosen. This sets the difference of time constants in the rate circuit at 0.01 second, which keeps the T_2 tanks in the order of 1 in^3 at 100°R. Exact values of volume versus temperature desired in T_2 require a consideration of the actual value of lag versus temperature in the "fast" branch of the circuit. Volume compensation to keep the rate circuit gain constant is the most straightforward method of holding the limit value of velocity as temperature changes.

Fortunately, a compact mechanism for getting large volume changes versus temperature is available. Spherical shells of one material with a rim of a material with lower coefficient of expansion can be made to exhibit large volume changes. This is treated in detail in Section 5.3.2 and Appendix IV.

Alternate methods considered were (1) changing the limit value on V_3 and V_4 (difficult because of bias changes which are propagated throughout the circuits) and (2) changing the gain in either the position error or rate channel (again difficult because gain has an associated bias level).

Since the gain of the error detection circuit is only about 0.02 psi per degree using practical orifice sizes, it is desirable to make the gain of V_1, V_2 and V_3, V_4 as high as practical, bearing in mind noise levels, biases, and error detector loading effects. If the inlets of V_1, V_2 are enlarged to get more gain, either the input and feedback transducers must have their orifice sizes increased (using more gas and increasing torque motor loads) or the gain of the error detector decreases by an amount almost compensating for the V_1, V_2 gain increase. A larger pressure swing would defeat the objective of making the rate sensor relatively insensitive to pressure level. By the nature of the interstage coupling, the position error detector must work on approximately the same pressure level as the rate sensor. Therefore, the most practical course is to accept the low gain in the position error circuit, use a low first stage gain to minimize loading and noise, and then make up the balance in V_3, V_4 and V_9, V_{10}. The noise problem is discussed further in Section 4.6.

A pressure gain as high as 3.8 has been shown for 0.25 in chamber diameter vortex valves with a pressure drop comparable to that shown in Figure 3-6, with enough load flow being drawn to justify using a 10 psi/psi gain in the following stage. The gains of V_1 and V_2 will be tentatively set at 2.73 psi/psi (each). The gains of V_3 and V_4 are 10 psi/psi (each). This makes the V_9 and V_{10} position error signal pressures have a swing of ±1.64 psi each for a ±3 degree position error. This is enough to saturate the V_3 and V_4 outputs when they are properly biased and adjusted. Thus, the position error limit is mechanized.

The rate sensor gain depends on both the orifice sizes and the difference of time constants. Consequently, final T_2 (Figure 3-6) sizing will determine the sensor gain. The amplifier string may be assumed to have the same pressure gains as the position error detector string, with the exception noted before that the V_9 and V_{10} inlet ports will be

larger for the rate signal inputs. V_9 and V_{10} gains must be set last, as there are other practical restraints on the mechanization of the rest of the circuit. The closed loop gain from ϵ_{10} to ϵ_4 (Figure 5-1) is 1.78 psi/psi. This lead lag circuit is mechanized by V_{11} and V_{12}, each of which must have a gain of 16 psi/psi. Gains of 13.8 psi/psi per stage have been demonstrated, and 16 psi/psi is not an unreasonable projection, especially considering the low required output pressure change. Valves V_{13} and V_{14} are operating in a manner analogous to an emitter follower circuit. The individual valve gain is, therefore, not critical. The supply pressure to each follows the input signal pressure, with a gain approaching 1. (Values of 0.8 and 0.9 are common.) The required lagged feedback signal is readily available at the required 0.5 psi/psi gain at the V_{11} and V_{12} feedback signal orifices. It appears that about 0.6 psi/psi gain would be the maximum value readily available.

Now that it is established that this portion can be mechanized as shown in the block diagram, V_9 and V_{10} gains can be set.

$$\frac{G_b K_1}{2} = \text{Gain of one side} = 291 \frac{\text{psi}}{\text{radian}}$$

Then:

$$\frac{291}{(1.146)(2.73)(10)} = V_9 \text{ gain} = 9.3 \text{ psi/psi}$$

The gain requirements of vortex devices, as loaded in the system shown schematically in Figure 3-6, are within the capabilities of the 0.250 in chamber diameter vortex amplifiers and valves that have been tested. The pressure levels indicated in the schematic are approximate. The interconnections between the vents of upper stage amplifiers and supplies of the lower stage amplifiers have been checked for proper balance of inlet and outlet flows at the pressure levels shown. Again, trimming will unquestionably be required, but the concept is entirely supported by test data and can be used for a revised flow estimate. The flow estimate is detailed in Section 4.7. The component pressure and gains are tabulated in Table 5-1.

The remaining generalized requirements from Figure 5-1 all pertain to the flapper valve described in detail in Section 5.5.

Table 5-1 - Component Specifications

Component	Supply Pressure (psia)	Vent Pressure (psia)	Mean Output Signal Pressure	Mean Input Signal Pressure	Gain	Remarks
Position Error Detector	115	P_s of V_1 and V_2	108.6	Not applicable	$0.02 \frac{psi}{deg}$	
V_1, V_2	105	100	102 5	106 6	$2.93 \frac{psi}{psi}$	
V_5, V_6	105	100	102 5	108 6	$1.865 \frac{psi}{psi}$	Each input
V_3, V_4, V_7, and V_8	100	54	97	102 5	$10 \frac{psi}{psi}$	
V_9, V_{10}	94	86	90	97	$9.3 \frac{psi}{psi}$	For V_3 and V_4 signals
					$18.6 \frac{psi}{psi}$	For V_7 and V_8 signals
V_{11}, V_{12}	86	50	60	90	$16 \frac{psi}{psi}$	Extra flow supplied by bleed from 215 psia
V_{13}, V_{14}	59 (mean)	50	Same as supply	60	$0.8 \frac{psi}{psi}$	Non-inverting follower circuit
Power valve	215	50	107.5	60	variable	Depends on load conditions assumed. See Appendix III.
Power valve bellows and lever					$0.09 \frac{lb\text{-}in}{psid}$	Output is torque about flapper pivot. $A_1 \ell_1$ on Figure 5-1.
Power valve spring constant					$200 \frac{\%\ D}{lb\text{-}in}$	K_3 on Figure 5-1
Power valve pressure feedback					$0.383 \frac{lb\text{-}in}{psid}$	$A_2 \ell_2$ on Figure 5-1 $2.5\ K_f$ in analog study
Positive pressure feedback lag						Bellows and orifices on power valve
T_2 tank						Requires variable volume estimated at 1 in^3 at 100°R
T_3 tank						Estimated at 3 in^3
T_5 tank						Estimated at 5 in^3

P-2975

5.2 ERROR DETECTOR CIRCUIT

The error detector produces a pneumatic push-pull signal, within the limits of its output, that is proportional to the difference between the commanded position and the actual position of the actuator's output shaft. An area-balancing circuit employing flappers and nozzles generates the error signal.

The error detector consists of a position input transducer and a position feedback transducer that positions flappers in the detecting circuit. The input signal to the detector is electrical,and the position input transducer converts the electrical signal to a proportional flapper position. The position feedback transducer converts the output shaft's position to proportional flapper position through a cam. The error detector has a gain of 0.02 psi per degree of rotation.

Description of the error detector circuit and its detailed specifications, resulting orifice area changes with position, and output pressure characteristics follow. The position input and position feedback transducers are also described, and specifications of the position input transducer's torque motor and an analysis of the position feedback transducer's flapper assembly are presented.

5.2.1 Overall Circuit

The error detector circuit is composed of the orifices varied by the input and feedback position transducers and the fixed orifices at the input of vortex amplifier V_1 and V_2 of Figure 3-6. A schematic of the error detector circuit is shown in Figure 5-3. The gas at supply pressure P_{SE} flows into the position input and position feedback nozzles to the control ports A_{V_1} and A_{V_2} of the vortex amplifiers V_1 and V_2.

No error signal is generated when the total inlet area of nozzles 1 and 1' is equal to the total inlet area of nozzles 2 and 2'. If either the flappers of the position input transducer or the flappers of the position feedback transducer are moved, the total inlet areas of nozzles 1 and 1' and 2 and 2' will differ. This difference in the control pressures is the error signal. Any movement of the flappers to bring the total inlet areas to the same value will, of course, reduce the error signal. The flappers of both transducers have strokes equivalent to the full stroke of the actuator. If one of the nozzle areas of the position input transducer is decreased, the corresponding area in the position feedback transducer will have to be increased to reduce the error signal.

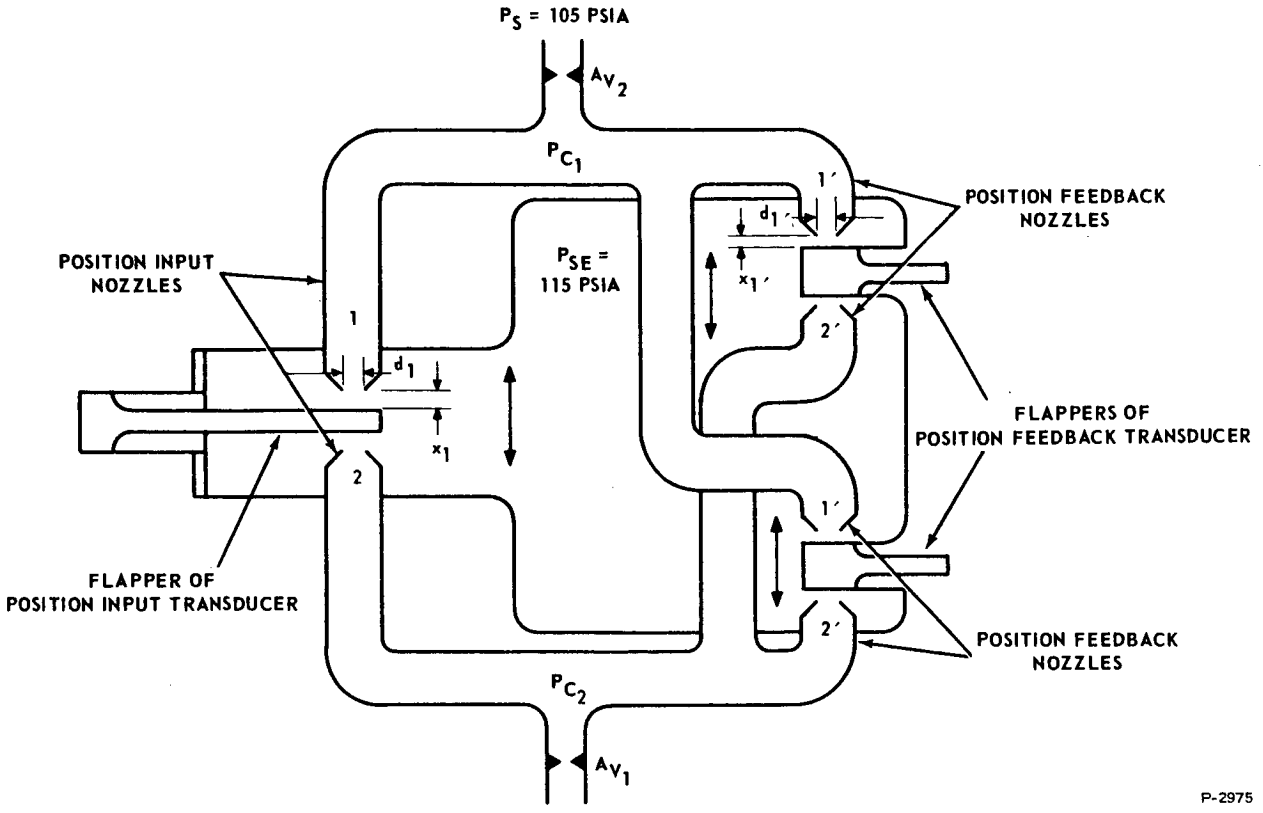

Figure 5-3 - Schematic of Error Detector Circuit

This arrangement with the supply gas flowing into a nozzle is used to reduce the gas consumption of the actuation control system.

Detailed specifications for the error detector circuit are:

A_N = total mean inlet flow area ($a_N + 2a_N'$) = 0.000578 in^2

a_N = flow area of position input transducer nozzle (πdX) = 0.000289 in^2 (mean value)

a_N' = flow area of position feedback transducer nozzle ($\pi d'X'$) = 0.000119 in^2 (mean value)

d_1 = position input transducer nozzle diameter = 0.047 in

x_1 = clearance between flapper and nozzle of position input transducer = 0.00196 in at mid position

d_1' = position feedback transducer nozzle diameter = 0.0297 in

x_1' = clearance between flapper and nozzle of position feedback transducer = 0.00138 in at mid position

P_{SE} = supply pressure to error detector circuit = 115 psia

P_S = supply pressure to vortex amplifiers = 105 psia

P_{C1} = control pressure at vortex amplifier = psi (see pressure gain curve of Figure 5-4)

K_p = pressure gain = 0.02 psi/deg

The change in inlet nozzle flow area and error detector control pressure as functions of position error are shown in Figure 5-4.

5.2.2 Position Input Transducer

The position input transducer is essentially an electromagnetic torque motor with an output flapper that fits between the position input nozzles. This transducer forms an interface between the input electrical signal and the pneumatic actuation system. Open-loop characteristics of the torque motor used in the transducer (linearity, hysteresis, threshold, and gain variations with temperature) are important since they are

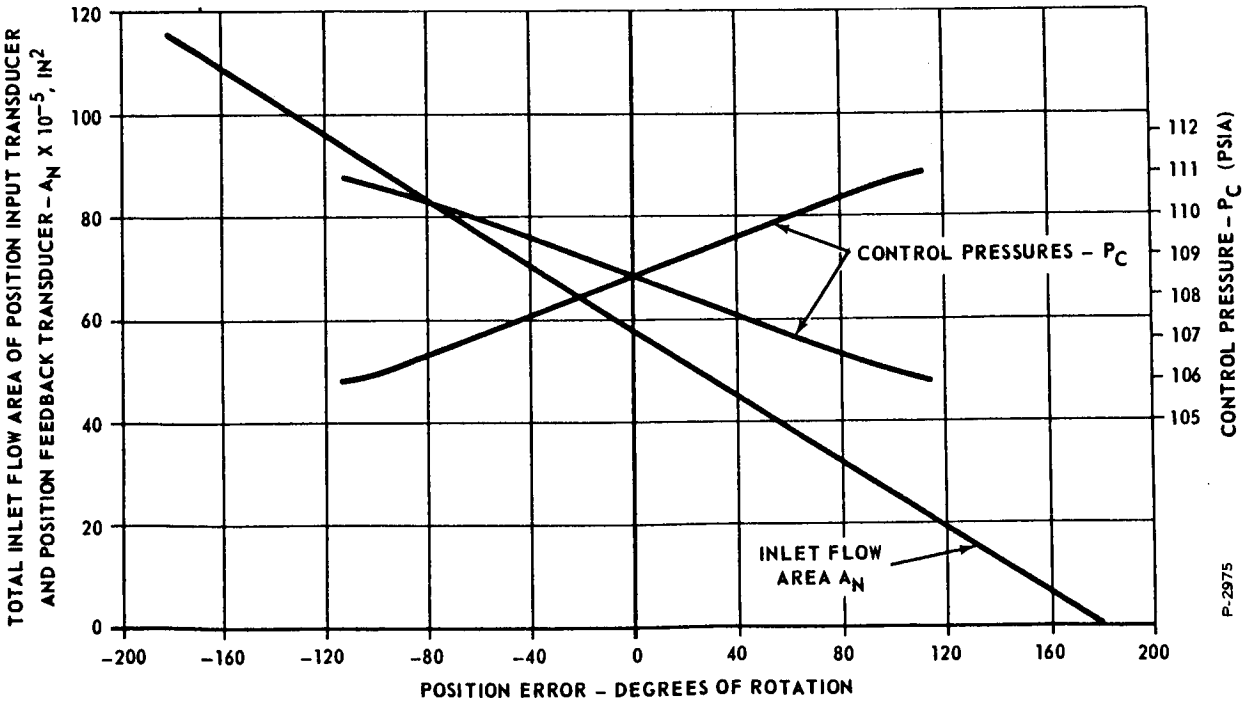

Figure 5-4 - Inlet Flow Area and Position Error Detector Control Pressures as Functions of Position Error

in series with the characteristics of the closed loop portion of the actuation system. Since the torque motor is outside the actuation system closed loop, the effect of its characteristics cannot be lessened by the loop compensation. The linearity of the torque motor and of the position feedback transducer cam establish the linearity of the closed loop actuation system.

An assembly drawing of the position input transducer is shown in Figure 5-5. The torque motor selected for this application is a D.G. O'Brien Model 121 torque motor which is capable of working in the specified environment. This torque motor has a dry coil (i.e., its flapper is sealed from the rest of the torque motor) making it ideal for this application. It is small in size, 1.0 in by 1.56 in by 1.7 in.

Table 5-2 compares required characteristics of the torque motor with those of the Model 121 torque motor.

5.2.3 Position Feedback Transducer

The position feedback transducer varies the orifices both in the error detector circuit and the rate sensor. The orifice variations are proportional to the angular position of the actuator's output shaft. The position feedback transducer is shown schematically in Figure 5-6.

The cam of the transducer is coupled to the output shaft of the actuator and is symmetrical around a signal axis. Dual spring tube flappers are preloaded against the cam. When the cam rotates, therefore, one flapper is driven by the cam and the other, due to the preload, is forced to follow the cam.

The dual set of flapper-nozzles in the error detector circuit eliminates changes in the position signal due to thermal expansion effects. Any dimensional changes in the cam due to temperature variations cause the flapper tubes to move in opposite directions, thus maintaining a constant total inlet orifice area. This technique is not used with the rate sensor nozzles, however, because rate of change is of interest, rather than exact positional accuracy.

The cantilevered flapper enables a greater cam displacement. This reduces the required dimensional accuracy of the cam compared to one with the nozzles placed directly over the cam. The spring tube assembly is used to seal the flapper from the nozzles. The spring tube flapper design is shown in Figure 5-7.

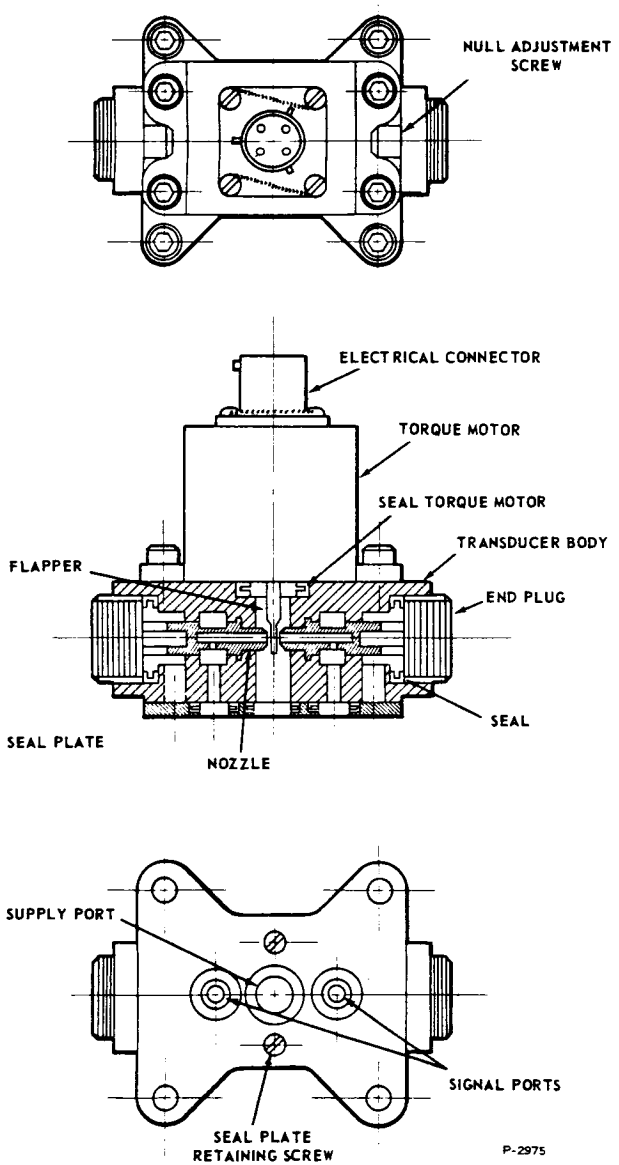

Figure 5-5 - Drawing of Position Input Transducer

Table 5-2 - Torque Motor Specification

Performance Parameter	Specification	Model 121 Torque Motor
Output displacement	± 0.00196 in	± 0.004 in
Input current (for maximum stroke)	200 milliamperes maximum at 20 volts	± 10 milliamperes
Maximum input power		180 milliwatts
Coil resistance		1800 ohms
Coil type	dry	dry
Temperature range	100°R to 600°R	100°R to 600°R
Static gain	not specified	$\frac{0.0005 \text{ inch}}{\text{milliampere}}$
Allowable static gain variation over temperature range	not specified	5% maximum
Linearity	± 4%	± 2%
Frequency response flat within ± 3 db 90° phase angle		 500 cps 500 cps
Minimum life at 100°R	200 hours	1000 hours

P-2975

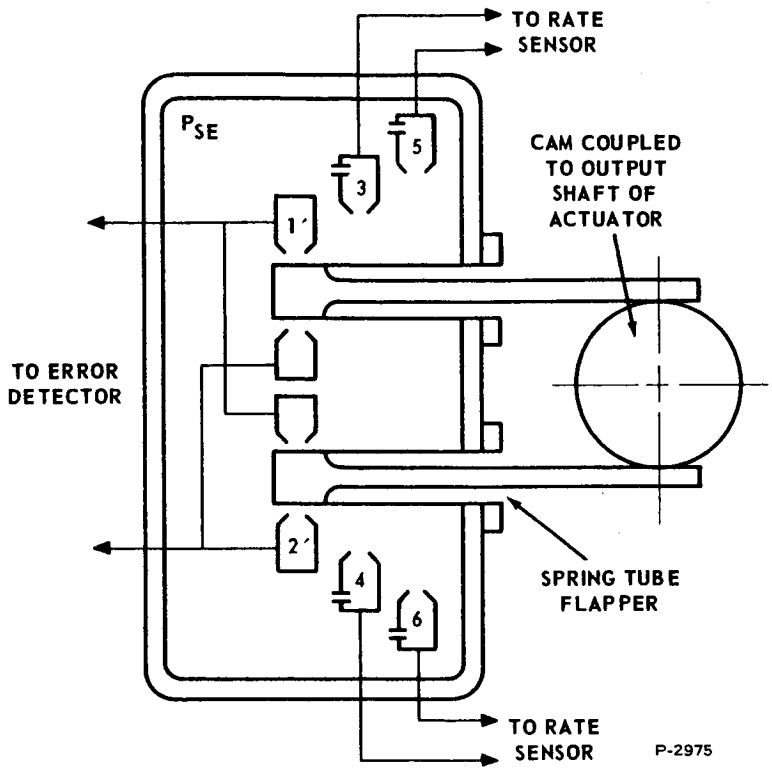

Figure 5-6 - Schematic of Position Feedback Transducer

In this design, the relatively low spring rate of the flapper bar, as compared to the sealing tube, allows the ratio of δ_c/δ_o to be high, thereby reducing the orifice area sensitivity to cam profile irregularities. For a required flapper deflection at the orifice δ_o, of ±0.00138 in, the maximum cam contact load W, (assuming a 10 percent deflection) is given by:

$$W = \frac{(0.2)\,(0.00138)\,EI_t}{\ell^2\left[\frac{L}{2} - \frac{\ell}{3}\right]}$$

where:

L = flapper bar beam length = 2.2 in

ℓ = sealing tube beam length = 0.7 in

E = modulus of elasticity = 30×10^6 psi

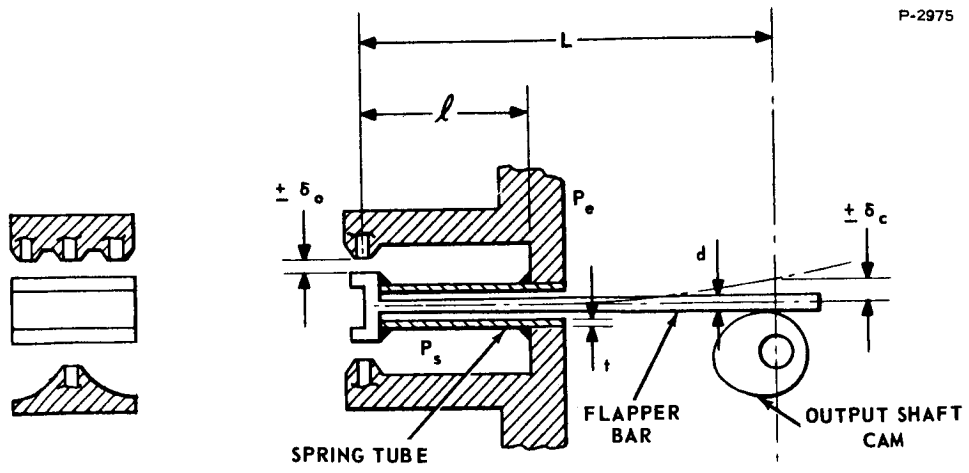

Figure 5-7 - Spring Tube Flapper Assembly

I_t = sealing tube cross section moment of inertia = 7.56×10^{-6} in^4

(tube mean radius - 0.070 in)
(tube wall thickness - 0.007 in)

The solution of the above equation indicates that the load exerted by the cam on the end of the flapper bar varies from 0.73 to 1.54 pounds. At the maximum load of 1.54 pounds, the maximum bending stress in the seal tube is 10,500 psi.

Assuming a flapper bar solid diameter of 0.084 in, the maximum bending stress in the flapper bar at a cam load of 1.54 pounds is 59,000 psi. An acceleration of 68 g's is required to lift the flapper from the cam at minimum load. These stress levels are within the endurance limits of materials suitable for use in this application.

The cam surface must impart a displacement to the cantilevered flapper tube assembly which is linearly proportional to the angular displacement of the cam. The required cam rise can be determined from the difference between maximum and minimum flapper bar loads (1.54 pounds maximum and 0.073 pounds minimum). Assuming the deflection of the flapper bar at the nozzle (δ_o) is negligibly small, compared to the deflection at the cam (δ_c), the required cam rise is given by:

$$\text{Cam rise} = \frac{(1.54 - 0.073)\, L^3}{3EI_f} = \frac{1.467\,(2.2)^3}{3\,(30 \times 10^6)\,(2.40 \times 10^{-6})}$$

$$2\,\delta_c = \text{cam rise} = 0.072 \text{ in}$$

The cam rise is much greater than $2\,\delta_o$, which equals 0.00276 in. The cam radius must change uniformly ±0.036 in as the cam contact point rotates ±90 degrees.

5.3 RATE SENSOR

The rate sensor generates a pneumatic push-pull signal that is proportional to the rotational velocity of the actuator's output shaft. The signal is generated by a pseudo differentiation of a pneumatic position signal using a volume and orifice network. The position signal is generated by the position feedback transducer of the error detector, using separate nozzles for the rate sensor. Because the gain of the rate sensor must remain relatively constant, the volumes used in the network vary as supply gas temperature changes from 100°R to 600°R.

Description of the rate sensor and a discussion of its design follow. The required sizes of the orifices and volumes in the network to achieve the desired performance, the specification of the variable volume, and the results of an analysis establishing the feasibility of the variable volume design are presented.

5.3.1 Rate Sensor Circuit

The rate sensor circuit and associated amplifier is shown schematically in Figure 5-8. The cam-operated position flappers are the flappers of the position feedback transducer of the error detector. Nozzle 3 is connected through a volume T_2 and nozzle 4 is connected directly to vortex amplifier V_5. These connections insure that the net static input signal to V_5 is always the same regardless of the position of the flapper. When the flappers are moving, the change in the pressure from nozzle 3 is lagged by the volume T_2, and the net input signal to V_5 is changed approximately in proportion to the rotational velocity of the actuator. The input signal to vortex amplifier V_6 is changed in the same manner except that the signal generated is opposite in sign.

Vortex amplifiers V_5 and V_6 each have two inputs. Because the same size amplifiers are to be used throughout the system, each input orifice must have half the area of the V_1 and V_2 amplifier input orifices, to achieve the same bias conditions with the same mean pressure. (V_1 and V_2 are in the position error channels.) This cuts the pressure gain of V_5 and V_6 in half relative to V_1 and V_2. If the rate

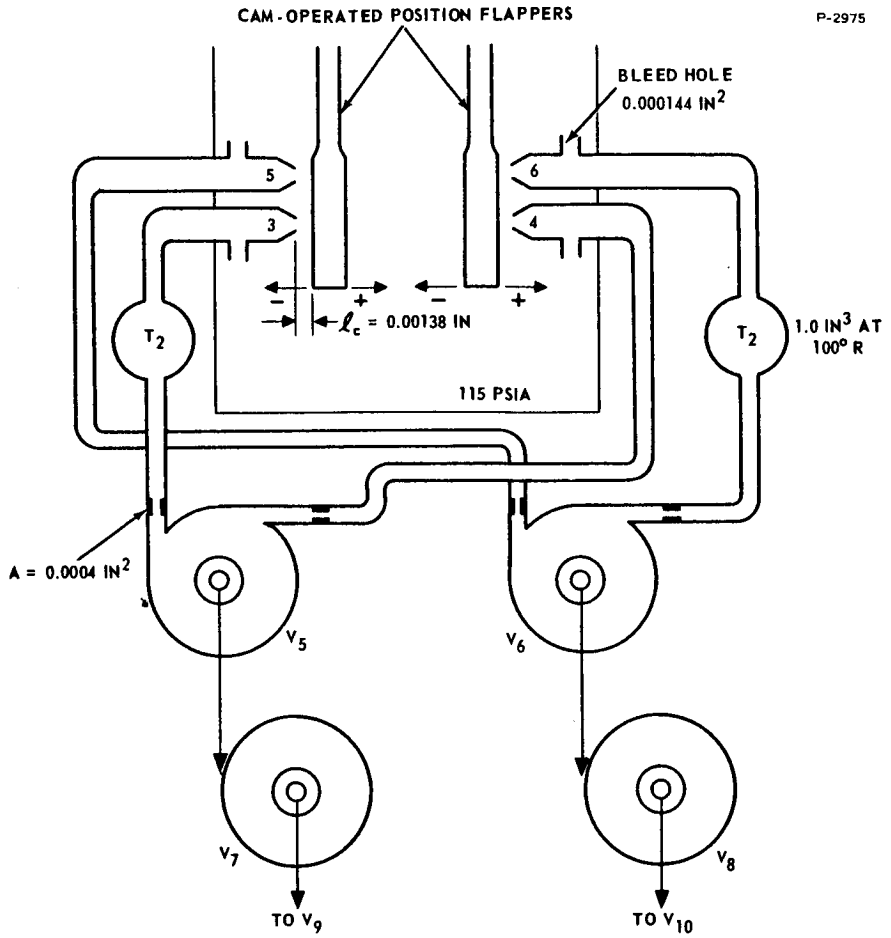

Figure 5-8 - Schematic of Rate Sensor Circuit and Associated Amplifiers

channel gain is to meet the requirements established, either the psi/deg gain of each input device must be twice that of one side of the push-pull error detector circuit or the gain must be made up elsewhere. Another design constraint on the flapper-nozzles of the rate sensor is that the pressure versus position curve must be as linear as possible throughout the travel of the actuator. The best compromise in circuit design results from making the flapper-nozzle gain the same as one side of the push-pull error detector circuit by using the dimensions shown in the schematic. Figure 5-9 shows the resulting psi/deg output of one rate sensor flapper-nozzle.

The gains of amplifiers V_5 and V_6 are set at essentially the same value as those of V_1 and V_3, 2.73 psi/psi, of the error detector

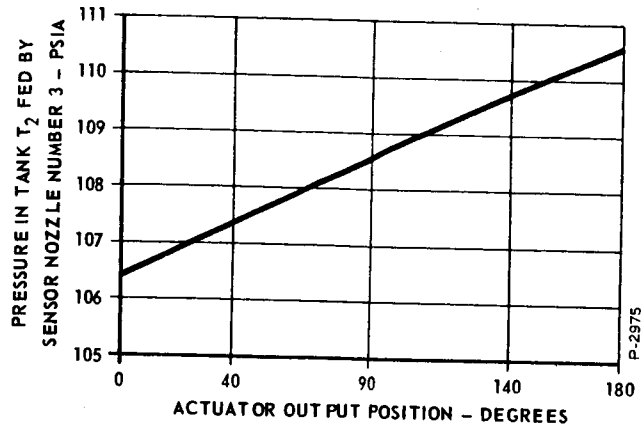

Figure 5-9 - Rate Sensor Input Pressure Versus Position

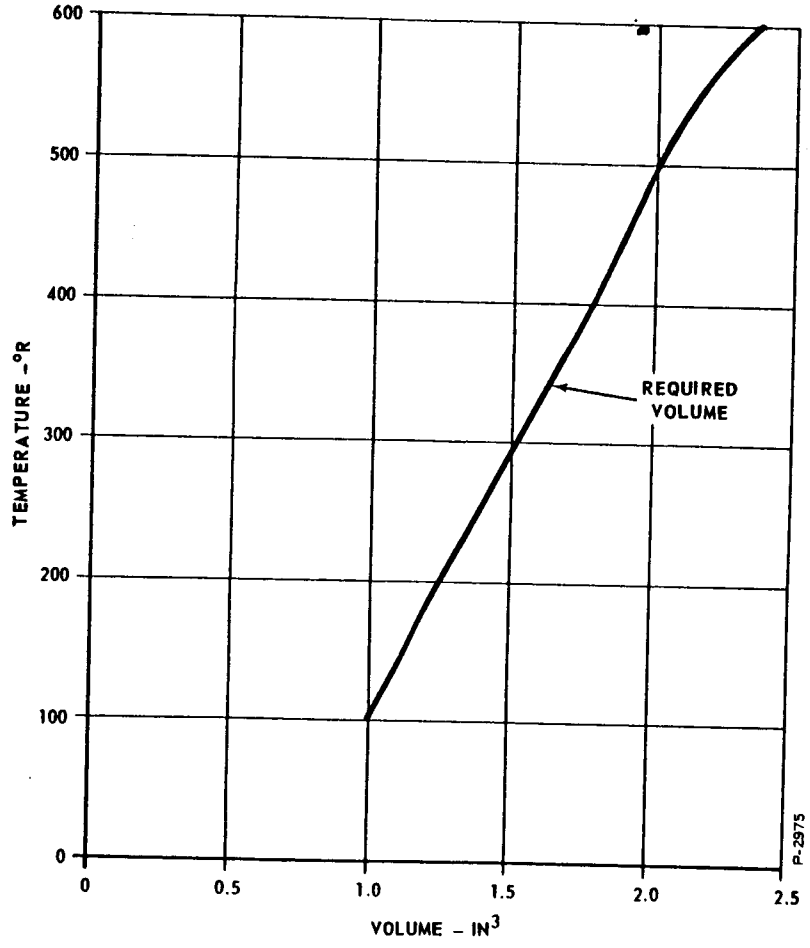

Figure 5-10 - Required T_2 Volume Versus Temperature

channel. Amplifiers V_7 and V_8 will have a gain of 10 psi/psi. Amplifiers V_7 and V_8 can supply enough flow to summation amplifiers V_9 and V_{10} to make the rate input gain twice as much as the position input gain, without stubstantial loss in output differential pressure V_7 and V_8. There will be a loss in the output pressure level, but the maximum pressure swing about the quiescent level is only 1.67 psi; therefore, these amplifiers are neither saturated nor are their output pressures below the chamber pressures of the following stages. The gain of the V_7 and V_8 inputs to V_9 and V_{10} are adjusted by varying the inlet control orifices of V_9 and V_{10}.

The T_2 lag minus the lag in the fast side of the circuit, T_1, must be 0.01 second. The estimated required volume per 0.01 second of lag at 100°R is 1.0 in^3. To keep the gain of the sensor constant throughout the specified temperature range of the supply gas, the lags must vary with temperature. The lag in the fast side of the circuit is small enough to be neglected, and the required volume of T_2 versus temperature is shown in Figure 5-10.

5.3.2 Compensating Volumes

There must be a 55 percent reduction in the T_2 volumes of the rate sensor circuit when the supply gas temperature goes from 600°R to 100°R.

The change in volume required is substantial. After a thorough investigation, the temperature-varying chamber shown in Figure 5-11 was selected. This chamber consists of two spherical shells made of a material with a high coefficient of expansion. The shells are fastened very securely to the inside of the rim as shown. The rim is made of a material with a low coefficient of expansion. The chamber

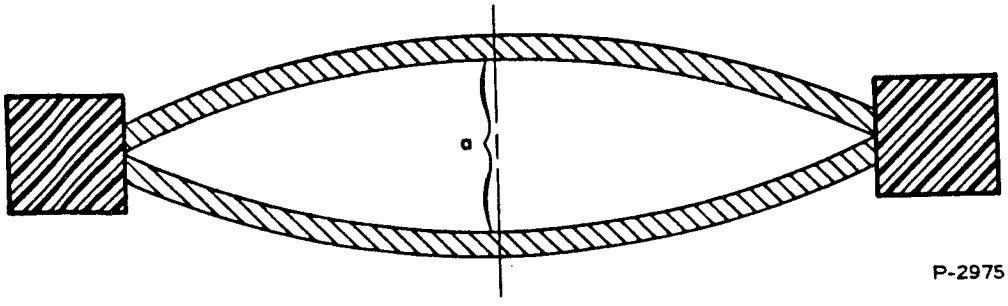

Figure 5-11 - Variable Volume Chamber

is assembled at its highest operating temperature, or in a state simulating the highest temperature. When the chamber is cooled, the outer ring does not shrink as much as the shell shrinks. Because the shell decreases more than the rim, a tension load is created and a moment imposed around the edge of the shell. These loads, along with the natural shrinking of the disk, decrease dimension a, changing the volume within the chamber.

Various dimensional relationships and materials were investigated using the equations developed in Appendix IV, to determine if a volume change could be achieved that would meet the requirements and withstand the loads resulting from pressure differential and induced stresses. The investigation established that a volume change greater than that required could be achieved with stress levels well within the structural capabilities of materials selected. The change in chamber volume as a function of temperature is compared with the required volume change in Figure 5-12. The shell thickness selected was more than adequate to resist the pressure loads existing. Although the change is greater than required, it is possible to match the change to that required by proper dimensional selection.

A drawing of one-half of the volume chamber is shown in Figure 5-13. Specifications for the chamber are:

Rim material	AISI 410 stainless steel (coefficient of expansion 5.3×10^{-6})
Shell material	AISI 304 stainless steel (coefficient of expansion 8.0×10^{-6})
Poisson's ratio	$\nu = 0.21$ (dimensionless)
Young's modulus	$E = 28{,}000{,}000$ psi
Radius of spherical shell at initial temperature	$r = 20.98$ in
Thickness of spherical shell	$t = 0.045$ in
Angle between axis and edge of shell	$\theta = 6$ deg
Outer diameter of shell	$D = 4.75$ in

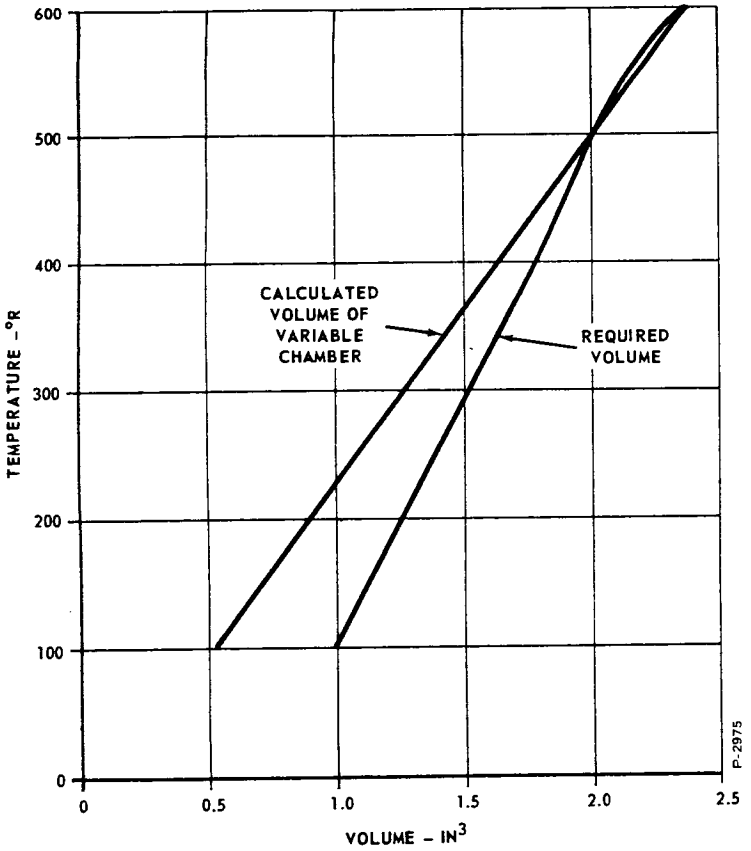

Figure 5-12 - Volume Change and Required Volume Change With Temperature

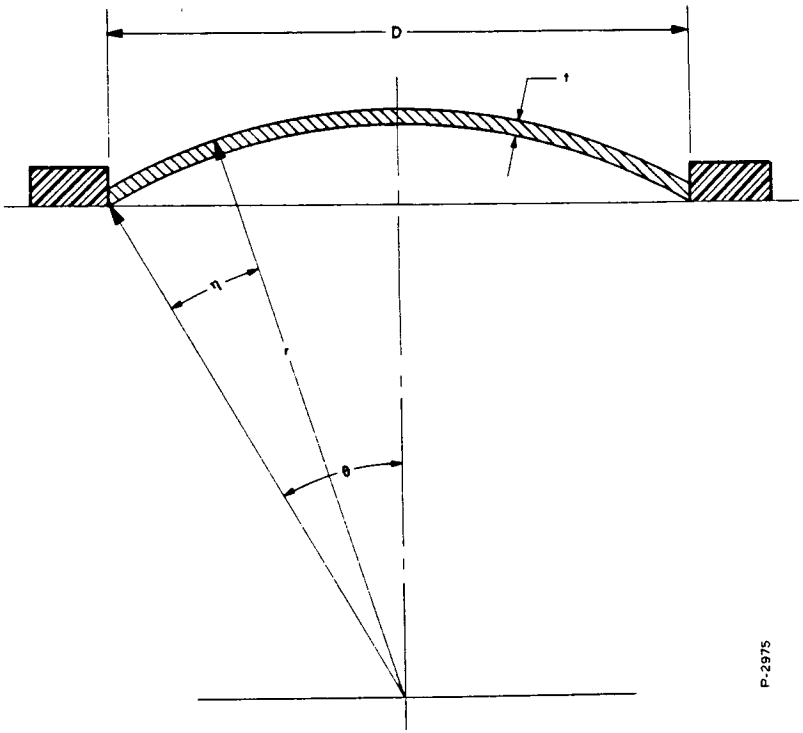

Figure 5-13 - Section of Variable Volume Chamber

In the analysis, the stresses in the shell were established from 600°R to 100°R and are presented in Table 5-3 for the worst case at 100°R. The stresses due to the pressure load are not set forth because they are small in comparison to thermally generated loads, as long as the pressure differential is small. The critical buckling stress, σ_{cr} is 35,490 psi for the shell. The table indicates that all compressive stresses are well below this value. The maximum tensile stresses are also within the capability of the materials selected.

5.4 VORTEX VALVES AND AMPLIFIERS

Vortex valves and pressure amplifiers are used to implement the amplification and frequency compensation circuits of the actuation system. Appendix II explains how these devices function. Table 5-1 lists gain characteristics required for all individual vortex elements used in the circuit. Experimental data relating to vortex valves and pressure amplifiers of the size selected for use in the actuation system are presented in this section. The data verify that the gain characteristics required for these devices can be achieved.

Table 5-3 - Stresses in Spherical Shell of Variable Chamber

h	σ_2	σ_M	σ
0	30,750	54,480	85,230
0.5	29,190	35,830	65,020
1.0	24,610	18,540	43,150
1.5	20,840	9,960	30,830
2.0	16,030	2,292	18,320
2.5	11,580	-2,645	8,933
3.0	7,763	-5,422	2,341
3.5	4,696	-6,615	-1,919
4.0	2,376	-6,726	-4,349
4.5	731	-6,162	-5,431
5.0	-345	-5,239	-5,584
5.5	-972	-4,181	-5,154
6.0	-1,266	-3,141	-4,407

P-2975

σ_2 = Hoop stress - psi

σ_M = Bending stress - psi

σ = Meridional normal stress in the extreme fiber of the shell - psi

h = Angle measured from edge of spherical shell - deg.

\- denotes compressive stress

Most of the tests were run at room temperature using nitrogen as the supply gas. To verify that these data are valid for other supply gases and temperatures, gain characteristics of a pressure amplifier were established using both nitrogen and helium. The results indicated that gain characteristics of these devices are not affected by the gas and, therefore, should not be affected by the temperature of the gas.

5.4.1 Vortex Valves

Vortex valves are used in the lead-lag circuit of the actuation system and are labeled V_{13} and V_{14} in the Figure 3-6 system schematic. The circuit function is analogous to an emitter-follower transistor circuit and, therefore, is called a pressure follower. The change in output flow as a function of control pressure is not critical but should be as high as possible to realize as large a pressure swing as possible at the supply port of the device. The maximum pressure gain of such a circuit is 1 psi/psi. A gain of 0.8 psi/psi is assumed for the circuit in the performance study and should be more than adequate.

Approximately 80 percent of the pressure swing realized at the supply port of the valve can be made available at the control inlet of the vortex amplifier V_{11}. With this available pressure swing, a potential feedback gain of 0.64 psi/psi can be achieved as compared to the required gain of 0.5 psi/psi. Figure 5-14 shows the operating test characteristics of a vortex valve used as a pressure follower. The test conditions simulated those encountered in the system circuit, and a gain of 0.916 psi/psi was achieved.

5.4.2 Vortex Pressure Amplifiers

Vortex pressure amplifiers with an external pressure pick-off are used for amplifiers V_1 through V_{12} in the system's amplification and frequency compensation circuits. All have essentially identical chamber and exit geometries, but control flow inlet orifice areas are varied to set gain. Exact conditions of operation for each stage have not been simulated in vortex amplifier tests; the ranges of operation have been tested, however, and effects of vent back pressure explored.

The range of gains required runs from 2.73 psi/psi for V_1, V_2, V_5, and V_6 to a maximum of 18.6 psi/psi for V_9 and V_{10}. Gains in excess of 13 psi/psi have been demonstrated with a vortex amplifier test model having a vortex chamber diameter of 0.25 in. No difficulty in meeting required gain values is anticipated, because the control flow inlet area can be enlarged to achieve the desired values.

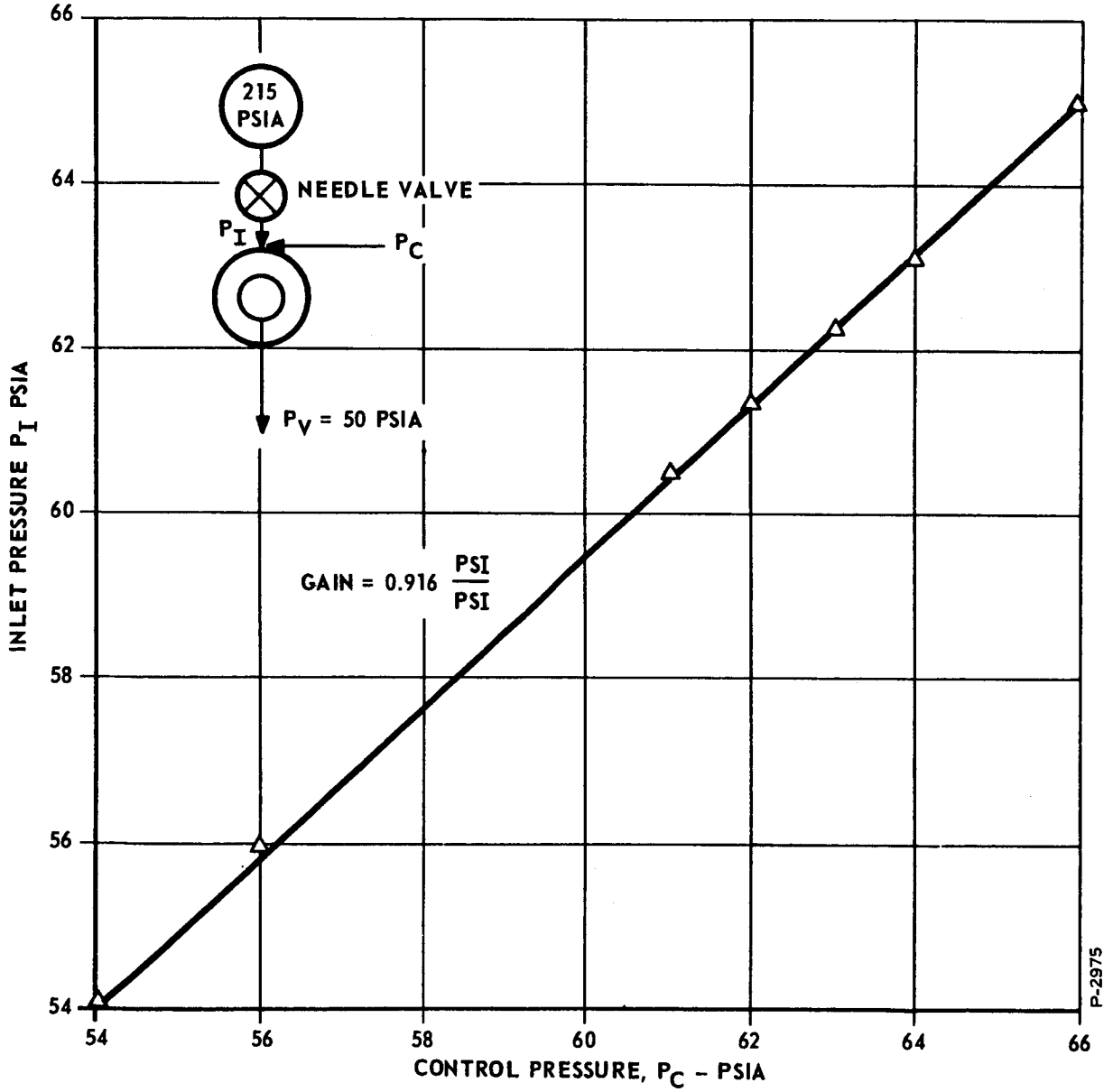

Figure 5-14 - Pressure Gain Characteristics of 0.25 in Chamber Diameter Vortex Valve in Pressure Follower Mode

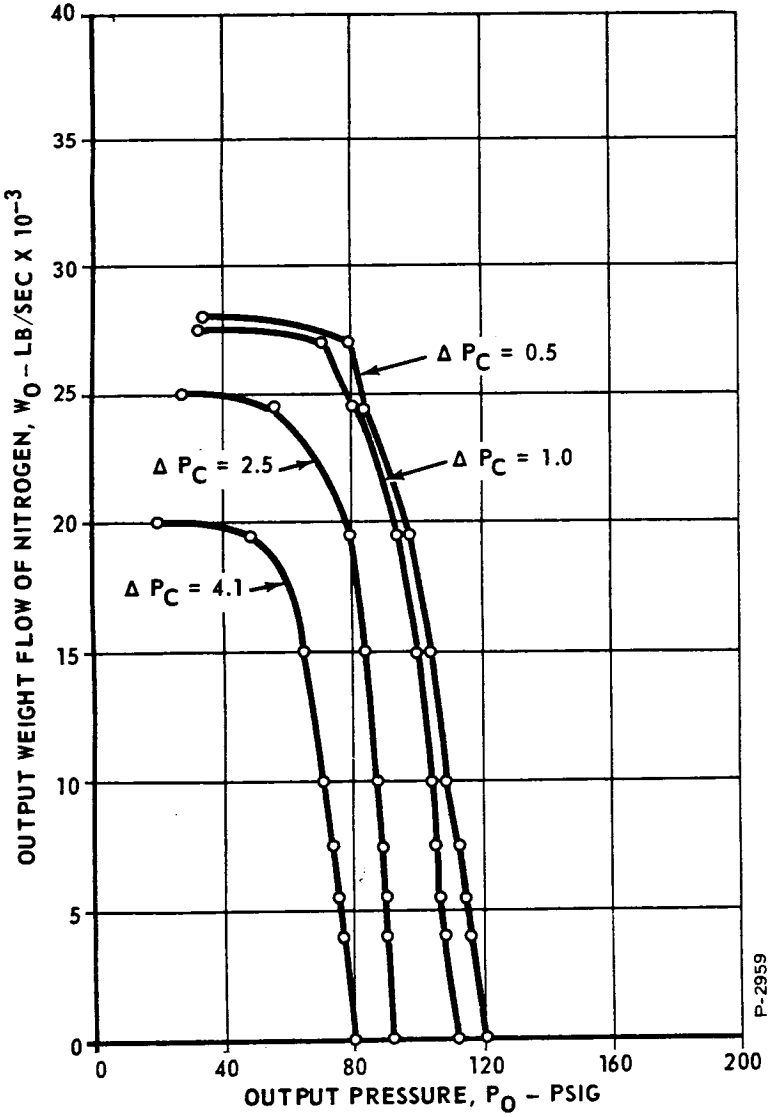

Figure 5-15 - Load Flow Versus Load Pressure for P_S of 150 psia

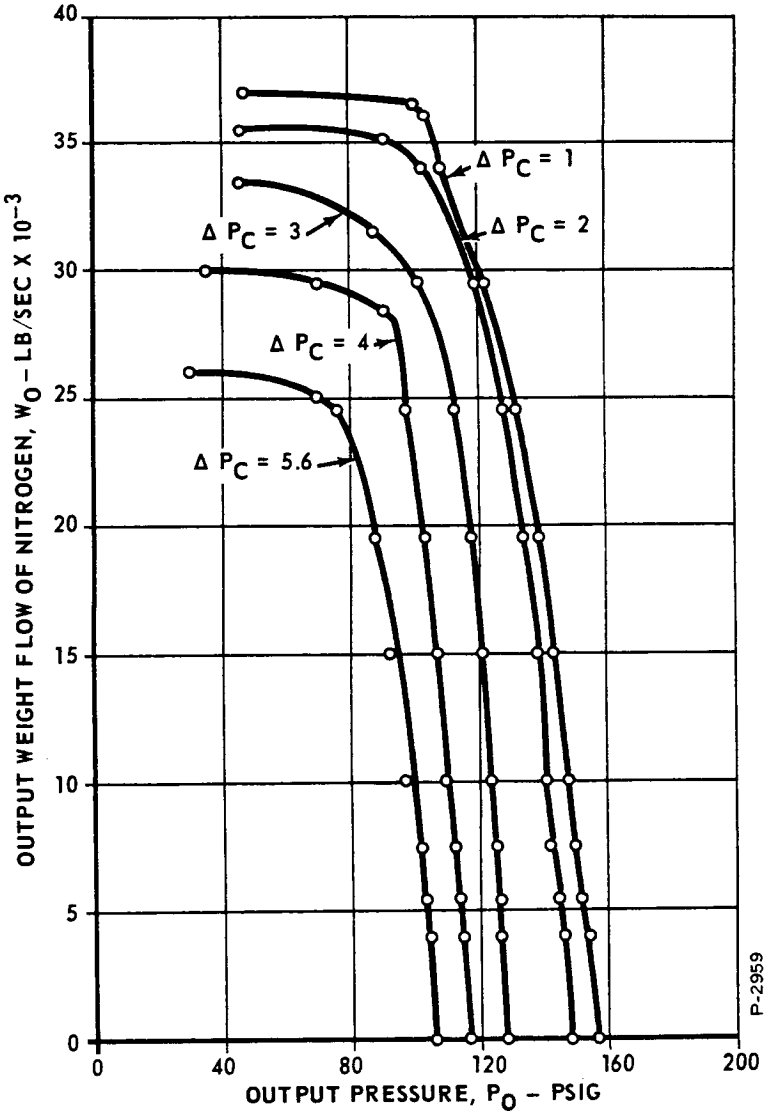

Figure 5-16 - Load Flow Versus Load Pressure for P_S for 200 psia

Figure 5-15 and 5-16 show load flow versus load pressure characteristics of the 0.25 in diameter amplifier test model. In these figures:

P_S = supply pressure to vortex valve

P_C = control pressure

P_O = pressure to the load

P_V = vent pressure

W_o = load flow

W_N = normalizing flow.

Figure 5-17 is a normalized plot derived from data of Figures 5-15 and 5-16. C can be interpreted as lines of constant control pressure, by proper conversions. The parameter C is a function of control gas angular momentum divided by a normalizing momentum.

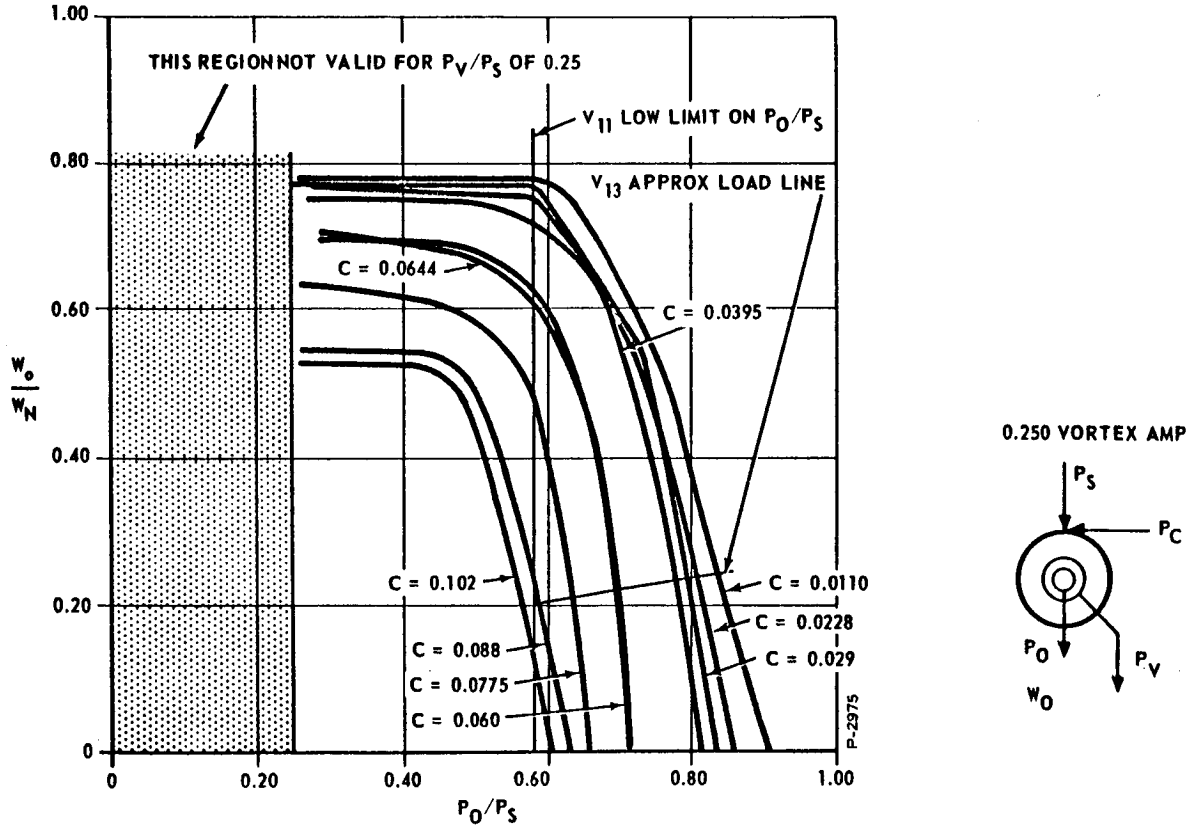

Figure 5-17 - Normalized Load Flow for Lines of Constant C

The normalizing momentum is a function of the vortex valve supply pressure, the vent pressure, and the vortex valve exit area. This plot allows the test data of a particular internal configuration of one size amplifier to be scaled from one set of operating pressures to another within a given range of P_V/P_S. For a given size amplifier of fixed geometry, it should be possible to predict pressure gain with a specified load within 5 percent.

With increasing values of P_V/P_S, the shaded section of Figure 5-17 becomes invalid. When the value of P_V/P_S gets above about 0.7, the valid area of the figure is substantially reduced, and the remainder of the plot shifts toward higher P_O/P_S values at the zero line of W_o/W_N. This shifting has been verified, and Figure 5-18 and 5-19 show the results of operating with a smaller separation of P_S and P_V. The mean value of P_O with a load is 193 psia or a P_O/P_S of 0.965. In this test, the load orifices used to derive the data are similar to those required if the following stage, of approximately the same size, is going to have a gain of 7 to 14 psi/psi.

It is established, therefore, that the operating regimes proposed are feasible with the present device.

Applying Figure 5-17 data, consider amplifier V_{11} of Figure 3-6 where the P_O/P_S range is on scale. The load in this case is nearly constant since the bellows draws only transient flow and V_{13} operates with a small difference between P_O of V_{11} and P_S of V_{13}. Assume P_O of V_{11} minus P_S of V_{13} is 1 psi. The normalized initial load flow, W_o/W_N, is equal to 0.22 at a P_O/P_S of 0.7. Since flow is almost constant, but does increase slightly as P_O increases, the load line is approximately as sketeched on Figure 5-17. This load line now shows the C values that are required by V_{11} to meet each value of output pressure. The C values in turn are used to determine P_C for a given control orifice or, conversely, the control orifice area required at a given value of input P_C.

When the normalized plot has been extended to lower values of P_V/P_S operation, a complete tool for systematic detailed stage design will be available. In the meantime, sufficient operating points have been examined to complete the system design and calculate maximum flow consumption.

Since this test was run on nitrogen, it was desirable to establish that use of a lighter gas would give essentially the same results. Figure 5-20 demonstrates the result of substituting helium for

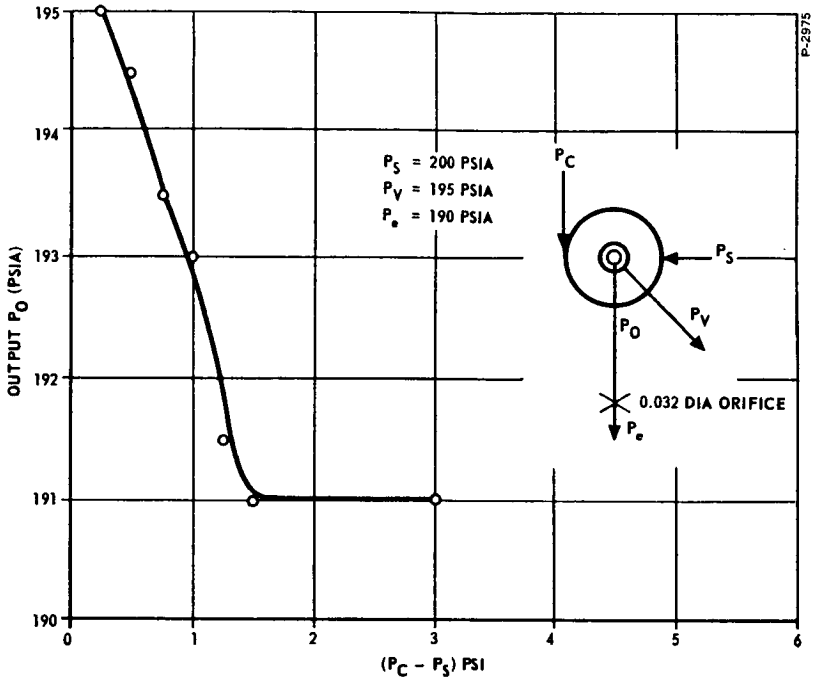

Figure 5-18 - Pressure Gain Characteristics of 0.25 in Chamber Diameter Vortex Amplifier Unit with 0.32 in Diameter Load Orifice

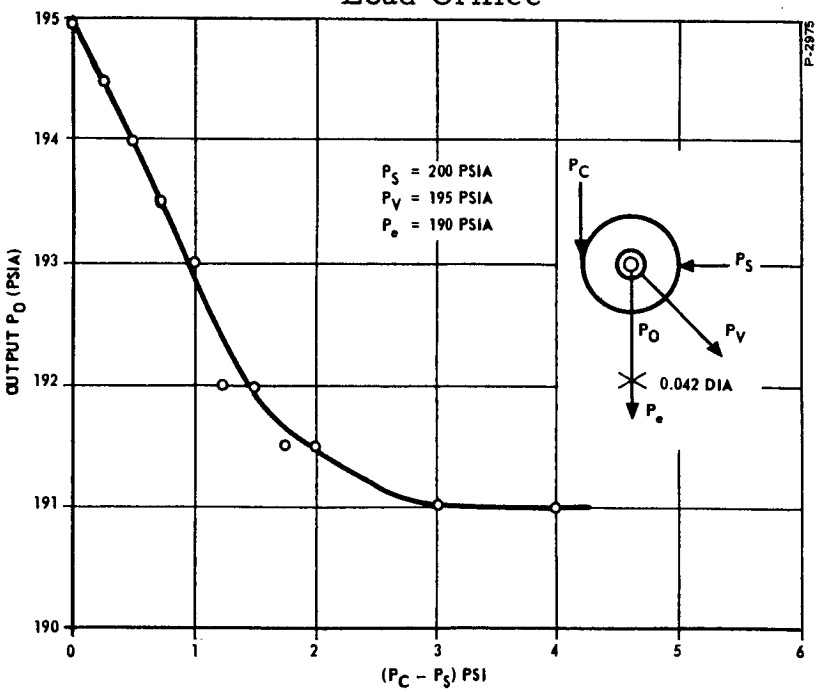

Figure 5-19 - Pressure Gain Characteristics of 0.25 in Chamber Diameter Vortex Amplifier with 0.042 in Diameter Load Orifice

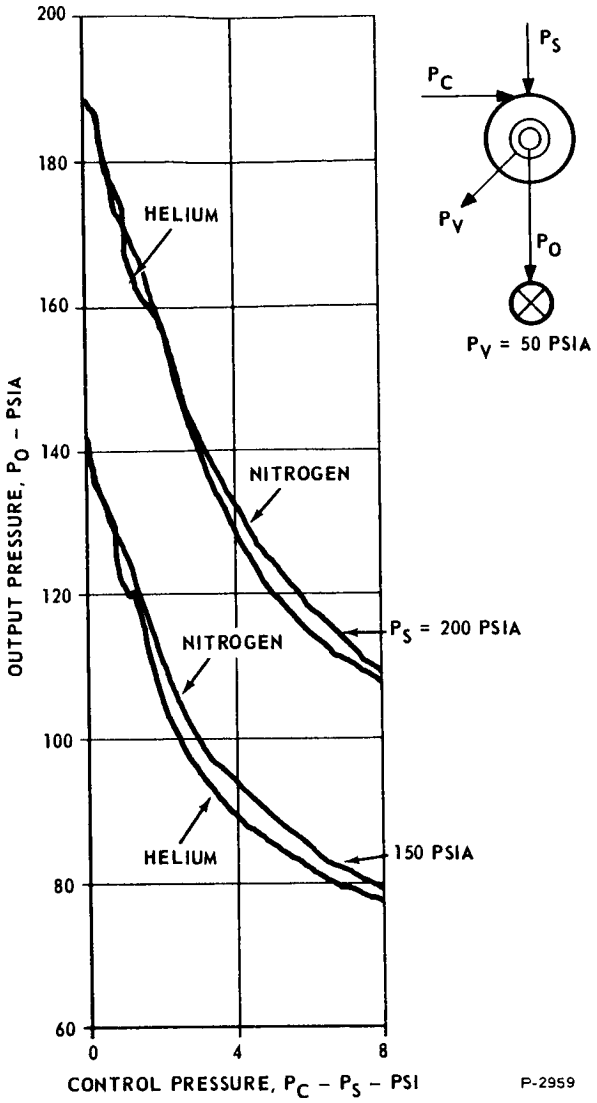

Figure 5-20 - Pressure Gain Characteristics of 0.25 in Diameter Vortex Amplifier with Helium and Nitrogen as the Supply Gas

nitrogen. The curve shift noted is slight and is within the error limits of the test set-up. This confirms theoretical reasoning that there should be no appreciable change of performance with changes in the square root of RT as long as both control and supply gas change. Since the ratio of specific heats, γ, of helium differs from both nitrogen and hydrogen, some changes in the f_1 function of the orifice flow equation occur which do not entirely cancel out. This indicates that the region below 200°R, where the γ of hydrogen changes appreciably, will be an area where

small gain changes can be expected. There are, however, no gains which are extremely critical in determining stability, and position accuracy is now a matter of area matching, rather than divider gain matching. Thus, hydrogen testing should not result in unexpected developments.

It is theoretically possible for the output flow of amplifiers V_{11} and V_{12} to be much smaller and still provide a negligible time constant for charging the driving bellows of the flapper valve. A reduction of 10 to 1 is theoretically possible. This would then reduce the size of all upstream vortex amplifiers, and if the position error detector orifices were kept the same size, would make it possible to get substantially more gain from the V_1 and V_2 amplifiers, possibly eliminating V_3 and V_4. The same reduction would apply to the rate channel. The lag tank sizes would reduce almost proportionately, since the resistance components of the circuits would be increased. This 10 to 1 reduction would result in valve diameters of $0.250/\sqrt{10}$ inch or about 0.079-in chamber diameter, and a vortex amplifier of 0.070 in chamber diameter.

The performance study assumes that internal stage lags do not exceed 0.001 second at 100 °F. This is the lag in probe pressure versus control pressure change. This lag is actually somewhat less than the pressurization time constant and is believed to be substantially below 0.001 second for the 0.250-in chamber diameter amplifier.

Orifices sizes within the 0.25-in chamber diameter vortex amplifier are equivalent to standard number size drills, and current techniques now being used allow these orifices to be drilled.

Figure 5-21 shows the blocked pickoff pressure gain of a vortex amplifier with a 0.072-in diameter chamber. While extensive test data are not yet available, the gain obtained is very promising and indicates the feasibility of scaling down from the 0.25-in diameter vortex amplifier wherever circuit conditions warrant.

5.5 POWER CONTROL VALVE

The power control valve, which is of the flapper-nozzle type and utilizes dynamic pressure feedback for compensation, converts the output signal of the amplification and compensation network to a power signal to the piston actuator. Figure 5-22 shows schematically the power control valve flapper-nozzle assembly. The mechanical design parameters were established using the sizing procedure presented in

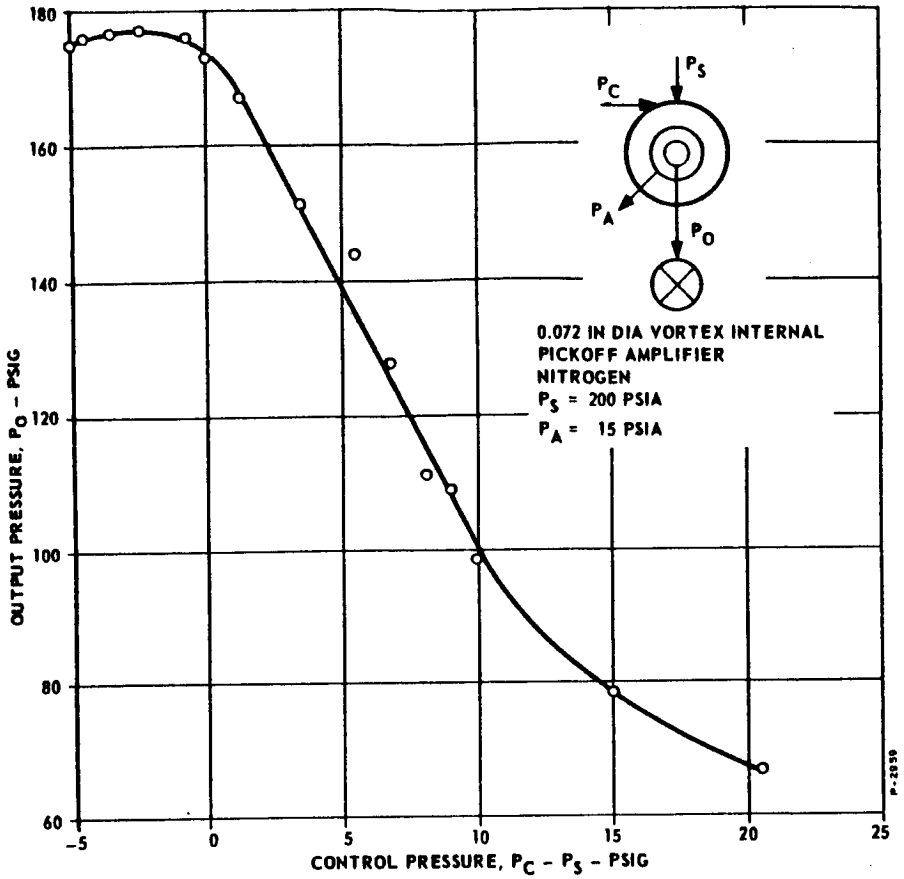

Figure 5-21 - Pressure Gain Characteristics 0.072 in Diameter Vortex Amplifier

P-2975

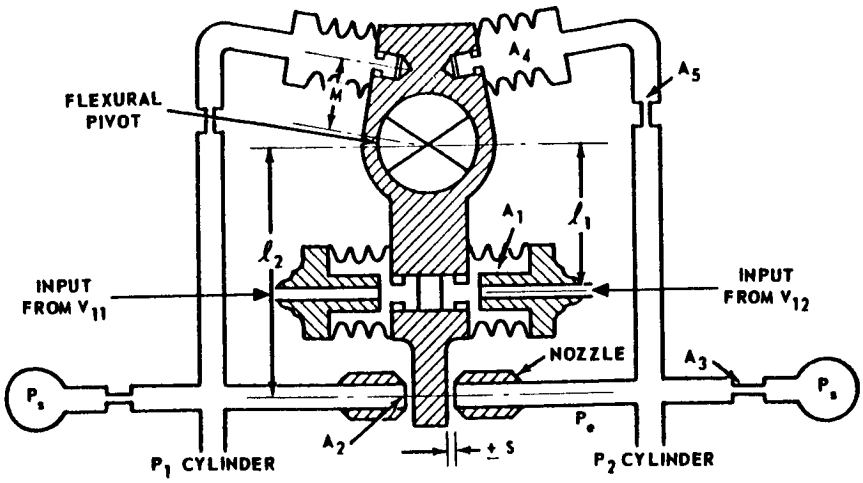

Figure 5-22 - Schematic of Flapper Nozzle Assembly of Power Control Valve

Appendix VI and in the valve simulation for the performance study. These design parameters are:

Supply orifice area	A_3	$= 0.00144\ in^2$
Mean variable orifice area generated by nozzle and flapper	A_0	$= 0.00288\ in^2$
Ratio of positive to negative pressure feedback	$\frac{A_4 M}{A_2 \ell_2}$	$= 0.90$
Gain for negative pressure feedback	$A_2 \ell_2$	$= 7.675\ \frac{\%\ stroke}{psi}$
Gain for differential input	$A_1 \ell_1 K_3$	$= 18\ \frac{\%\ stroke}{psi}$
Estimated polar moment of inertia of flapper assembly used in the simulation of the valve	J_F	$= 17.6\ 10^{-6}\ lb\text{-}in\text{-}sec^2$
Minimum allowable value for the undamped natural frequency of the flapper assembly squared	ω_F^2	$= 1{,}960{,}000\ \frac{radian^2}{sec^2}$

Using these general parameters and selecting values for variables, specific design values were developed. Variables were dictated by size limitations and the desire to use standard parts for the flexural pivot and the bellows. Generation of the valve's specific design values is presented. The specifications are also presented for the bellows selected because they are a critical item in the design of the valve.

The valve flapper is supported by a Bendix flexural pivot. The control pressures to the flapper are ported to bellows area A_1 at a moment arm of distance ℓ_1 from the flexural pivot with a resulting flapper stroke S, at a moment arm of distance ℓ_2. The cylinder Pressures, P_1 and P_2, are sensed through orifice area A_5 by the positive pressure feedback bellows area A_4 at a moment arm of distance M from the pivot.

The square of the undamped natural frequency of the flapper nozzle assembly is given by the expression:

$$\omega_F^2 = \frac{K}{J_F}$$

where K is equal to the effective spring rate of the flapper assembly about its pivot and includes the effect of the bellows and the flexural pivot. From this expression and using an estimated polar moment of inertia of the flapper from the simulation and the minimum value for ω_F^2, a minimum spring rate of 34.5 lb-in per radian was established. With this as a basis, a flexural pivot with a spring rate of 52.0 in-lbs per radian was selected and, when combined with a bellows acting on the flapper, gave the flapper an effective spring rate of 78.5 lb-in per radian. This is substantially higher than required. The section modulus of the flapper was sized to limit the cantilevered deflection of the flapper at the nozzles to less than 5 percent of the stroke amplitude when in a worst-case loaded condition. The polar moment of inertia was then re-estimated at 13.8×10^{-6} in-lb-sec^2, which is less than the maximum allowable value.

Now the negative pressure feedback and A_O values must be satisfied simultaneously.

$$0.07675\ S = \frac{A_2\, \ell_2^{\,2}}{78.5} \qquad \text{inches of arc at radius } \ell_2 \text{ for one psi of negative feedback}$$

$$(0.00288) = \pi \sqrt{\frac{4\, A_2}{\pi}}\ S$$

This is derived from the relationship between the area of A_2, the stroke in inches, and the area A_O.

If ℓ_2 is set at 1.1 in, then A_2 and S can be derived.

$$S = 0.0051 \text{ in}$$

$$A_2 = 0.0257 \text{ in}^2$$

Now:

$$A_4 M = 0.90\ (A_2 \ell_2) \text{ in}^3$$

$$A_4 M = 2.54\ 10^{-2} \text{ in}^3$$

A_4 is selected from stock bellows sizes and M is determined.

$$A_4 = 0.0705 \text{ in}^2$$

$$M = 0.364 \text{ in}$$

Similarily, the input bellows area can be chosen as 0.145 in^2. Since $A_1 \ell_1 K_3$ is equal to 18 percent of the stroke, K_3 has the units of percent stroke per lb-in. The value from previously calculated stroke and flapper spring rate values is:

$$K_3 = 169.5 \frac{\% \text{ stroke}}{\text{lb-in}}$$

Then:

$$\ell_1 = \frac{18}{(169.5)(0.145)} = 0.732 \text{ in}$$

This completes the power control valve sizing except for the details of the bellows. When the bellows lever arm lengths are established, a check must be made to see that the assumed spring rate is correct. If it is off slightly, only the gains are affected. The gain ratios remain unchanged.

Using the bellows spring rates and the established lever arm lengths, the flapper assembly spring is 71.4 lb-in per radian versus the initially estimated 78.5 lb-in per radian value. Since the estimated value is needed to calculate stroke and establish lever arms, the only way to get a final set of figures in perfect agreement is to go through the calculation again with an adjusted spring rate value. The resulting changes would approach the limits of accuracy of much of the catalog data; therefore, the values already calculated may be considered final, pending more precise component data.

The bellows used are of electro-deposited nickel made in a standard size. The required stroke of the bellows is less than 10 percent of the maximum allowable stroke at maximum pressure differential. The maximum pressure differential acting on the bellows is considerably below their nominal rating. This short stroke will contribute to a long fatigue life for the bellows. An insert is used in bellows A_1 to reduce the volume of compressed gas. The specifications for the bellows are given below.

(A) Input Pressure Bellows (A_1)

Number of convolutions	=	8
Effective area	=	0.145 in^2
Spring rate	=	7.0 lb/in

Outside diameter	=	0.50 in
Inside diameter	=	0.36 in
Wall thickness	=	0.0012 in
Bellows active length	=	0.256 in
Nominal pressure rating	=	71 psid
Allowable stroke at nominal pressure rating (for minimum life expectancy of 100,000 strokes)	=	0.048 in
Maximum required stroke	=	0.0035 in
Maximum pressure differential	=	10 psid
Allowable stroke at maximum pressure differential (100,000 strokes)	=	0.096 in

(B) Positive Feedback Bellows (A_4)

Number of convolutions	=	6
Effective area	=	0.0705 in^2
Spring rate	=	45 lb/in
Outside diameter	=	0.375 in
Inside diameter	=	0.250 in
Wall thickness	=	0.002 in
Bellows active length	=	0.193 in
Nominal pressure rating	=	247 psid
Allowable stroke at nominal pressure rating (100,000 strokes)	=	0.0225 in
Maximum required stroke	=	0.0016 in
Maximum pressure differential	=	165 psid
Allowable stroke at maximum pressure differential (100,000 strokes)	=	0.044 in

APPENDIX I

REQUIREMENTS AND SPECIFICATIONS

This appendix lists the system component requirements, performance specifications, and environmental conditions under which the actuation system must operate, as specified in the contract.

I.1 SYSTEM COMPONENT REQUIREMENTS

In the analysis, all fluid interaction components used in the actuation system shall be described. The description shall contain performance calculations substantiated by sufficient experimental evidence to support the use of the proposed components.

I.1.1 Input Transducer

The input transducer shall be capable of receiving an electrical command signal and converting it to a pneumatic command signal. This shall be the only electronic component permitted in the servo system and may contain moving mechanical parts. Selection of the electro-mechanical input transducer shall be based upon the following requirements:

(a) System performance specifications shall be met without subtracting out errors, nonlinearities, etc., of the input transducer.

(b) The input transducer shall be capable of functioning under the environmental conditions described in subsection I.3.

(c) The input transducer shall not require a driving signal larger than 20 volts at 200 milliamperes.

(d) The system static and dynamic characteristics shall be specified only in terms of voltage or only in terms of current applied to the input transducer.

I.1.2 Summing Junction

The summing junction shall be a pneumatic device with no moving parts.

I.1.3 Preamplifier and Frequency Compensator

The preamplifier and frequency compensator shall be fluid interaction devices which contain no moving mechanical parts.

I.1.4 Power Valve

The power valve shall be a pneumatic valve which may contain moving mechanical parts. It is desirable that the power valve be a fluid interaction device with no moving mechanical parts, but this is not a requirement of this investigation.

I.1.5 Actuator

The actuator shall be a General Electric AG-20 actuator-motor. The rotation of the actuator-motor output shaft shall be considered the output of the servo system. A scram spring shall be provided to drive the output shaft to zero when pneumatic power to the actuator-motor is stopped.

I.1.6 Position Transducer

The output shaft position pickoff transducer shall be a pneumatic device which may contain moving mechanical parts.

I.2 ACTUATION SYSTEM PERFORMANCE SPECIFICATIONS

I.2.1 Rated Load Characteristics

(a) Total inertia of load	92.5 lbm $-in^2$
(b) Load friction	32 in-lbf static 25 in-lbf dynamic
(c) Bias (scram) spring loading in direction of 0° drum rotation (± 10 in-lbf)	50 in-lbf @ 15° rotation

I.2.2 Static Performance Characteristics

(a) Travel	0° to 180° ± 1° maximum 15° to 165° ± 1° working
(b) Static position resolution at the actuator output shaft	± 0.2°

(c)	Static linearity of output shaft position to electrical command signal to input transducer	± 4% of full travel (specification) ± 1% of full travel (goal)

I.2.3 Dynamic Performance Characteristics

(a)	Transient response to an 18° step input	
	(1) Rise time to 62.5% of step command	0.055 sec
	(2) Settling time to within 0.9% of command	0.15 sec
	Allowable overshoot (maximum)	6°
(b)	Frequency response to a ± 2° input	
	(1) Phase shift at 6 cps (maximum)	90°
	(2) Phase shift at 12 cps (maximum)	180°
	(3) Output shaft amplitude variation from 0 to 8 cps	Less than ± 3 db
(c)	Maximum dynamic resolution at 3 degrees/sec slewing velocity	± 0.5°
(d)	Maximum slewing velocity	± 300°/sec

I.2.4 Fluid Requirements

(a)	Actuator power	
	(1) Working fluid	Hydrogen (dry air, nitrogen, or helium or any combination of these gases may be used to

	simulate hydrogen at temperatures at/or less than 400°R, providing that the contractor offers proof that the substitution of these gases approximates the use of hydrogen at those temperatures.)
(2) Supply pressure	215 psia ± 10 psi
(3) Exhaust pressure	50 psia ± 5 psi
(4) Supply gas temperature	Arbitrary
(5) Gas consumption	0.04 lbm/sec of hydrogen at a temperature of 100°R The NRTO Project Manager shall have the option of relaxing this requirement, under certain circumstances, by permitting the flow rate to be increased to 0.075 lbm/sec of hydrogen at 100°R.

I.2.5 Operational Life

All components, except the basic G.E. AG-20 actuator-motor, shall be capable of operating continuously for at least 200 hours without breakdown when subjected to the vibration environment listed in subsection I.3.

I.3 ENVIRONMENTAL CONDITIONS

The prototype actuation system shall be capable of operation under the environmental specifications denoted by asterisk (*) in the following list. Performance under the environmental conditions preceded with a dagger (†) shall be considered as a desirable goal, that will ultimately be required for an actuation system. Therefore, no materials or components shall be selected that are inherently incompatible with this environment.

I.3.1 Environmental conditions during non-operation

(a)*	Shock along all axes	6 g's
(b)*	Vibration along axes	6 g's amplitude from 0 to 20 cps. Vibration increases linearly to 20 g's amplitude at 200 cps and remains constant up to 2000 cps.
(c)*	Acceleration	8 g's along output shaft axis 1 g normal to ouput shaft axis;
(d)†	Ambient air pressure	Sea level to 0.5 in. Hg
(e)†	Ambient air temperature	Room temperature to -70°F
(f)†	Radiation field	Essentially negligible before reactor startup. Not known after reactor shutdown but

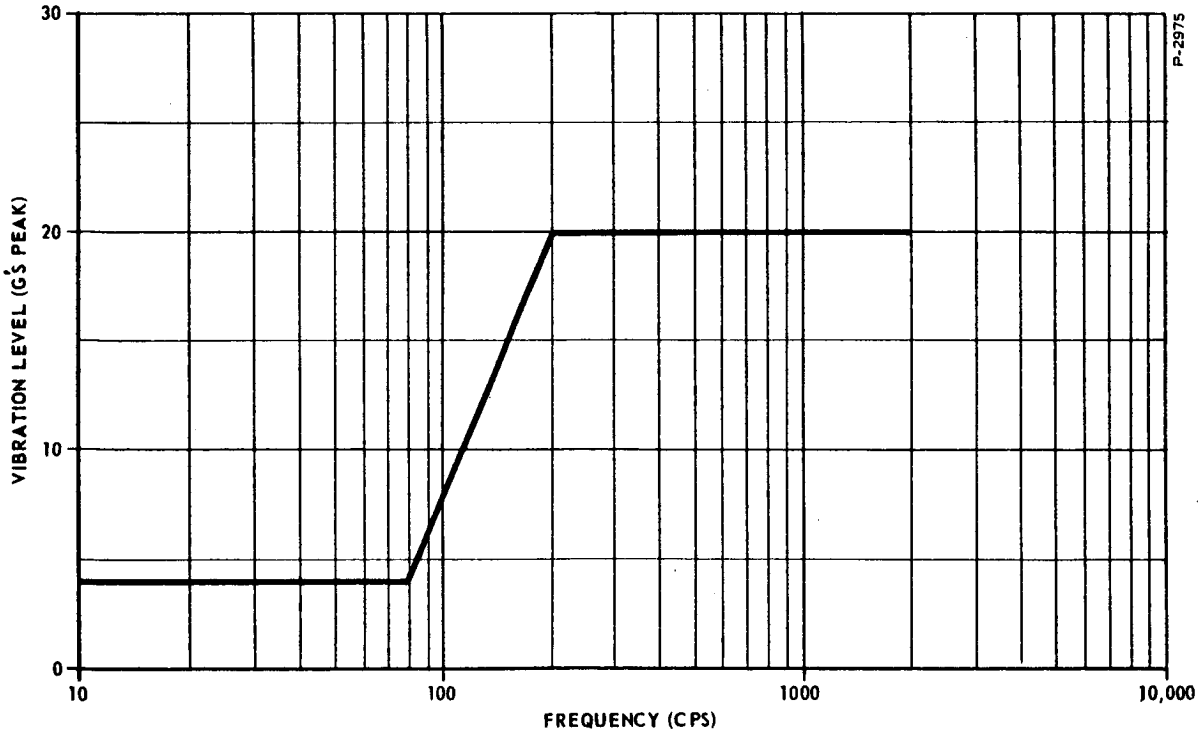

Figure I-1 - Variation of Vibration Level Versus Frequency

estimated to be small in comparison to that existing during reactor operation.

I.3.2 Environmental conditions during system operation

(a)*	Shock loading	Negligible
(b)*	Vibration	4 g's from 0 to 50 cps. 20 g's from 80 cps to 2000 cps (See Figure I-1).
(c)*	Acceleration	1.2 g's along output shaft axis. 0.6 g's normal to output shaft axis.
(d)‡	Radiation field	
	(1) Total dose	6×10^6 rads (ethylene) 1 hour.
	(2) Fast neutron flux rate (E 1.0 mev)	3×10^{11} neutrons/cm^2 sec
	(3) Gamma heating (equivalent)	350 watts/lbm aluminum
(e)‡	External pressure	Less than 10^{-9} mm Hg

APPENDIX II

VORTEX DEVICES

Three basic types of fluid interaction devices were considered during the preliminary system design. Two of the devices are used in the final design. These are the "vortex valve" and the "vortex pressure amplifier." These devices will therefore be described first and in the most detail.

The other device considered was a vorjet amplifier. It is described briefly.

II.1 Vortex Valve

The basic vortex valve consists of a cylindrical chamber with supply flow and control flow inlets and an outlet orifice as illustrated in Figure II-1. The supply flow of gas enters the chamber and, in the absence of control flow as indicated in Figure II-1(a), proceeds radially inward without resistance and then flows out of the outlet orifice. In the absence of control flow the maximum total flow through the valve is achieved with the main pressure drop occurring across the output orifice. The chamber pressure is slightly less than the supply pressure. Control flow at a pressure above chamber pressure is injected tangentially into the chamber, as shown in Figure II-1(b). The tangential control flow

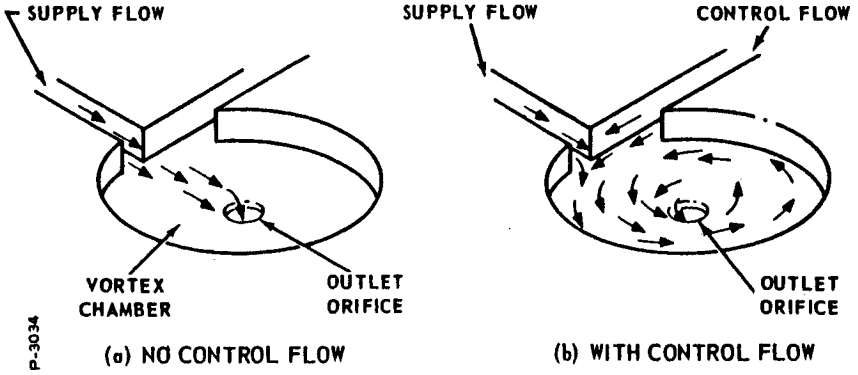

Figure II-1 - Vortex Valve

imparts a rotational component to the supply flow. The combined flow has both a tangential and a radial component. The conservation of momentum requires that the tangential velocity and the radial velocity both increase as the flow moves inward. The centrifugal force due to the fluid rotation results in a radial pressure gradient. For a constant supply pressure, this drop in pressure across the chamber reduces the pressure differential across the outlet orifice, and thus reduces the outlet flow.

A reduction in the total outlet flow as high as 7:1 has been achieved with vortex valves. At the lowest outlet flow the supply flow to the valve is virtually zero. At this point, the outlet flow is being supplied almost entirely by the control flow.

The schematic symbol of the vortex valve is shown in Figure II-2. In this figure P_v is the pressure downstream of the vent orifice, P_c is the control pressure, and P_s is the supply pressure.

II.2 Vortex Pressure Amplifier

A vortex pressure amplifier is similar to a vortex valve with the exception that a pickoff or receiver is placed in the gas stream of the outlet orifice; the pickoff acts in much the same manner as a pitot tube. The receiver pressure and flow is the output of the device. When there is no control flow, the flow out of the outlet orifice is directed into the receiver, Figure II-3(a), and the pressure and flow recovered under the condition is at a maximum. As control flow is added, the exit

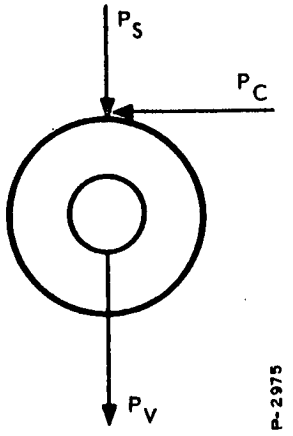

Figure II-2 - Schematic Symbol of Vortex Valve

flow fans out as shown in Figure II-3(b), and the recovered pressure decreases. Hence, the vortex pressure amplifier uses the combined effects of the vortex valve and flow diversion for obtaining amplification.

The pickoff is capable of supplying a significant amount of flow with some decrease in pickoff output pressure but very little loss in total available pressure change or in the available increment of change of output pressure versus control pressure. That is to say, the pressure gain is nearly constant for a wide range of load impedance. Figures II-4 and II-5 are examples of performance of the 0.25 inch chamber diameter vortex pressure amplifier. The weight flows shown are for nitrogen. On hydrogen, the blocked load pressures will be virtually identical, but of course the weight flow scale will change. The schematic symbol for the vortex pressure amplifier is shown in Figure II-6.

As with the vortex valve, P_s is the supply pressure, P_c is the control pressure, and P_v is the pressure downstream of the vent orifice. P_o is pickoff or receiver pressure.

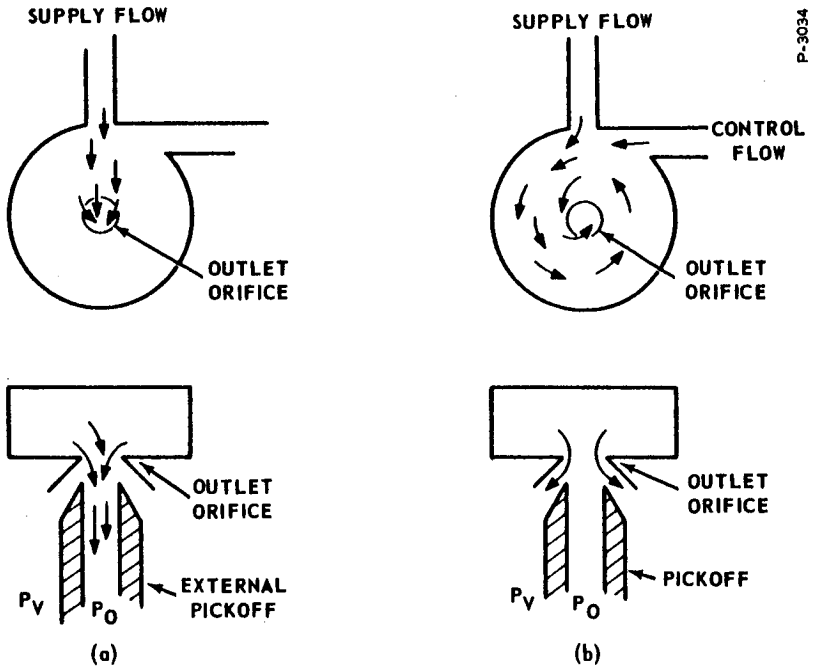

Figure II-3 - Vortex Amplifier

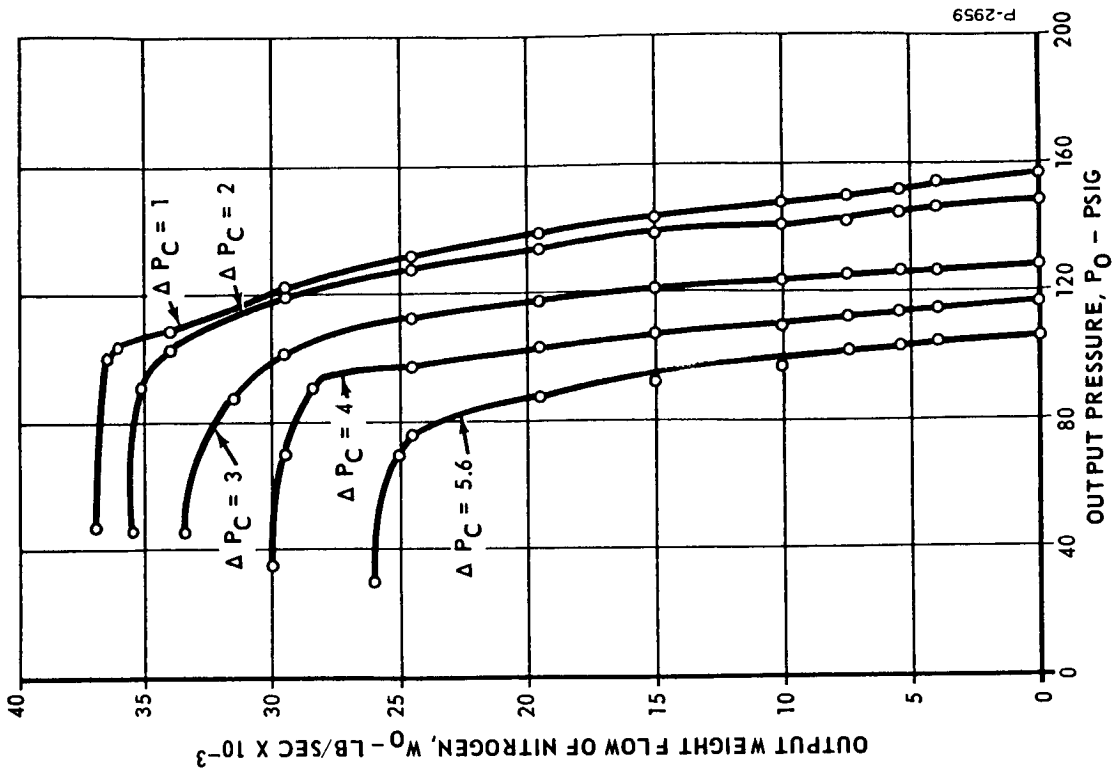

Figure II-5 - Load Flow Versus Load Pressure for P_s for 200 psia

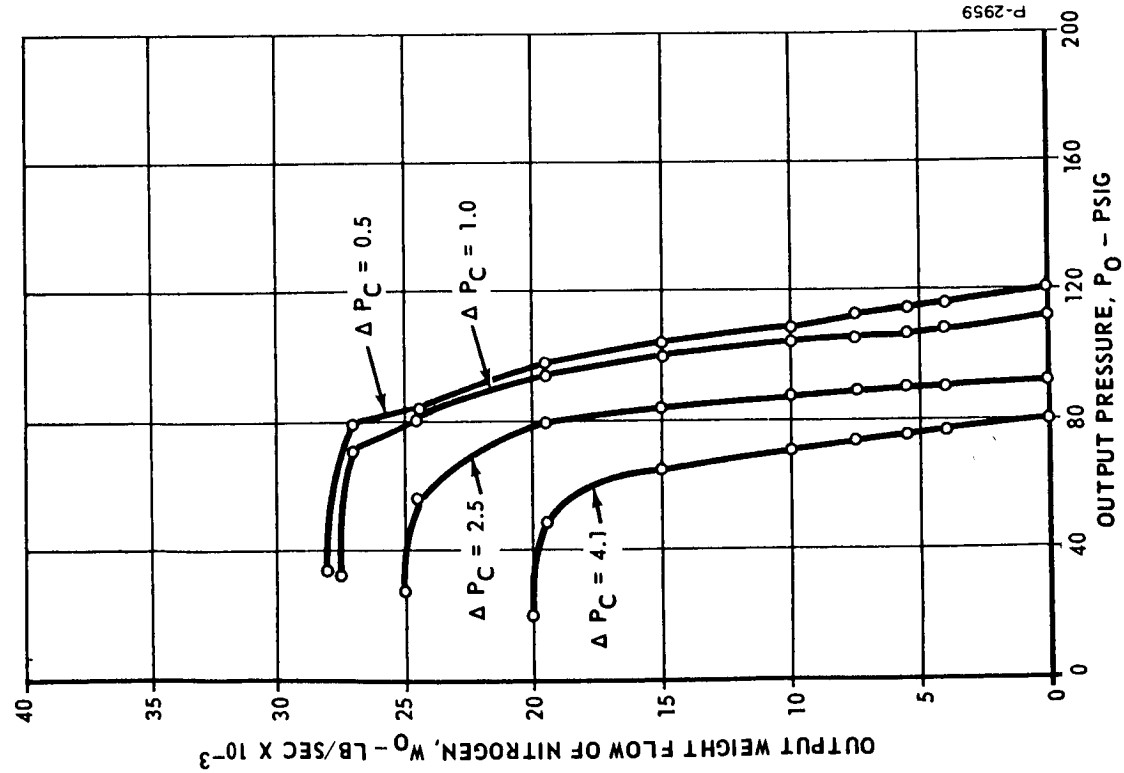

Figure II-4 - Load Flow Versus Load Pressure for P_s of 150 psia

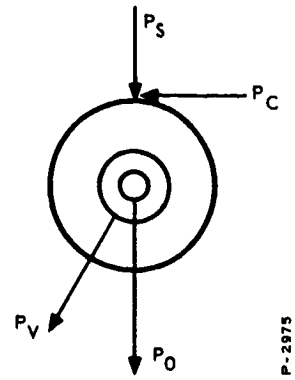

Figure II-6 - Schematic Symbol of Vortex Pressure Amplifier

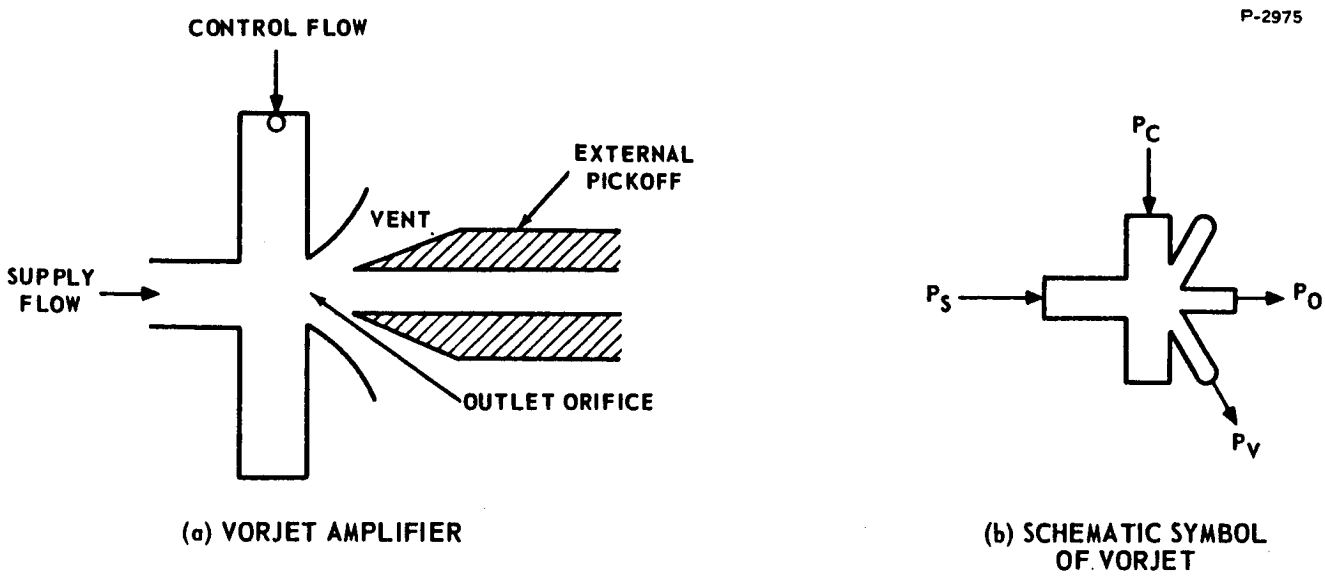

Figure II-7 - Vorjet Amplifier

II.3 Vorjet Amplifier

This amplifier was originally proposed to perform the necessary pressure level change in feedback signals around a vortex pressure amplifier. The change in pressure level is necessary since the maximum vortex output pressure is below its supply pressure and its input signals are above its supply pressure.

The construction is very much like a vortex pressure amplifier except that supply flow is introduced directly in line with the outlet orifice. See Figure II-7(a). If the control ports are blocked, a very low pressure is achieved in the vortex chamber due to the entrainment of vortex chamber gas by the supply jet. It is therefore possible to introduce a control signal at a pressure considerably below supply pressure. Since the control flow is introduced tangentially, it still has a tangential component when it mixes with the supply flow. This causes a change in the pressure recovered by the external pickoff.

Figure II-7(b) shows the schematic symbol of the device.

APPENDIX III

ANALOG SIMULATION OF AG-20 ACTUATOR-MOTOR

The AG-20 actuator-motor consists of a rotary output member driven by a relatively short stroke piston and rack arrangement. There are two separate pistons on opposite ends of the rack, with a constant pressure region between them which eliminates crossport leakage. Individual leakage to ambient is low relative to valve flow, and therefore was not simulated.

Table III-1 presents a comparison of the parameter values specified and those values used in the Bendix simulation of the actuator. Figure III-1 shows a block diagram of the power control valve and actuator simulation.

The simplest possible piston actuator simulation would assume mid-stroke conditions, without any spring loading or friction, and with the pressure source at a constant value. Then the two piston chambers would have equal volumes and initially equal pressures; so, the chambers would also have equal time constants. The simulation of the piston chambers could then be reduced to

$$P_1 - P_2 = \left(\frac{K}{T S + 1} \right) (Q_L)$$

where

P_1 and P_2 = the pressures in the two piston chambers

T = the average time sonstant of the two chambers

K = the appropriate gain and Q_L = the load flow.

Since this centered condition yields the highest pressure gain and the greatest phase lag, it is a valuable simplification for preliminary analysis. Unfortunately, near the ends of the available stroke, the chamber volumes P_1 and P_2 are very different. However, the characteristics of the actuator under these conditions can be approximated by using half of the center position gain and the time constant of the smaller chamber, since the other chamber does not change pressure fast enough to have any appreciable effect on dynamic performance.

Table III-1 - Parameter Values Used for Performance Analysis

Actuator and Load Parameter	Specified	Used In Performance Analysis	Remarks
Mid-Position Volume (V_o)	3.71 in^3 (minimum) 3.85 (maximum)		
P_1 Line	0.317 in^3		The value used in the performance analysis includes the estimated volume in the power control valve.
P_2 Line	0.381 in^3		
Total	4.23 in^3 (maximum)	4.36 in^3	
Displacement Volume	2.2 in^3/rad	2.2 in^3/rad	
Actuator Friction	Equivalent to ± 10 psi pressure differential		
Load Friction	32 lb-in static	54 lb-in static	In the performance analysis the actuator friction was added to the load friction.
	25 lb-in dynamic	47 lb-in dynamic	
Actuator Inertia	0.00183 in-lb-sec^2		The actuator inertia is considered negligible and was not included in the performance analysis.
Load Inertia	92.5 lbm-in^2 (0.24 in-lb-sec^2)	0.24 in-lb-sec^2	
Actuator Spring Load	75 in-lb @ 15° and 124 to 145 in-lb @ 180°	75 in-lb @ 15° 24.3 in-lb/rad gradient	
Leakage	60×10^{-6} lb/sec of He @ room temperature for 2 pistons		This leakage was not considered in the performance analysis because it is two orders of magnitude below the power control valve flow

P-2975

In the presence of an appreciable spring load, the situation is further altered; the maximum phase lag point is now shifted toward the end with maximum spring load, since if P_1 is higher than P_2 the higher pressure allows the volume at pressure P_1 to be larger than the volume at pressure P_2 for equal time constants. The situation is complicated even further by the valve operating off center, since the orifice resistance values are no longer equal.

In view of these general considerations and the original contract

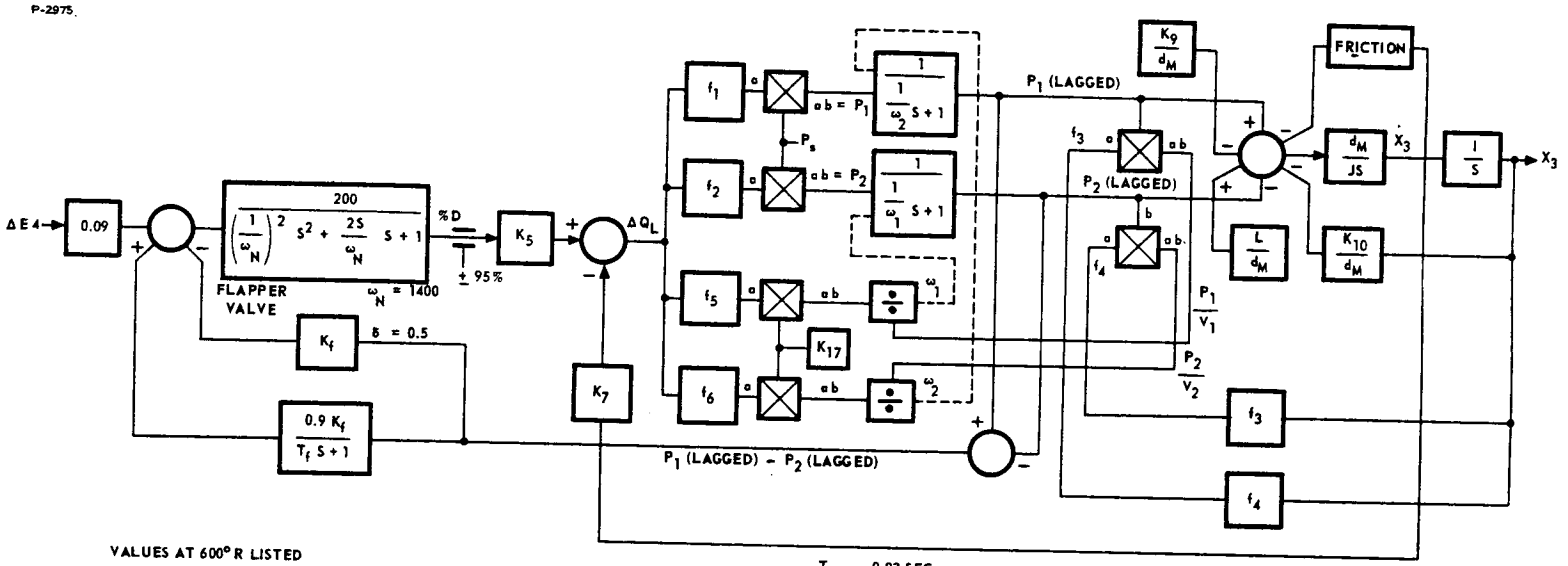

VALUES AT 600° R LISTED

- J — EFFECTIVE POLAR MOMENT OF LOAD AND ACTUATOR – LB/IN SEC^2
- K_5 — VALVE FLOW GAIN AT 600° F – IN^3/SEC PER %D
- K_7 — EFFECTIVE DISPLACEMENT FLOW = $d_M \frac{\left(\sqrt{RT}\right)\ 600° R}{\left(\sqrt{RT}\right)\ \text{SIMULATED TEMP}}$
- K_9 — SPRING PRELOAD AT – X_3 = 90° LB-IN
- K_{10} — SPRING RATE – LB-IN/RADIAN
- L — EXTERNAL TORQUE LOAD – LB-IN
- d_M — EQUIVALENT DISPLACEMENT – IN^3/RADIAN
- Δ E4 — DIFFERENTIAL PRESSURE TO FLAPPER VALVE (PSID)
- X_3 — OUTPUT ROTATION, RADIANS. ZERO X_3 = 90° MINUS X_3 = 90° TO 0°, PLUS X_3 = 90° TO 180°
- P_1 — PRESSURE TO CAUSE POSITIVE CHANGE IN X_3 – PSI
- P_2 — PRESSURE TO CAUSE NEGATIVE CHANGE IN X_3 – PSI
- P_S — SUPPLY PRESSURE – PSI
- Q_L — LOAD FLOW – IN^3/SEC
- T_f — 0.03 SEC
- K_{19} — NON-DIMENSIONAL MULTIPLIER, VALUE SCALES WITH RT LIKE K_7
- f_1 — $\frac{P_1}{P_S}$ vs ΔQ_L
- f_2 — $\frac{P_2}{P_S}$ vs ΔQ_L
- f_3 — $\frac{1}{V_1}$
- f_4 — $\frac{1}{V_2}$
- f_5 — % f_5 MAX WHERE $f_5 = \left|\left(\frac{\partial P_1}{\partial Q_L}\right)_{MAX} \left(d_M\right)\left(\frac{1}{\gamma}\right)\right|$
- f_6 — % f_6 MAX WHERE $f_6 = \left|\left(\frac{\partial r_2}{\partial Q_L}\right)_{MAX} \left(d_M\right)\left(\frac{1}{\gamma}\right)\right|$

Figure III-1 - Block Diagram of Power Control Valve and Actuator Simulation

objective of studying the effects of source pressure variations, the simulation generates P_1 and P_2 individually and each is then lagged by an amount dependent upon individual chamber volume, existing pressure in the chamber, and the effective valve resistance including effects of actuator displacement flow.

The formula for a volume-orifice system time constant is

$$T = \left(\frac{V}{\gamma P}\right) (-\partial P/\partial Q)$$

where

V = volume in^3

γ = ratio of specific heats

P = pressure lb/in^2

$\frac{V}{\gamma P}$ = volumetric adiabatic capacitance, in^5/lb

$\frac{\partial P}{\partial Q}$ = valve pneumatic resistance, $lb\text{-}sec/in^5$

and adiabatic compressibility is assumed.

Referring to Figure III-1 it can be seen that the volume lags are mechanized in a manner which adjusts the time constant in accordance with the current chamber volume, pressure, and valve flow resistance.

The effects of temperature changes are easily simulated by changing two gains (K_7 and K_{17} in Figure III-1. The first gain change simulates a fictitiously increased actuator displacement flow at low temperatures. The effect is equivalent to the reduction of valve volume flow which actually occurs. The second gain change represents an increase in the effective valve resistance sufficient to yield proper chamber time constant values.

Generation of required functions started with a study of the actuator-motor torque-speed requirements. The results are shown in Figure III-2. Note that valve operation is entirely on one side of the center except for very large transients. This is due to the heavy spring load. With this function available, the next step is to calculate P_1 and P_2 versus valve stroke for various size inlet and outlet orifices. The most desirable plot results from outlet orifices with a nominal (flapper centered) area equal to twice the inlet area. From these flow

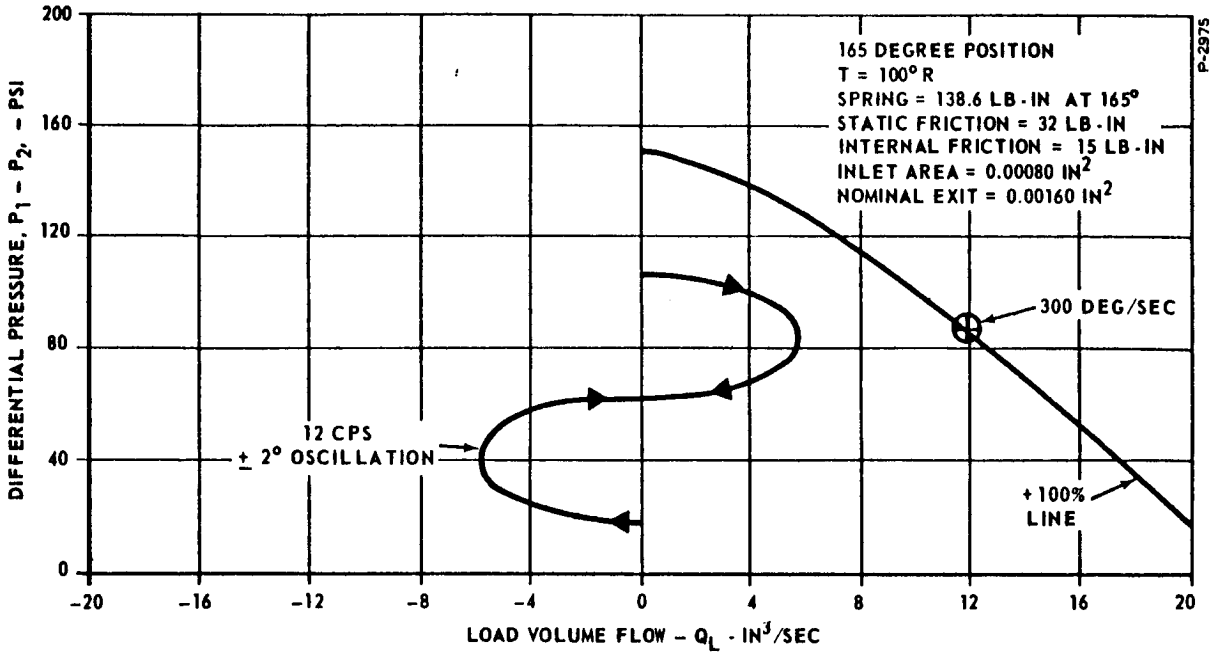

Figure III-2 - Differential Pressure Versus Load Volume Required of Power Control Valve

curves, functions f_1 and f_2 follow immediately. Functions f_5 and f_6 essentially depend on the slope of the flow plot, with certain added restrictions to keep P_1 and P_2 chamber lag frequencies, ω_1 and ω_2, within the computer capability. The allowable range in the existing mechanization is 5 to 500 radians per second. With the nominal size valve, based entirely on torque-speed considerations, ω_1 and ω_2 are around 10 radians per second at 100°F. Drastic changes do occur during transients and the effects are noticeable in the analog record. The effects, however, are not as great as one would expect at first glance and therefore fixed time constants can be used to simplify the analysis when small signals are being considered.

Since the block diagram includes references to all pertinent functions, the analog wiring diagram is not included the referenced functions are all included as figures (Figures III-3 through III-12).

The simulation accuracy was checked by calculating linear performance (without friction) and then testing the simulation with an appropriately time scaled sine wave. The frequencies shown are the simulated frequencies. Since the simulation was slowed by 10 to 1 relative to real time, the actual test signals were only 1/10 of the frequencies plotted. Phase data were available but were not reduced beyond spot

checks since it was obvious that they compared very closely with the computed values.

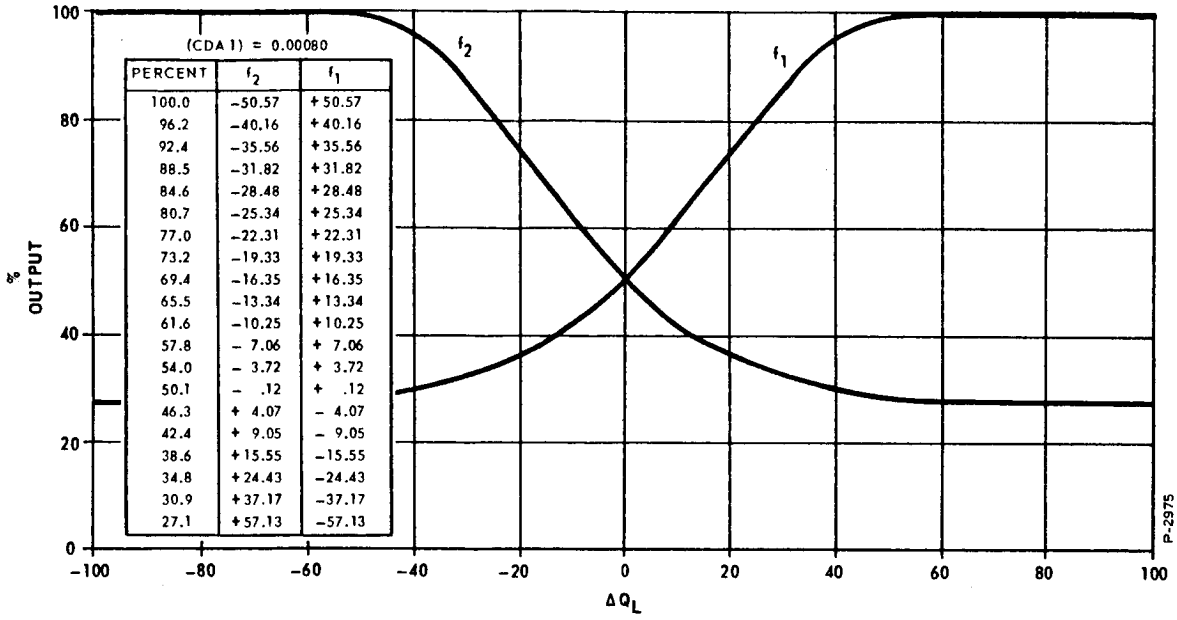

Figure III-3 - Functions f_1 and f_2

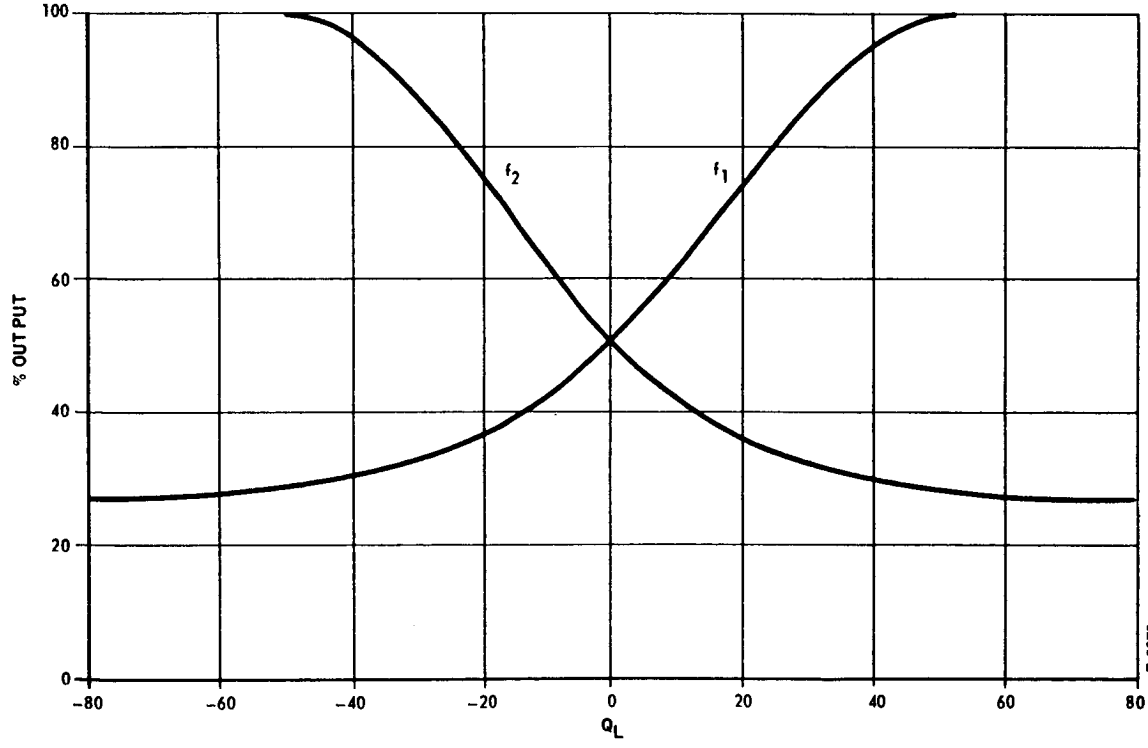

Figure III-4 - Functions f_1 and f_2 as Simulated

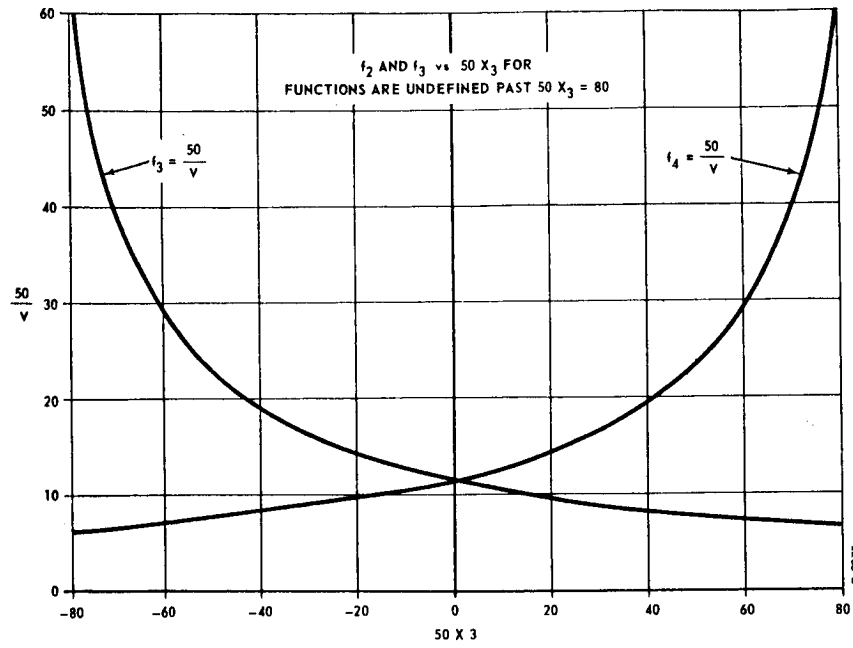

f_4 FOR V_o = 4.36	
50 X_3	1/V
+80	1.1905
+75	0.9434
+70	0.7812
+65	0.6667
+60	0.5814
+55	0.5155
+50	0.4630
+45	0.4202
+40	0.3846
+35	0.3546
+30	0.3289
+25	0.3067
+20	0.2874
+15	0.2703
+10	0.2551
+ 5	0.2415
0	0.2294
- 5	0.2183
-10	0.2083
-15	0.1992
-20	0.1908
-25	0.1832
-30	0.1761
-35	0.1695
-40	0.1634
-45	0.1577
-50	0.1524
-55	0.1475
-60	0.1429
-65	0.1385
-70	0.1344
-75	0.1305
-80	0.1269

f_3 FOR V_o = 4.36	
50 X_3	1/V
-80	1.1905
-75	0.9434
-70	0.7812
-65	0.6667
-60	0.5814
-55	0.5155
-50	0.4630
-45	0.4202
-40	0.3846
-35	0.3546
-30	0.3289
-25	0.3067
-20	0.2874
-15	0.2703
-10	0.2551
- 5	0.2415
0	0.2294
+ 5	0.2183
+10	0.2083
+15	0.1992
+20	0.1908
+25	0.1832
+30	0.1761
+35	0.1695
+40	0.1634
+45	0.1577
+50	0.1524
+55	0.1475
+60	0.1429
+65	0.1385
+70	0.1344
+75	0.1305
+80	0.1269

Figure III-5 - Functions f_3 and f_4 for Equal P_1 and P_2 Chamber Volumes, V_o = 4.36 in^3

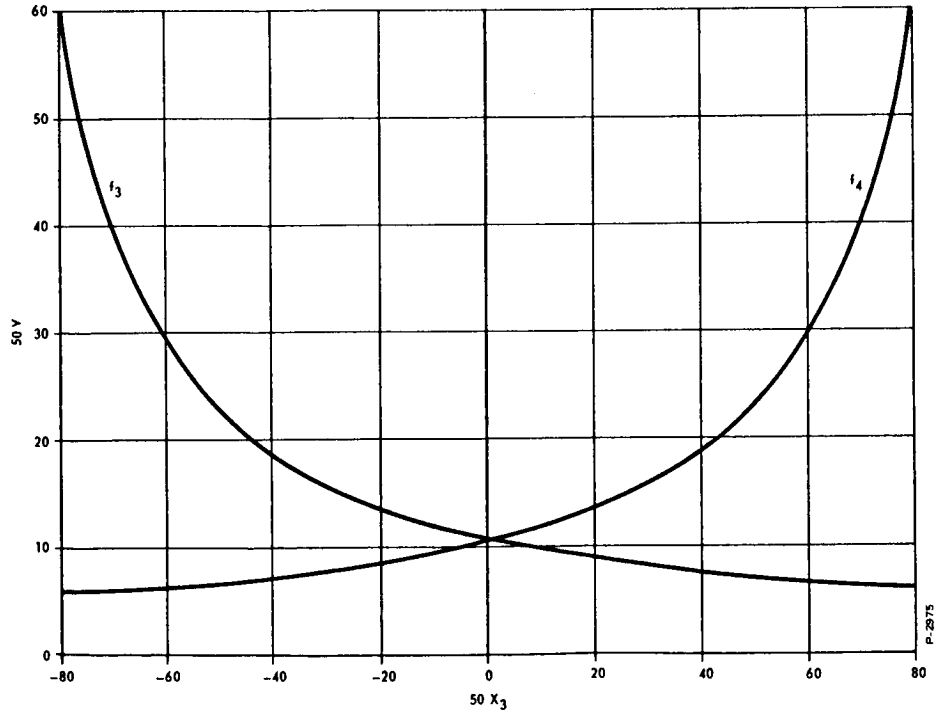

Figure III-6 - Functions f_3 and f_4 as Simulated

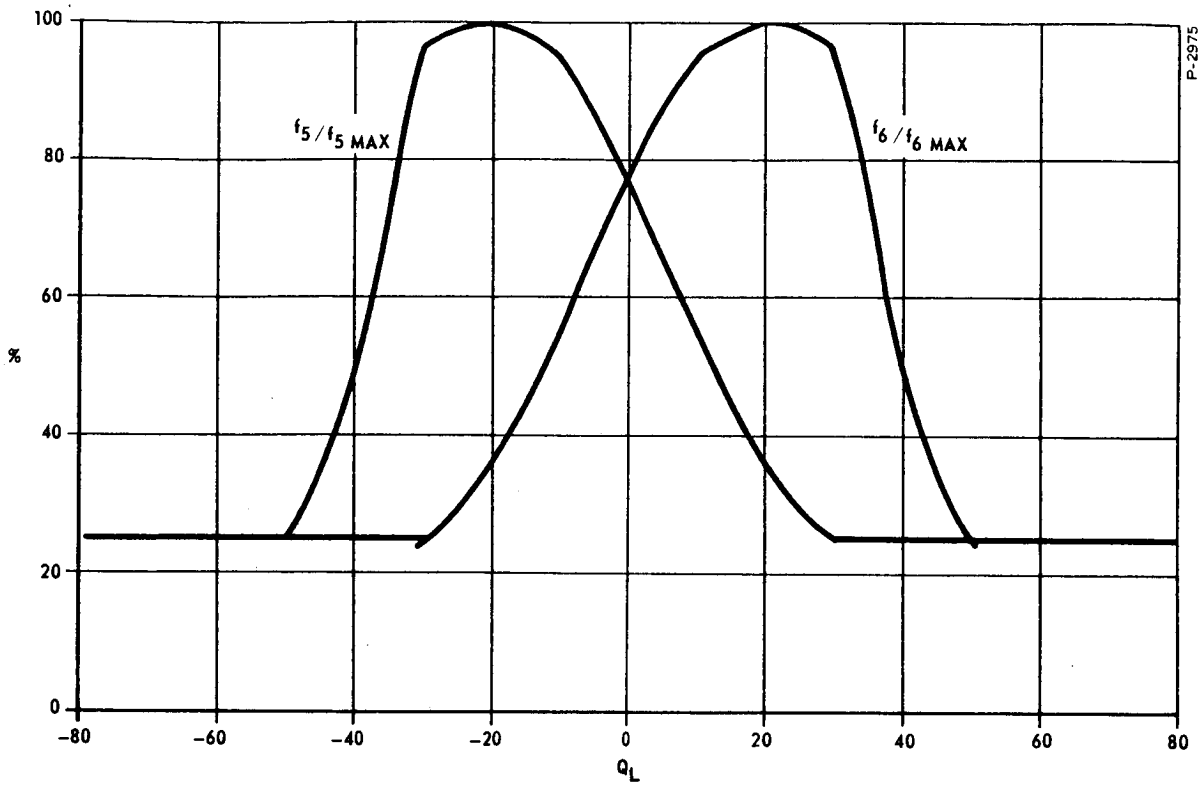

Figure III-7 - Functions f_5 and f_6

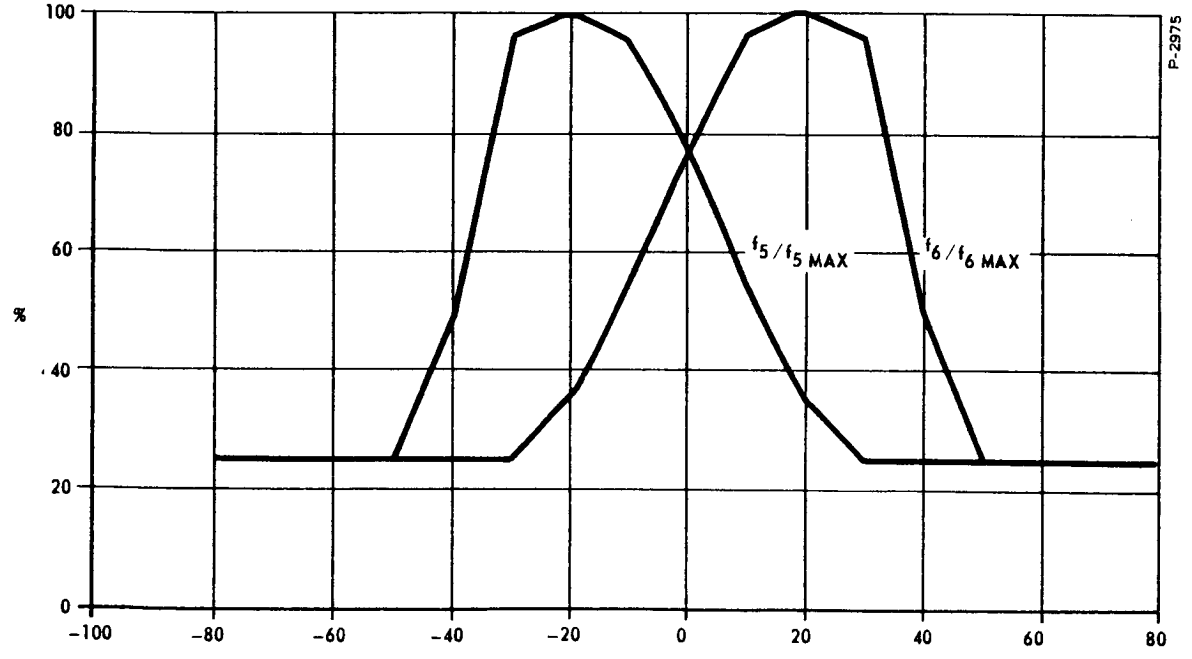

Figure III-8 - Functions f_5 and f_6 as Simulated

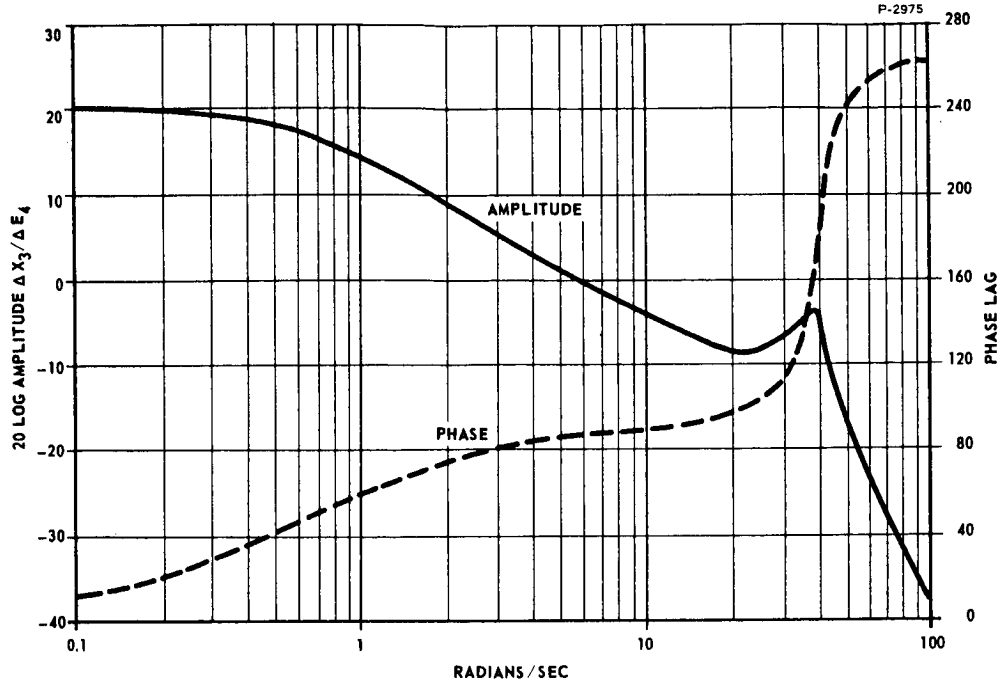

Figure III-9 - Calculated Actuator Response at 100°R

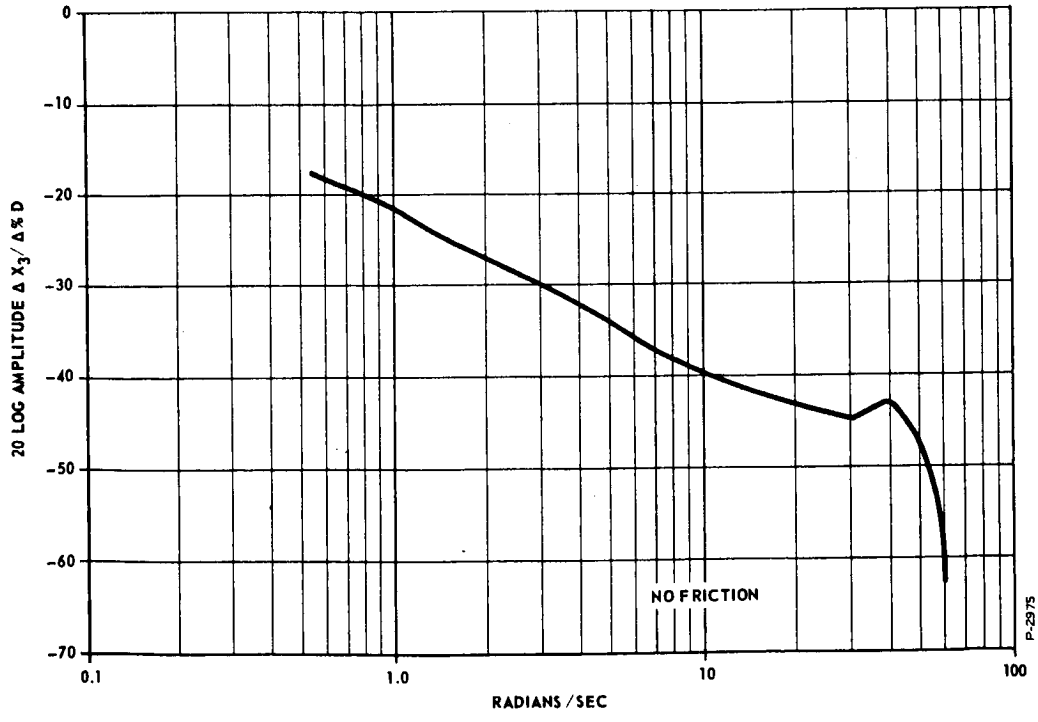

Figure III-10 - Measured Amplitude Response of Simulated Actuator at 100°R, Without Friction

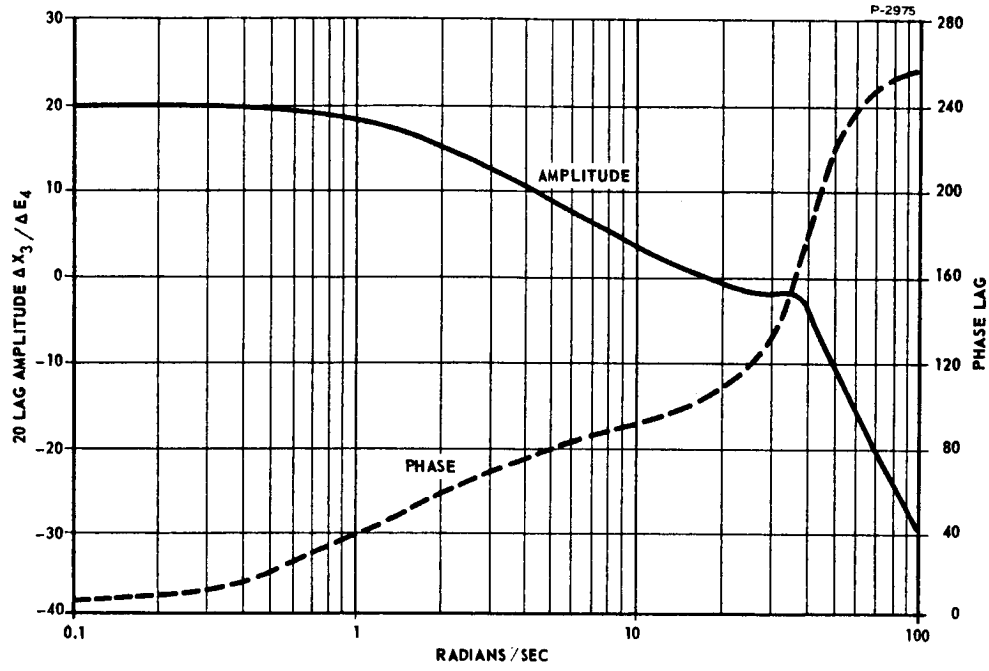

Figure III-11 - Calculated Actuator Response at 600°R

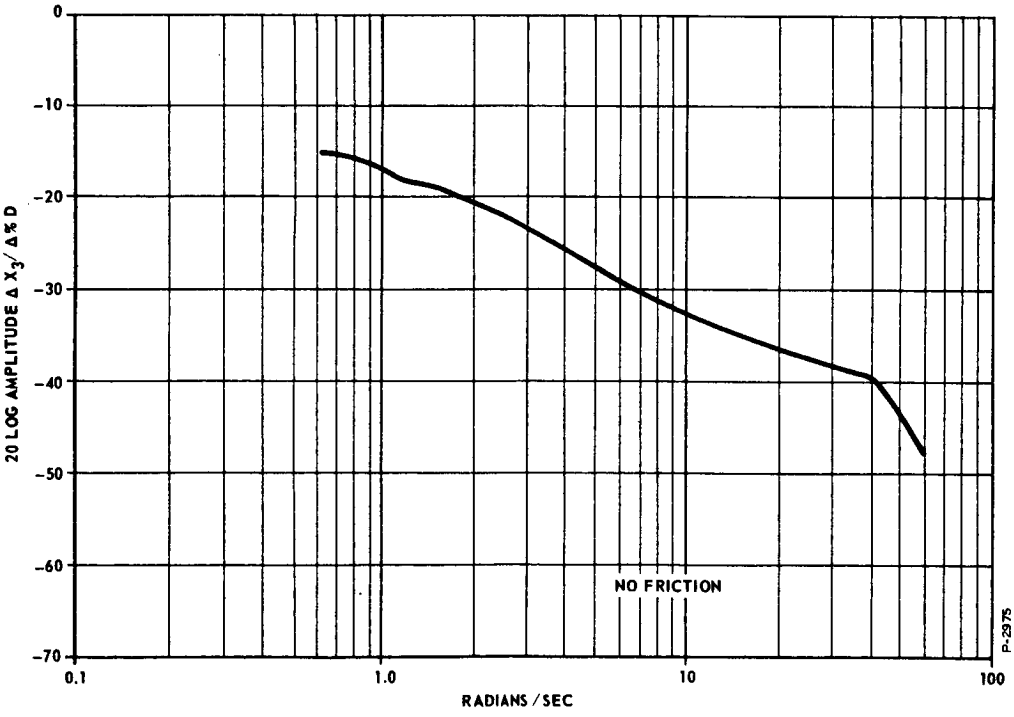

Figure III-12 - Measured Amplitude Response of Simulated Actuator at 600°R, Without Friction

APPENDIX IV

ANALYSIS OF THERMAL STRESSES AND DEFLECTIONS OF A SPHERICAL SHELL SUBJECTED TO EDGE CONSTRAINT AND UNIFORM PRESSURES -- APPLICATION TO A VELOCITY SENSOR

In designing a velocity sensor in which a pneumatic signal proportional to velocity is generated by pseudo differentiating a position signal, a concept has been employed whereby a volume is varied as a function of temperature using a temperature sensitive curved diaphragm. Such a design appears to produce the greatest change in volume for the least change in size due to the effect of temperature variation. The volume must vary as a predetermined function of temperature.

To investigate the feasibility of achieving the required volumetric change as a function of configuration (e.g., a spherical or an eliptical shape, choice of materials, combination of dimensions, etc.), it is necessary to have full knowledge of the deflections and stresses caused by the temperature change.

This analysis approximates the deflection and thermal stresses occurring in a thin spherical shell under pressure due to a temperature change. Specifically, a segment of the spherical shell is assumed to be welded to an internal rigid frame at temperature T_1, and then heated or cooled to temperature T_2 while a pressure differential, Δp is being exerted upon the shell. The solutions are obtained as a sum of the solutions of the membrane equations and of the equations for the so-called "edge-effect," which incorporate the effect of different thermal expansions at the welded junction and which display "local-effect" characteristics explicitly. The criterion necessary to prevent buckling is also stated.

The rigorous approach to the problem under consideration requires the solution of the differential equation for a spherical shell of the form

$$\frac{1}{12\,(1-\nu^2)}\left(\frac{t}{r}\right)^2 r^4\,\nabla^4\left(\frac{w}{r}\right) - r^2\,\nabla^2\left(\frac{\phi}{Er^2t}\right) - \frac{rp}{Et} = 0$$

where

$$r^2 \nabla^2 = \frac{\partial^2}{\partial \zeta^2} - \tan \zeta \frac{\partial}{\partial \zeta} + \sec^2 \zeta \frac{\partial^2}{\partial \theta^2}$$

$$\nabla^4 = \nabla^2 \nabla^2$$

ϕ = stress function

p = pressure per unit area of the middle surface with the compatibility equation as given by

$$r^4 \nabla^4 \left(\frac{\phi}{Er^2 t}\right) + r^2 \nabla^2 \left(\frac{w}{r}\right) = 0$$

and appropriate boundary conditions as shown in Figure IV-1.

The scope of this analysis is confined to the steady state conditions. All materials are considered to be homogeneous, isotropic, and within their elastic limits. The physical properties such as Young's modulus E, Poisson's ratio ν, and the coefficient of thermal expansion α, are

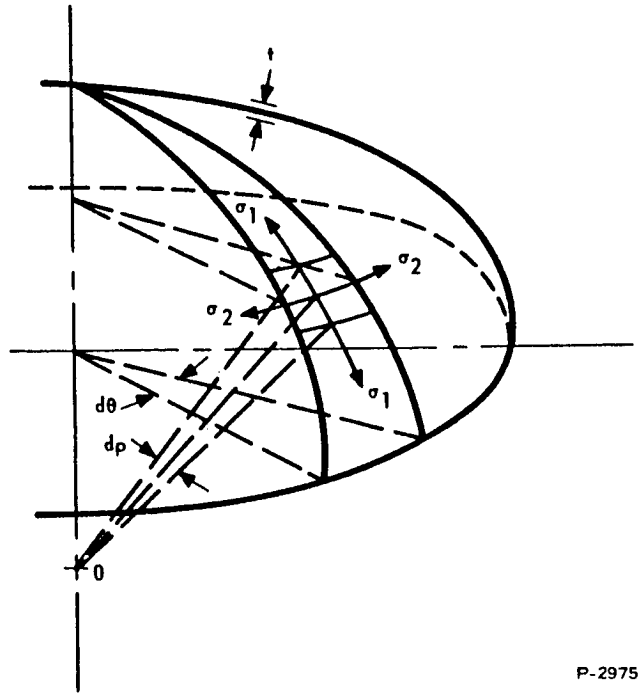

Figure IV-1 - Nomenclature of the Spherical Shell

assumed to possess constant values at the average operating temperature. The problem will be treated within the framework of Gol'demweizer and Rabotnov. (See Subsection IV-4, reference IV-1.)

Since only the feasibility of using curved diaphragms is being established, only an approximate solution is sought which is adequate for the feasibility study.

IV-1 ANALYSIS

Consider a thin spherical shell welded to a ring-shaped frame of dissimilar material, where the mid-plane of the shell has a uniform radius of curvature r_1 at temperature T_1 and the system is in a stress-free state. The assembly is then assumed to be heated to temperature T_2 by a gas admitted into the plenums with a pressure differential $(p_i - p_o)$, where p_o and p_i are the supply and signal pressure acting on the convex and concave sides of the shell, respectively. Because the shell and the ring possess different coefficients of thermal expansion (α_s for the shell and α_r for the ring), the shell is restrained at its edge. The edge would normally expand to a new radius according to the relationship.

$$r_2 = r_1 (1 + \alpha_s T)$$

where

$$T = T_2 - T_1$$

The analysis, however, must consider that the ring also experiences a change in radius from R_1 at T_1 to R_2 at T_2; thus,

$$R_2 = R_1 (1 + \alpha_r T) = r_1 (1 + \alpha_r T) \text{ Sin } \theta_{01}$$

If the ring-shaped frame is thick and made of rigid material (i.e., has a large value of Young's modulus E_r), it is reasonable to assume that the radial displacement of the ring, except for undergoing its independent thermal expansion, is not affected by the radial displacement of the thin shell; i.e., only the shell edge will be affected by the radial displacement where the amount it is affected is

$$- \delta_0 = - w_{\theta_0} = a - R_2 \doteq r_1 (\alpha_s - \alpha_r) T \text{ Sin } \theta_0 \qquad \text{(IV-1)}$$

Thus in terms of the boundary loadings and the influence coefficients α_{ij} (i, j = 1,2) which completely characterize the deformation of the edge under the influence of the force $Q_0 = 1$ (uniformly distributed) and the moment $M_0 = 1$ (Figure IV-2) for the edge of a symmetrically loaded shell of revolution, the displacement δ_0 and angle of rotation (slope) Γ_0 at the edge are given in Reference IV-1 as

$$\delta_0 = \alpha_{11} Q_0 + \alpha_{12} M_0 - \alpha_{11} Q_0^* + \delta_0^* \qquad \text{(IV-2)}$$

and

$$\Gamma_0 = \alpha_{21} Q_0 + \alpha_{22} M_0 - \alpha_{21} Q_0^* + \Gamma_0^* \qquad \text{(IV-3)}$$

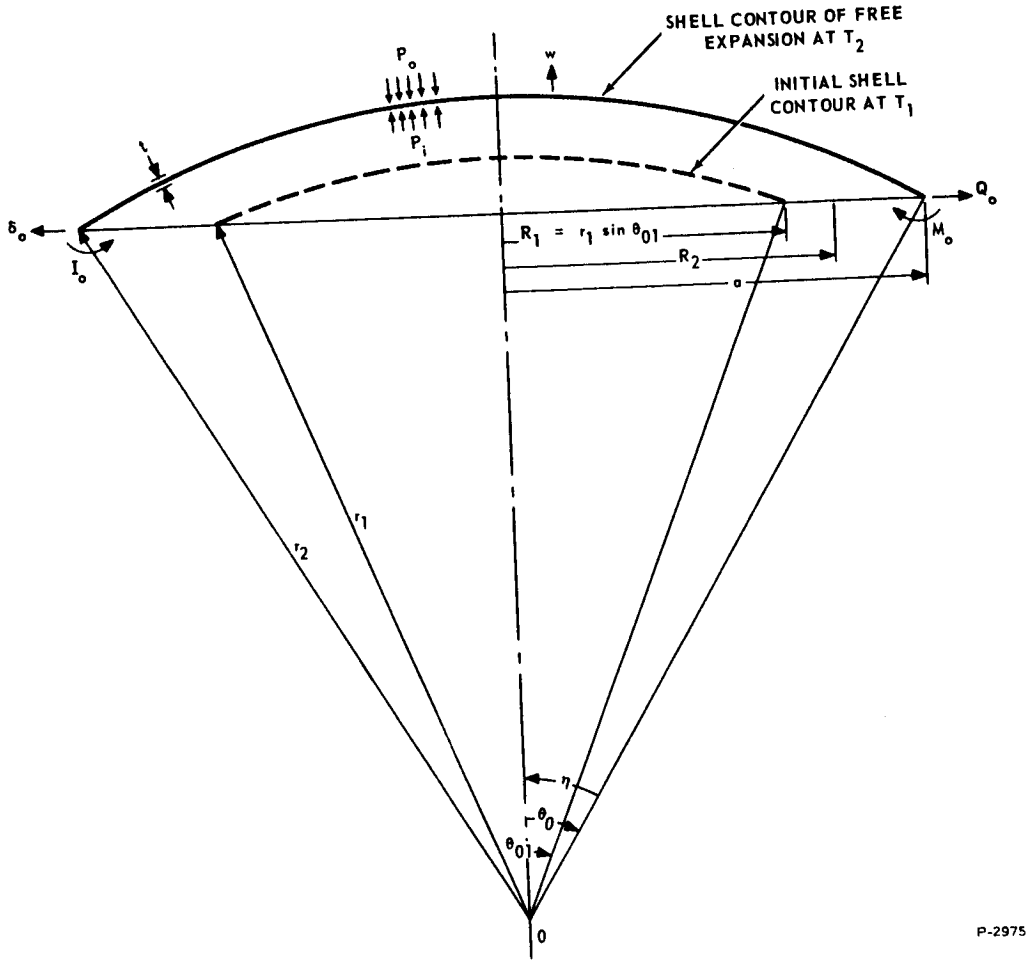

Figure IV-2 - Exaggerated View of the Spherical Shell

where the quantities with an asterisk indicate those being obtained by the membrane theory, and the influence coefficients a_{ij} are given as

$$\begin{cases} a_{11} = \dfrac{2\sqrt[4]{3(1-\nu^2)}}{E}\left(\dfrac{a}{t}\right)^{\frac{3}{2}}\sqrt{\sin\theta_0} \\ a_{12} = a_{21} = -\dfrac{2\sqrt{3(1-\nu^2)}}{E}\dfrac{a}{t^2} \\ a_{22} = \dfrac{4\left[3(1-\nu^2)\right]^{\frac{3}{4}}}{E}\sqrt{\dfrac{a}{t^5\sin\theta_0}} \end{cases}$$

The edge force contributed by the pressure differential $\Delta p = p_i - p_o$ in accordance with the membrane theory can be written as

$$Q_o^* = \frac{\Delta p\, r_2}{2}\cos\theta_0 \qquad \text{(IV-4)}$$

and the corresponding edge deflection δ_0^* and angle of rotation Γ^* are

$$\begin{cases} \delta_0^* = \dfrac{\Delta p\, r_2^2}{2t}\dfrac{(1-\nu)}{E}\sin\theta_0 \\ \Gamma_0^* \approx 0 \end{cases} \qquad \text{(IV-5)}$$

On substituting equations (IV-4) and (IV-5) into equations (IV-2) and (IV-3) and solving for Q_o and M_o yields

$$Q_0 = \frac{\xi_1 a_{22} - \xi_2 a_{12}}{a_{11}a_{22} - a_{12}^2}$$

$$M_0 = \frac{\xi_2 a_{11} - \xi_1 a_{21}}{a_{11}a_{22} - a_{12}^2}$$

where

$$\begin{cases} \xi_1 = a_{11} \dfrac{\Delta p a}{2} \cot \theta_0 - \dfrac{\Delta p a^2}{2t \sin \theta_0} \dfrac{(1 - \nu)}{E} - r_1 (a_s - a_r) T \sin \theta_0 \\ \xi_2 = a_{21} \dfrac{\Delta p a}{2} \cot \theta_0 \end{cases} \qquad \text{(IV-6)}$$

These expressions, equation (IV-6), incorporate the interference of thermal expansion equation (IV-1) and the conditions of a non-rotating rigid ring ($\Gamma_o = 0$).

Therefore, the radial (normal) deflection from the free expansion equilibrium position of the shell at temperature T_2 is of the form

$$w = \frac{\sqrt{2}\, r_2}{E t} \left[+ \sqrt{\frac{r_2}{c}} (Q_0 - Q_0^*) \sin \theta_0 \cos \beta - \frac{M_0}{c} \cos \left(\frac{\pi}{4} + \beta\right) \right] e^{-\beta} + w^* \qquad \text{(IV-7)}$$

where

$$c = \frac{t}{2\sqrt{3 (1 - \nu^2)}}$$

and

$$\beta = \frac{1}{\sqrt{2}} \int_{\theta_0}^{\theta} \frac{r_2}{\sqrt{c}}\, d\theta = \sqrt{\frac{r_2}{2c}}\, \eta$$

It is to be noted that η is defined by

$$\eta = \int_{\theta_0}^{\theta} d\theta = \theta - \theta_0 \qquad 0 \leq \eta \leq \theta_0$$

i.e., it is the angle measured from the edge of the spherical shell from $\theta = \theta_0$.

In equation (IV-7), the normal deflection of the shell as given in Reference IV-2 is

$$w^* = \frac{\Delta p\, r_2^2}{2t} \frac{(1 - \nu)}{E} \sin \theta_0$$

Similarly, the sum of the meridional normal stress in the extreme fiber of the shell is defined as

$$\sigma = \sigma_m + \sigma_2$$

where the bending stress is

$$\sigma_M = \left[\frac{6\sqrt{2}\,M_0}{t^2} \cos\left(\beta - \frac{\pi}{4}\right) - \frac{6}{\sqrt{3(1-\nu^2)}} \sqrt{\frac{r_2}{t}} \frac{\sin\theta_0}{t} (Q_0 - Q_0^*) \sin\beta \right] e^{-\beta} \qquad \text{(IV-8)}$$

and the hoop stress is

$$\sigma_2 = \sigma_1 = \left[+2^4 \sqrt{3(1-\nu^2)} \sqrt{\frac{r_2}{t}} \frac{\sin\theta_o}{t} (Q_o - Q_o^*) \cos\beta - 2\sqrt{2}\sqrt{3(1-\nu^2)} \frac{M_o}{t^2} \cos\left(\frac{\pi}{4} + \beta\right) \right] e^{-\beta} + \sigma_2^*$$

In equation (IV-8) the hoop stress in Reference IV-2 is

$$\sigma_2^* = \sigma_1^* = \frac{\Delta p\, r_2}{2t}$$

If the resultant compressive pressure ($p_o \geq p_i$) reaches a certain limit, the spherical form of equilibrium of the compressed shell can become unstable and buckling then occurs.(IV-3) Therefore, the buckling criterion is used to ensure the elastic stability; i.e.,

$$\sigma_{critical} = \frac{t}{r_2} \frac{E}{\sqrt{3(1-\nu^2)}}$$

In application, it is

$$\sigma_{compressive} = |-\sigma| \geq \sigma_{cr}$$

IV.2 LIST OF SYMBOLS AND DEFINITIONS

a	Radius of the base circle of the spherical shell at T_2 (in)
c	A parameter defined in Eq. (13)
E	Young's modulus of elasticity (psi)
M_o	Bending moment at the shell edge, (in-lb/in of peripheral length)
p_i	Pressure intensity on the concave side of the spherical shell (psi)
Δp	Pressure differential exerted on the shell, $\Delta p = p_i - p_o$ (psi)
Q_o	Shear force at the shell edge, (lb/in of peripheral length)
r_1	Radius of curvature of the shell at T_1 (in)
r_2	Radius of curvature of the shell at T_2 in stress-free state (in)
R_1	Radius of restraining ring at temperature T_1 (in)
R_2	Radius of restraining ring at temperature T_2 (in)
t	Thickness of the spherical shell (in)
T	Temperature change from the initial state T_1 $T = T_2 - T_1$ (°F)
T_1	Initial temperature (°F)
T_2	Final temperature (°F)
w	Normal (radial) deflection of the shell from the equilibrium state at T_2 (in)
α_k	Coefficients of thermal expansion pertaining to the shell (k=s), and the ring-frame (k=r), respectively, (in/in-°F)

a_{ij} Influence coefficients of the edge effect defined in Eq. (7) (i, j=1,2)

β An angular parameter defined in Eq. (14)

δ_o Normal (radial) deflection of the shell at the shell edge (in)

η Angle measured from the edge of the spherical shell toward its apex (rad.)

θ_o Angle between the normal through the apex and the radius of curvature connecting the edge of the spherical shell at T_2 (rad.)

Γ_o Angle rotation or slope of the shell at the edge

ν Poisson's ratio pertaining to the shell material

$\xi_{1,2}$ Parameters defined in Eq. (11)

σ Meridional normal stress in the extreme fiber of the shell (psi)

σ_2 Hoop stress (psi)

σ_M Bending stress (psi)

$*$ The variables with an asterisk refer to the solutions using the membrane theory.

IV.3 REFERENCES

(IV-1) V. V. Novozhilov, The Theory of Thin Shells, translated by P. G. Lowe, P. Noordhoff, Ltd., The Netherlands, 1959, pp. 260-304.

(IV-2) W. M. Coates, "The State of Stress in Full Heads of Pressure Vessels," ASME Transactions, 1929, pp. 117-131.

(IV-3) S. Timoshenko, Theory of Elastic Stability, First Ed., McGraw-Hill Book Co., Inc., 1936, pp. 491-497.

APPENDIX V

DESCRIPTION OF DIGITAL COMPUTER PROGRAM FOR NUMERICALLY EVALUATING BODE PLOTS (AMPLITUDE AND PHASE) OF GENERALIZED FORMS OF TRANSFER FUNCTIONS

In analyzing a servo system, with possible multiple feedbacks and where each block of the system can be represented by a transfer function having the form of Equation (V-3), the amplitude and phase as a function of frequency is often desired. Consequently, a digital computer program for numerically evaluating Bode plots of generalized forms of transfer functions was developed. Essentially, the program obtains the roots for the following system of equations:

$$\sum_{k=1}^{n} a_{jk} x_k = a_{n+1} x_{n+1} \qquad (V-1)$$

where

$j = 1, 2, 3, \ldots, n \leq 12$

a_{jk} = complex coefficients (given as functions of frequency ω)

$\omega = \omega_0 \, 10^{\left(\frac{m}{N}\right)}$

$m = 0, 1, 2, \ldots, 30$

N = number of ω-values per decade.

The roots of this system of equations are: $\left|\frac{x_k}{x_{n+1}}\right|$ for $k = 1, 2, 3, \ldots, n \leq 12$.

The coefficients are complex; i.e., they have the form $a_{jk} = u_{jk} + iv_{jk}$ and represent the constants and parameters associated with a particular system of transfer functions.

V.2 FORM OF EQUATIONS

The response of a specified system of transfer functions is represented by the set of equations (equivalent to the system of equations V-1)

$$\begin{aligned} a_{11}x_1 + a_{12}x_2 + \cdots + a_{1n}x_n &= a_{1n+1}x_{n+1} \\ a_{21}x_1 + a_{22}x_2 + \cdots + a_{2n}x_n &= a_{2n+1}x_{n+1} \\ \cdots & \\ a_{n1}x_1 + a_{n2}x_2 + \cdots + a_{nn}x_n &= a_{nn+1}x_{n+1} \end{aligned} \qquad \text{(V-2)}$$

where

$$n \leq 12.$$

Letting $a_{jk} = u_{jk} + i\, v_{jk}$, the coefficients a_{jk} may be real or complex. If the coefficient is real, the $v_{jk} = 0$ and $a_{jk} = u_{jk}$. However if the coefficient is complex, then a_{jk} is defined by

$$a_{jk} = \frac{K(T_1 s + A)(T_2 s + 1)(T_3 s + 1)(T_4^2 s^2 + 2\zeta_4 T_4 s + 1)}{(T_s s + B)(T_6 s + 1)(T_7 s + 1)(T_8^2 s^2 + 2\zeta_8 T_8 s + 1)} e^{-T_9 s} \qquad \text{(V-3)}$$

where

$$s = i\omega$$

$$\omega = \omega_0 (10)^{\frac{m}{N}}$$

$$m = 0, 1, 2, \ldots, 30$$

N = number of ω-values per decade μ

and

$$i = \sqrt{-1}$$

It should be noted that all of the coefficients a_{jk} could be computed from equation (V-3) provided the choices for the parameters K, T_1, T_2, ... , A, B are judiciously chosen. Furthermore, selected factors $(T_e s + d)$ can be eliminated from the network representation by setting $T = 0$ and $d = 1$. Thus, considerable flexibility is afforded in specifying the coefficients a_{jk}.

However, under normal conditions, the roots of the system, equation (V-2), are established by determining the coefficients a_{jk} for several values of ω. This technique yields sets in roots for the system at each value of ω, namely the values $\omega = \omega_0 (10)^{m/N}$.

V.3 METHOD OF SOLUTION

Letting $a_{jk} = u_{jk} + i\, v_{jk}$, the first step in arriving at a solution for the roots $\left|\frac{x_k}{x_{n+1}}\right|$ is to construct matrices for the real part and imaginary part of a_{jk}. Thus,

$$U = \begin{bmatrix} u_{11} & u_{12} & \cdots & u_{1n+1} \\ u_{21} & u_{22} & \cdots & u_{2n+1} \\ \cdots & & & \\ u_{n1} & u_{n2} & \cdots & u_{nn+1} \end{bmatrix}$$

and

$$V = \begin{bmatrix} v_{11} & v_{12} & \cdots & v_{1n+1} \\ v_{21} & v_{22} & \cdots & v_{2n+1} \\ \cdots & & & \\ v_{n1} & v_{n2} & \cdots & v_{nn+1} \end{bmatrix}$$

These two matrices are used, in the computer program, to store the results of complex arithmetic operation, where complex multiplication is given by

$$(a + b\,i)(c + d\,i) = (ac - bd) + (ad + bc)\,i \qquad \text{(V-4)}$$

and complex division is given by

$$\frac{(a + bi)}{(c + di)} = \frac{ac + bd}{c^2 + d^2} + \frac{bc - ad}{c^2 + d^2}\,i \qquad \text{(V-5)}$$

Under the multiplication and division operations defined by equations (V-4) and (V-5), the real part of the result is stored in the U matrix and the imaginary part is stored in the V matrix.

Using complex arithmetic, the elements $a_{11} x_1$, $a_{21} x_1$, ... , $a_{n1} x_1$, $a_{22} x_2$, ... are eliminated from the system of equations until $g_{nn} x_n = h x_{n+1}$ remains. At this point the root $\left|\frac{x_n}{x_{n+1}}\right|$ can then be computed, and successive substitution will yield the remaining roots.

V.4 UTILIZATION OF THE COMPUTER PROGRAM

In order to utilize the digital computer program for evaluating particular Bode plots, certain input information must be supplied:

(a) The values of ω_0, N, and n

where

ω_0 = initial value of ω in radians

N = the number of ω-values per decade; N must be an integer between 1 and 30.

and

n = the number of linear equations; $n \leq 12$.

(b) A table of real coefficients a_{jk}, where the row and the column identification and the value of the coefficient are provided. A form has been constructed for entering these quantities; the form is shown in Figure V-1 under the title "Real Coefficient Table."

(c) A table of parameter values for computing complex coefficients a_{jk}. The row and the column idenficiations and the values

T_1, T_2, T_3, T_4, T_5, T_6, T_7, T_8, T_9, ζ_4, ζ_8, K, A, B

must be provided. A form for entering these numerical values is shown in Figure V-2 under the title "Table of Parameters for Complex Coefficients." It should be noted that the number of complex coefficients can not exceed 50 and the total number of coefficients supplied is restricted to 156.

THE Bendix CORPORATION

RESEARCH LABORATORIES DIVISION

REAL COEFFICIENT TABLE

ω_0 = _____

N = _____

n = _____

(1) $\omega = \omega_0 (10)^{\frac{m}{N}}$, m = 0, 1, 2, ···, 30; N = NUMBER OF ω-VALUES/DECADE

(2) n = NUMBER OF LINEAR EQUATIONS; $\sum_{k=1}^{n} a_{jk} X_k = a_{n+1} X_{n+1}$, i = 1, 2, 3, ···, n

(3) SOLUTIONS: $\frac{X_k}{X_{n+1}}$, k = 1, 2, 3, ···, n

ENTRY FORMAT: ± · 1234567 E ± 89 OR FIXED DECIMAL · IF COEFFICIENT IS COMPLEX, ENTER C ·

COL → / ROW ↓	1	2	3	4	5	6	7	8	9	10	11	12	13
1													
2													
3													
4													
5													
6													
7													
8													
9													
10													
11													
12													

Figure V-1 - Real Coefficient Table

THE Bendix CORPORATION
RESEARCH LABORATORIES DIVISION

COMPLEX COEFFICIENT PARAMETERS

$$C = U + iV = \frac{K(T_1 S + A)(T_2 S + 1)(T_3 S + 1)(T_4^2 S^2 + 2\zeta_4 T_4 S + 1)}{T_5 S + B)(T_6 S + 1)(T_7 S + 1)(T_8^2 S^2 + 2\zeta_8 T_8 S + 1)} e^{-T_9 S}, \quad S = i\omega$$

ENTRY FORMAT: ± · 1 2 3 4 5 6 7 8 E ± 9 0
(± · 0 1 2 3 4 5 6 7 8 · 10 ± 9 0)

ROW	COL					
		T_1	T_2	T_3	T_5	T_6
ROW	COL					
		T_7	T_9	ζ_4	T_4	ζ_8
ROW	COL					
		T_8	K	A	B	

1 2 3 4 5 6 7 8 9 10 11 12 13 14 15 16 17 18 19 20 21 22 23 24 25 26 27 28 29 30 31 32 33 34 35 36 37 38 39 40 41 42 43 44 45 46 47 48 49 50 51 52 53 54 55 56 57 58 59 60 61 62 63 64 65 66 67 68 69 70 71 72 73 74 75 76 77 78 79

Figure V-2 - Table of Parameters For Complex Coefficients

V.5 COMPUTED OUTPUTS

The evaluation program has a specialized print format for the output quantities. The line print displays (1) the value of ω, (2) the amplitude of the k $\underline{\text{th}}$ root, (3) the amplitude of the k $\underline{\text{th}}$ root in decibels, (4) the phase of the k $\underline{\text{th}}$ root in degrees. All values of ω and the corresponding k $\underline{\text{th}}$ root appear on the same page. A second page displays all values of ω and the corresponding (k + 1) root. This print format is designed to facilitate graphing the data points.

APPENDIX VI

DIGITAL COMPUTATIONS FOR SIZING FLAPPER VALVE

VI.1 INTRODUCTION

Digital computations were used to size the flapper valve.

VI.1.1 Objectives

The objective was generation of numerical values to be used in the analog simulation.

VI.1.2 Description

A program was developed for flapper valve sizing. This program assumes initial values for input orifice effective area, exit orifice effective area, supply pressure, exit pressure, gamma, gas constant, and temperature. The program then arbitrarily chooses an intermediate pressure and calculates the flow to or from a load to realize the assumed intermediate pressure values covering the range from exhaust pressure to supply pressure. Then the exit is automatically stepped, and the process is repeated. After all exit steps are run through, the initial entrance and exit areas are stepped, and the whole process is repeated.

The results are then plotted by hand as lines of constant exit area on coordinates of pressure and negative or positive load flow.

The lines of exit area are in equal generated increments above and below the mean value. Now to size the flapper valve, one enters the graph at a value of positive load flow and finds the intersection of that load flow with a line of mean area minus some percentage. This defines one load pressure. Entering the other side of the graph (negative load flow) and finding the intersection with the line of mean area plus the same percentage defines the other pressure. In this way a line of differential pressure versus flapper valve stroke can be rapidly and accurately built up. This plot can then be superimposed on a plot of required differential pressure versus required load flow and checked to see if the assumed valve sizes are adequate. Since

four valve sizes were computed each time the program was run, a range could be rapidly covered. Only portions of the data were plotted in the initial scanning process, so the work is both rapid and accurate. The spread in sizes calculated is controlled by input, so the first run is made with a big spread and subsequent runs examine narrower and narrower ranges of orifice area. The lines of load flow versus pressure at constant valve area have another value. The time constant of the divider, assuming adiabatic compressibility, is $T = \frac{V\,\partial P/\partial Q_L}{\gamma P}$. Also, since the complete torque speed plot can be built up, the value of the partial of torque versus load flow is defined for all conditions. Thus we have not only chosen the sizes for the orifices but have also generated all the data needed to simulate the device dynamically.

VI.2 ANALYSIS

The detailed equations used are listed in the following subsections. Note that a linear correction of R and gamma for pressure effects is possible. This is adequate for the pressure range used on this project but might not be adequate if higher pressures, (more than a few hundred psia) were used. The corrections may be determined by reference to Figures VI-1 and VI-2.

VI.2.1 Principle Equations

$$(1)\quad Q_{A1} = (CdA_1)\left(\sqrt{R_1T_1}\right)\left(\frac{B_3}{B_1}\right) C_3A_1f_1\left(\frac{B_1}{B_3}\right)$$

$$(2)\quad Q_{A2} = (CdA_2)\left(\sqrt{R_2T_2}\right) C_3A_2f_1\left(\frac{B_0}{B_1}\right)$$

$$(3)\quad Q_L = Q_{A1} - Q_{A2}$$

VI.2.2 Auxillary Equations

$$(4)\quad (CdA_1)\,i = (CdA_1)_0\,(1 + K_1n_1)$$

Input is $(CdA_1)_0$ and K_1. K_1 is 3 digit 0.000 to 2.00. n_1 has successive values of 0, 1, 2, 3, and for each value of n_1, all values of CdA_2 are processed.

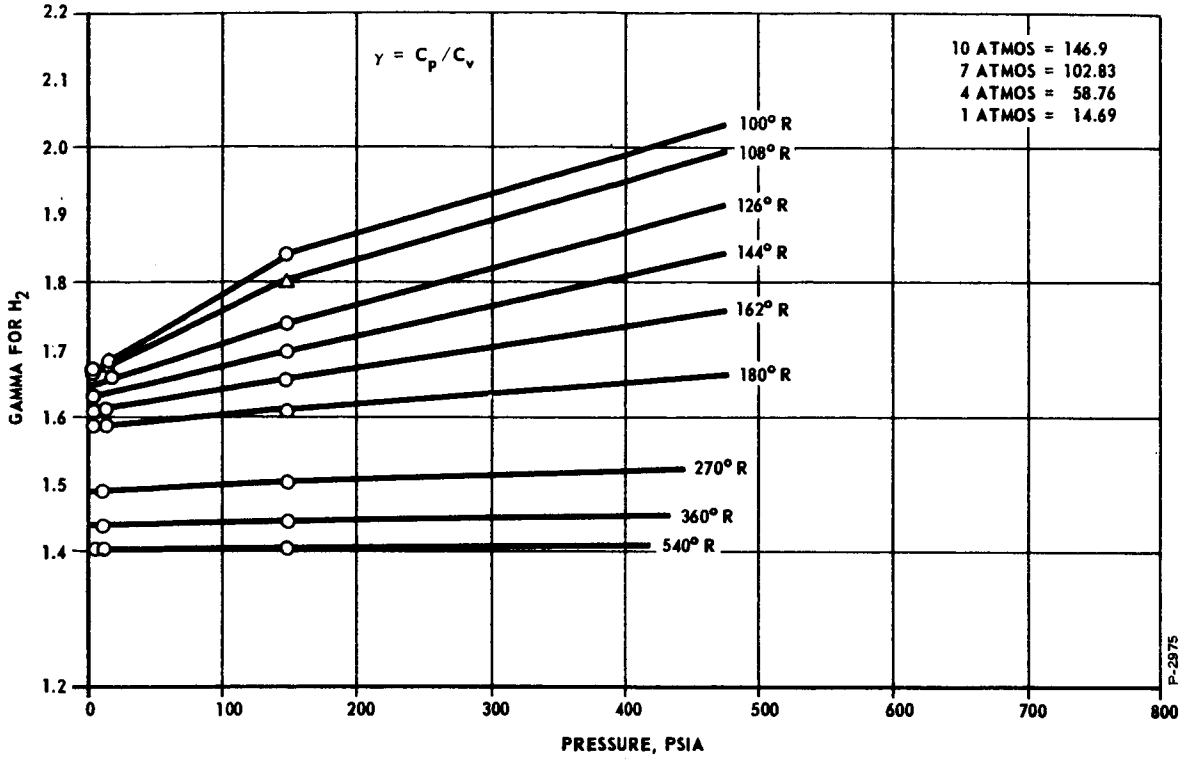

Figure VI-1 - Gamma for H_2 Versus PSIA

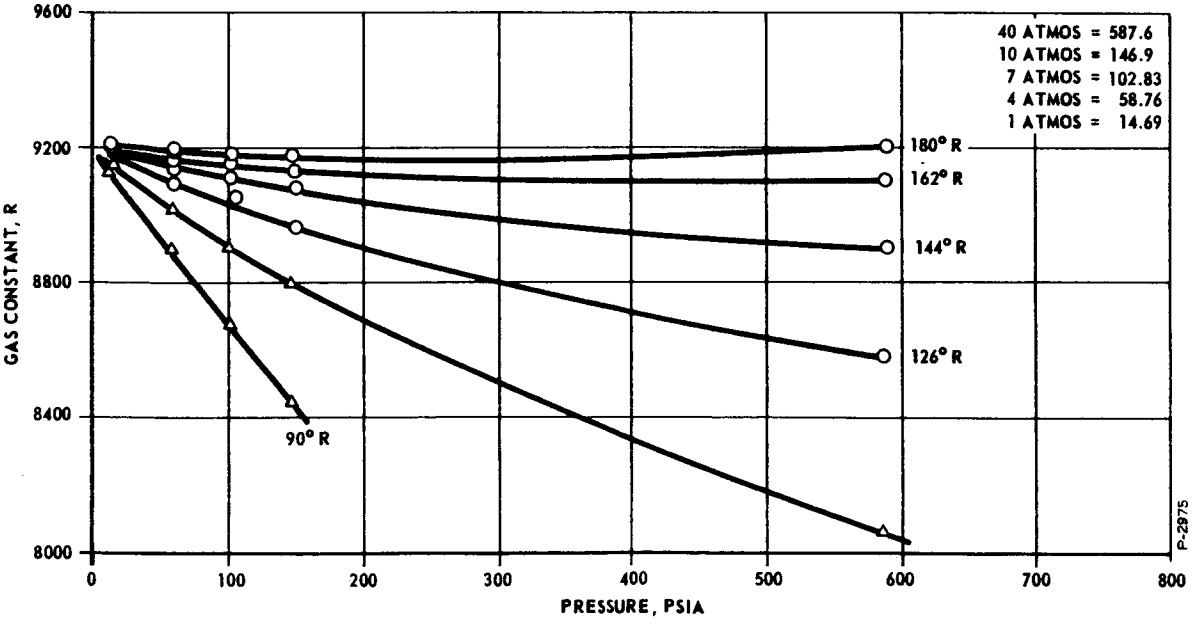

Figure VI-2 - Gas Constant for H_2 Versus PSIA

(5) $(CdA_2)_i = (C_dA_1)_0 \quad K_2 \left(1 + \frac{n_2}{10}\right)$

Input is K_2. n_2 has successive values of -10, -9, -8, -7, -6, -5, -4, -3, -2, -1, 0, 1, 2, 3, 4, 5, 6, 7, 8, 9, 10 and for each value of n_2, all values of B_1 are processed. (Equation 7)

(6) $\sqrt{R_1T_1} = \sqrt{T}\ \sqrt{R_1}$ where $T_1 = T$ and $R_1 = 9200 - K_3B_3$ where K_3 can be 0.00 to 6.00.

(7) $\sqrt{R_2T_2} = \sqrt{T}\ \sqrt{R_2}$ where $T_2 = R_2 = 9200 - K_3B_1$

(8)

$$C_3A_1 f_1\left(\frac{B_1}{B_3}\right) = \sqrt{\gamma_1 g}\left(\frac{2}{\gamma_1 + 1}\right)^{\left(\frac{\gamma_1 + 1}{2(\gamma_1 - 1)}\right)} \frac{\left[\left(\frac{B_1}{B_3}\right)^{\frac{1}{\gamma}} \sqrt{1 - \left(\frac{B_1}{B_3}\right)^{\left(\frac{\gamma_1 - 1}{\gamma_1}\right)}}\right]}{\left[\left(\frac{B_1}{B_3}\right)^{\frac{1}{\gamma}} \sqrt{1 - \left(\frac{B_1}{B_3}\right)^{\left(\frac{\gamma_1 - 1}{\gamma_1}\right)}}\right]_{max.}}$$

where

$$\left[\left(\frac{B_1}{B_3}\right)^{\frac{1}{\gamma}} \sqrt{1 - \left(\frac{B_1}{B_3}\right)^{\left(\frac{\gamma_1 - 1}{\gamma_1}\right)}}\right]_{max.}$$ occurs at $\left(\frac{B_1}{B_3}\right)$ critical

The appropriate value of C_3 for use in hand computations may be determined by reference to Figure VI-3.

and

$$\left(\frac{B_1}{B_3}\right) \underset{crit}{\equiv} \left(\frac{2}{\gamma_1 + 1}\right)^{\left(\frac{\gamma_1}{\gamma_1 - 1}\right)}$$

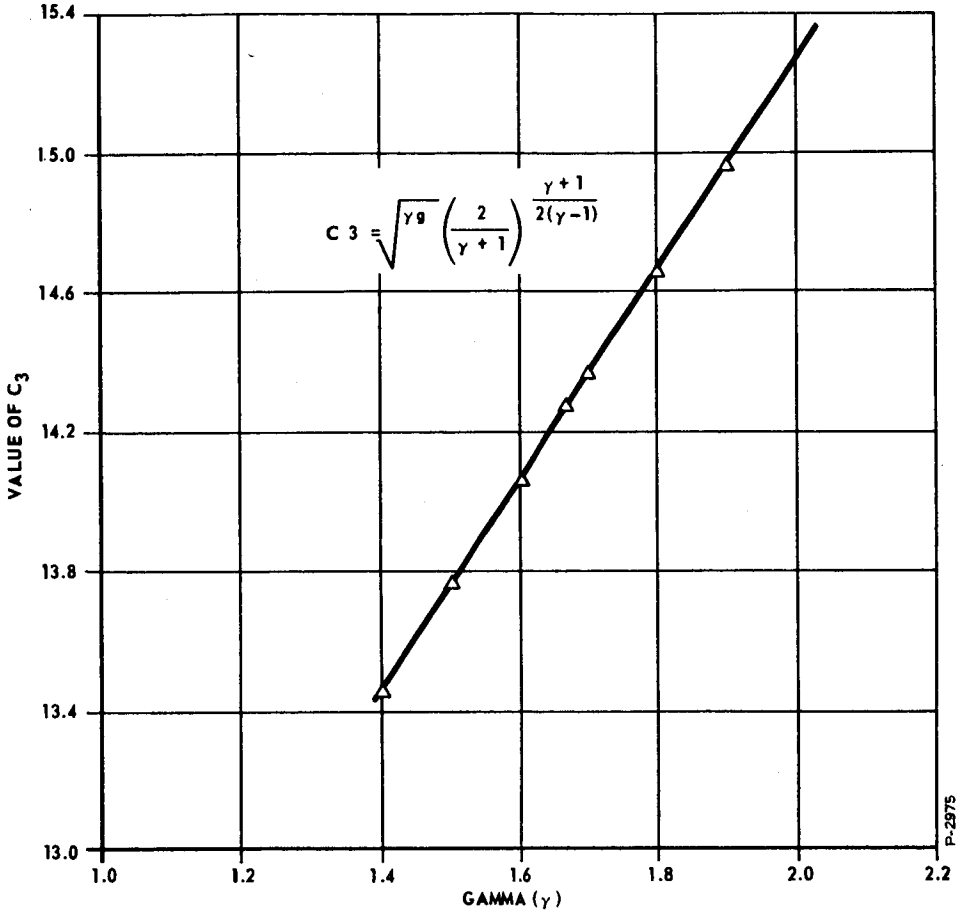

Figure VI-3 - Flow Coefficient C_3 Versus γ

In addition,

$$f_1 \left(\frac{B_1}{B_3}\right) \equiv 1 \quad \text{for}$$

$$\frac{B_1}{B_3} \leq \frac{B_1}{B_3}_{crit}$$

also

$$\gamma_1 = \gamma_0 + K_4 B_3$$

Values of f_1 for a range of values of γ are shown in Table VI-1.

Table VI-1 - f_1 Function Versus γ

GAMMA = 1.4000		GAMMA = 1.5000		GAMMA = 1.600		GAMMA = 1.6700		GAMMA = 1.7000		GAMMA = 1.8000		GAMMA = 1.9000		GAMMA = 2.0000	
PD/PU	F(PD/PU)	PD/PU	F(PD/PU)	PD/PU	F(PD/PU)	PD/PU	F(PD/PU)	PD/PU	F(PD/PU)	PD/PU	F(PD/PU)	PD/PU	F(PD/PU)	PD/PU	F(PD/PU)
0.5283	1.0000	0.5120	1.0000	0.4968	1.0000	0.4867	1.0000	0.4825	1.0000	0.4690	1.0000	0.4564	1.0000	0.4444	1.0000
0.5519	0.9988	0.5364	0.9987	0.5219	0.9987	0.5123	0.9987	0.5084	0.9987	0.4956	0.9986	0.4836	0.9986	0.4722	0.9985
0.5755	0.9951	0.5608	0.9949	0.5471	0.9948	0.5380	0.9947	0.5342	0.9947	0.5221	0.9945	0.5107	0.9944	0.5000	0.9942
0.5990	0.9889	0.5852	0.9886	0.5723	0.9883	0.5637	0.9881	0.5601	0.9880	0.5487	0.9877	0.5379	0.9874	0.5278	0.9871
0.6226	0.9801	0.6096	0.9796	0.5974	0.9791	0.5893	0.9788	0.5860	0.9786	0.5752	0.9781	0.5651	0.9777	0.5556	0.9772
0.6462	0.9687	0.6340	0.9680	0.6226	0.9672	0.6150	0.9667	0.6119	0.9665	0.6018	0.9658	0.5923	0.9651	0.5833	0.9645
0.6698	0.9546	0.6584	0.9536	0.6477	0.9526	0.6407	0.9519	0.6377	0.9516	0.6283	0.9507	0.6195	0.9498	0.6111	0.9489
0.6934	0.9375	0.6828	0.9362	0.6729	0.9350	0.6663	0.9341	0.6636	0.9338	0.6549	0.9326	0.6467	0.9314	0.6389	0.9303
0.7170	0.9174	0.7072	0.9159	0.6981	0.9144	0.6920	0.9133	0.6895	0.9129	0.6814	0.9114	0.6738	0.9101	0.6667	0.9087
0.7406	0.8941	0.7316	0.8923	0.7232	0.8905	0.7177	0.8892	0.7154	0.8887	0.7080	0.8871	0.7010	0.8854	0.6944	0.8839
0.7641	0.8672	0.7560	0.8651	0.7484	0.8631	0.7433	0.8617	0.7412	0.8611	0.7345	0.8592	0.7282	0.8574	0.7222	0.8556
0.7877	0.8365	0.7804	0.8341	0.7735	0.8318	0.7690	0.8303	0.7671	0.8297	0.7611	0.8275	0.7554	0.8255	0.7500	0.8236
0.8113	0.8014	0.8048	0.7988	0.7987	0.7963	0.7947	0.7947	0.7930	0.7940	0.7876	0.7917	0.7826	0.7895	0.7778	0.7874
0.8349	0.7614	0.8292	0.7586	0.8239	0.7560	0.8203	0.7542	0.8189	0.7535	0.8142	0.7510	0.8097	0.7487	0.8056	0.7465
0.8585	0.7157	0.8536	0.7128	0.8490	0.7100	0.8460	0.7081	0.8447	0.7073	0.8407	0.7048	0.8369	0.7024	0.8333	0.7001
0.8821	0.6629	0.8780	0.6600	0.8742	0.6572	0.8717	0.6553	0.8706	0.6545	0.8673	0.6519	0.8641	0.6494	0.8611	0.6471
0.9057	0.6015	0.9024	0.5985	0.8994	0.5957	0.8973	0.5939	0.8965	0.5931	0.8938	0.5905	0.8913	0.5881	0.8889	0.5858
0.9292	0.5282	0.9268	0.5253	0.9245	0.5227	0.9230	0.5209	0.9224	0.5201	0.9204	0.5177	0.9185	0.5154	0.9167	0.5132
0.9528	0.4371	0.9512	0.4346	0.9497	0.4322	0.9487	0.4306	0.9482	0.4299	0.9469	0.4278	0.9456	0.4258	0.9444	0.4238
0.9764	0.3132	0.9756	0.3112	0.9748	0.3094	0.9743	0.3082	0.9741	0.3077	0.9735	0.3060	0.9728	0.3045	0.9722	0.3030
1.0000	0.0000	1.0000	0.0000	1.0000	0.0000	1.0000	0.0000	1.0000	0	1.0000	0	1.0000	0	1.0000	0

(9) $C_3 A_2 f_1 \left(\frac{B_0}{B_1}\right)$

Same form as (5) with $\frac{B_0}{B_1}$ in place of $\frac{B_1}{B_3}$ and

γ_2 in place of γ_1

$$\gamma_2 = \gamma_0 \pm K_4 B_1$$

(10) $$B_1 = B_0 + \frac{B_3 - B_0}{20}(n_3)$$

where n_3 has successive values of 1 to 20.

VI.2.3 List of Inputs and Definitions

B_3	psia	Supply pressure
B_0	psia	Exhaust pressure
$(C_d A_1)_0$	in^2	Base value of inlet orifice
K_1		Additive % increment for CdA_1 i.e., K_1 = 0.1 produces values of CdA_1 spaced 10% apart
K_2		Multiplying factors = $\frac{(CdA_2)_0}{(CdA_1)_0}$
T	°R	Temperature
γ_0	Ratio of specific heats	Value at "0" psia for given T
K_3		Slope of Gas Constant (R) versus psia for given T
K_4		Slope of γ versus psia for given T

VI.2.4 Print Out

(A) Input data above, once for each complete set.

(B) CdA_1 once, each time it changes.

CdA_2 each time it changes.

B_1 $\qquad$ $Q_L/2.2$

Q_L $\qquad$ $Q_{A1}(B_1)\left(\frac{1}{R_1 T_1}\right) = W_1$

Figure VI-4 is a typical plot which may be constructed from the data printed out by this program.

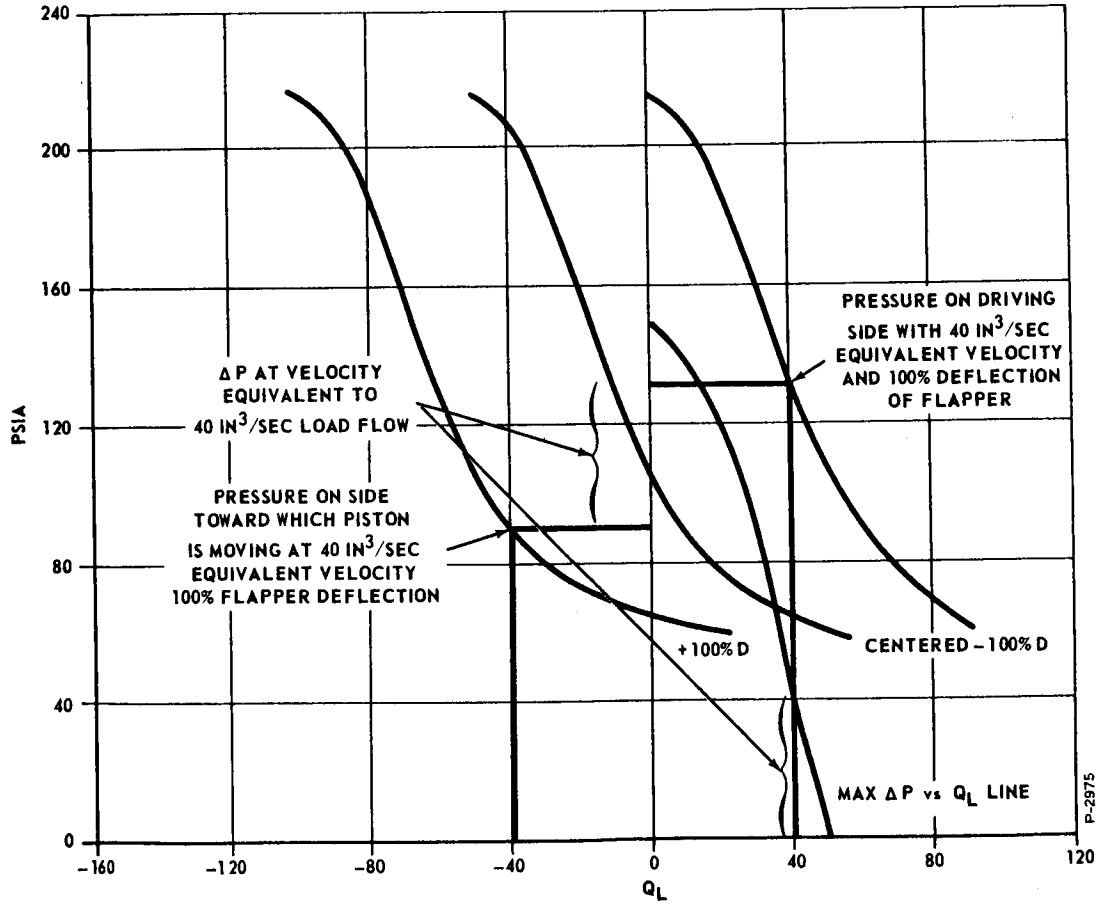

Figure VI-4 - Sample Result of Sizing Calculation